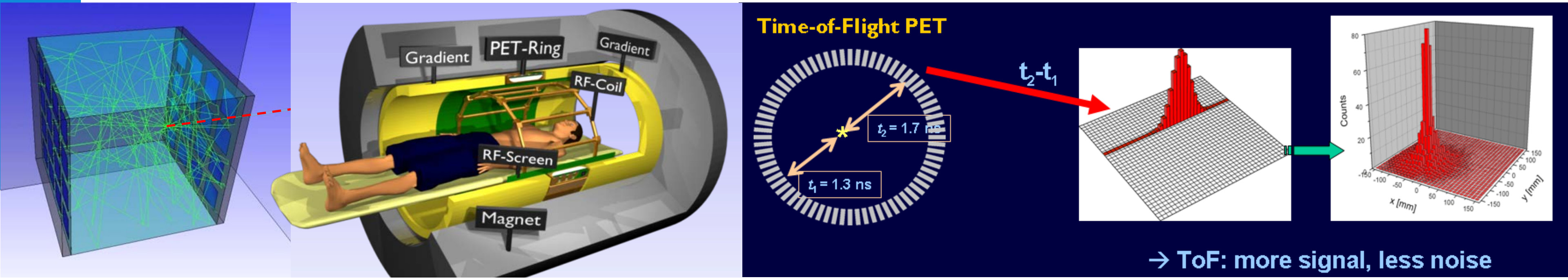

Emerging Technologies in Positron Emission Tomography:

TOF-PET, PET/MRI, In-beam PET

D.R. Schaart, LPC Clermont, 9-Mar-2012

Radiation Detection & Medical Imaging
Delft University of Technology

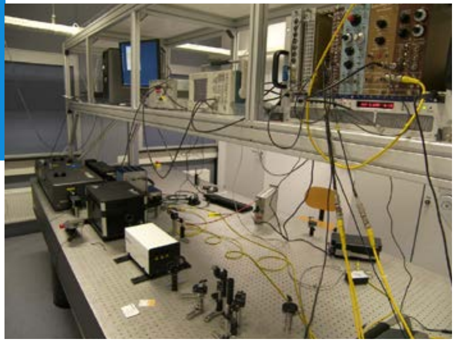

materials research

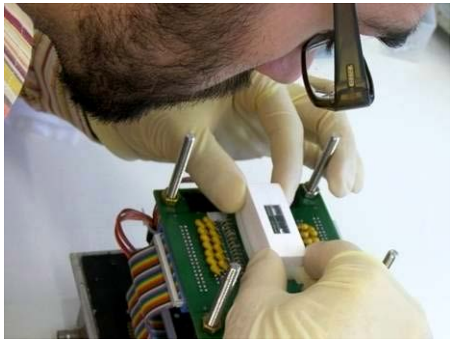

detector research

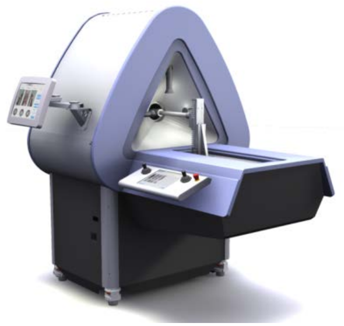

better imaging systems

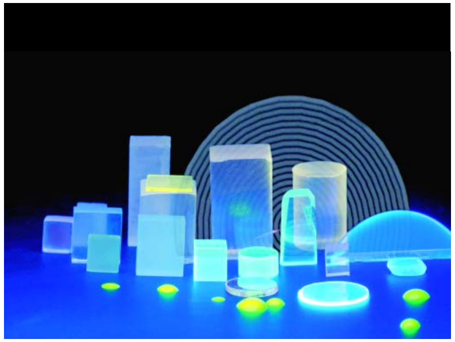

better scintillators

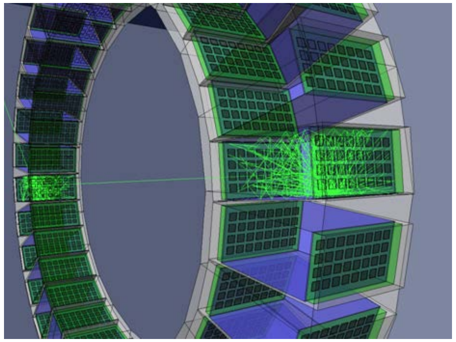

modeling & reconstruction

Positron Emission Tomography

Scanner: ring of gamma ray detectors

Collinearly emitted annihilation quanta detected in coincidence

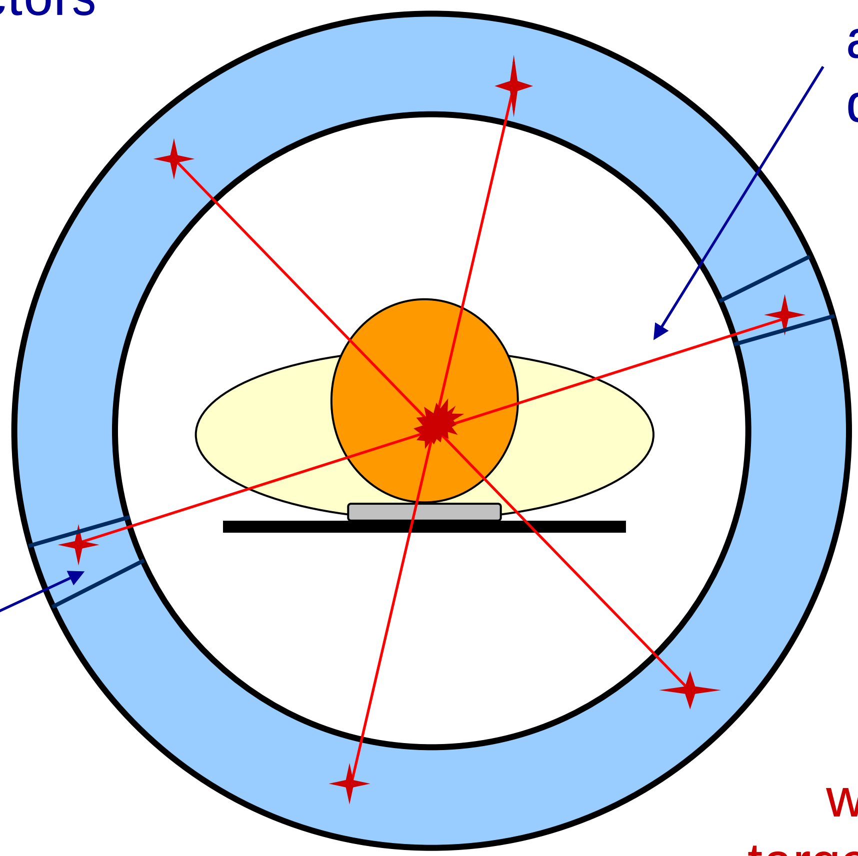

Detectors: scintillator + light sensor

Radiopharmaceutical which binds to a specific target, such as tumour cells

Positron Emission Tomography

Rectal carcinoma and multiple metastases
Data courtesy of J. Karp, Univ. of Pennsylvania

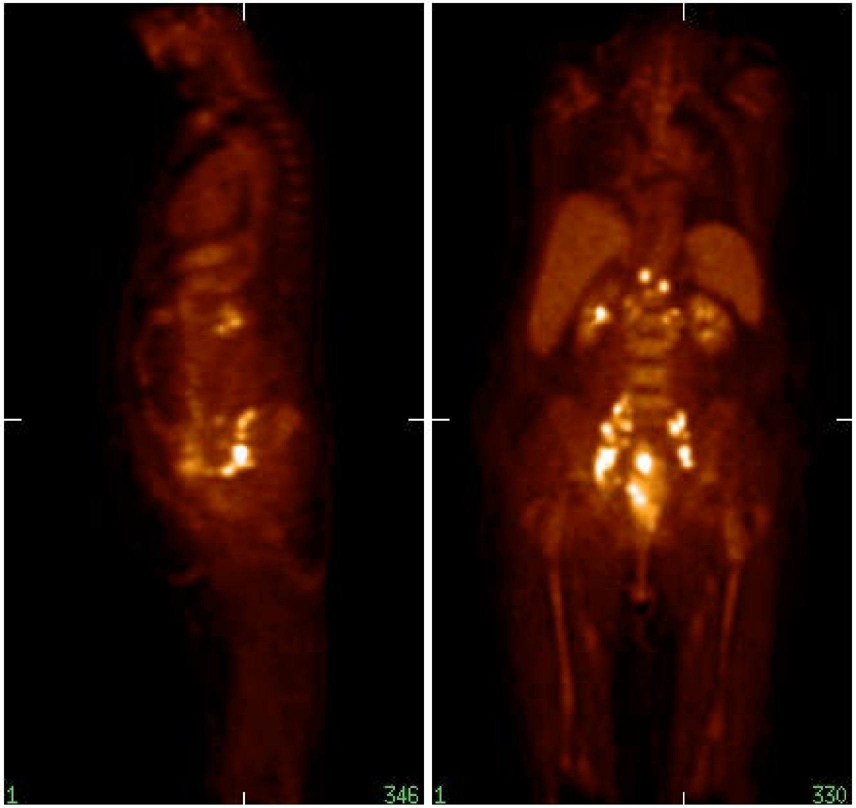

Applications of PET:

- Cancer / oncology
- Heart tissue viability
- Neurology
- Etc.

→ *PET images Function, not Anatomy!*

TU Delft
Dennis R. Schaart
Delft University of Technology

Clinical use: PET/CT

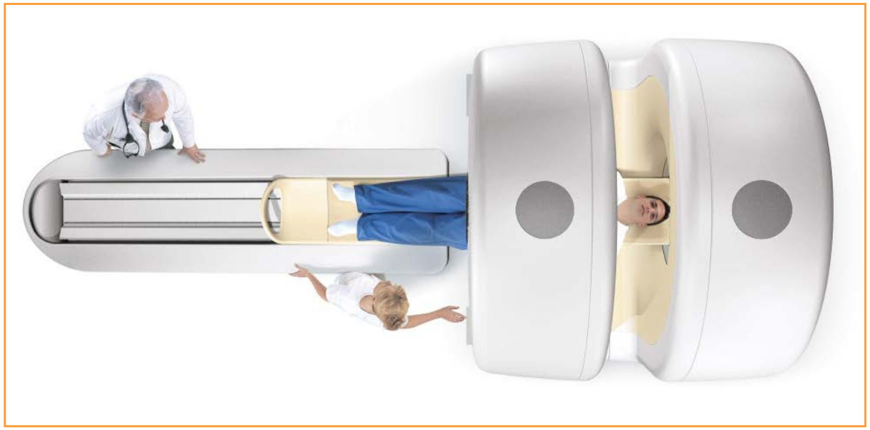

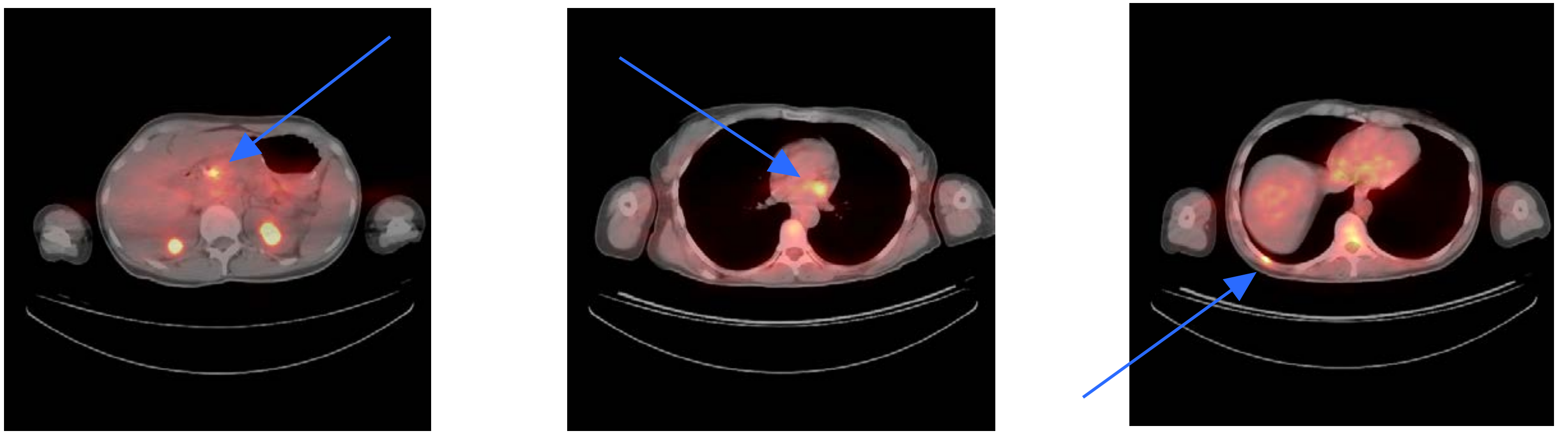

PET/CT (fused images): primary pancreatic cancer with suspicious chest wall and mediastinum lesions

Time of Flight PET Systems

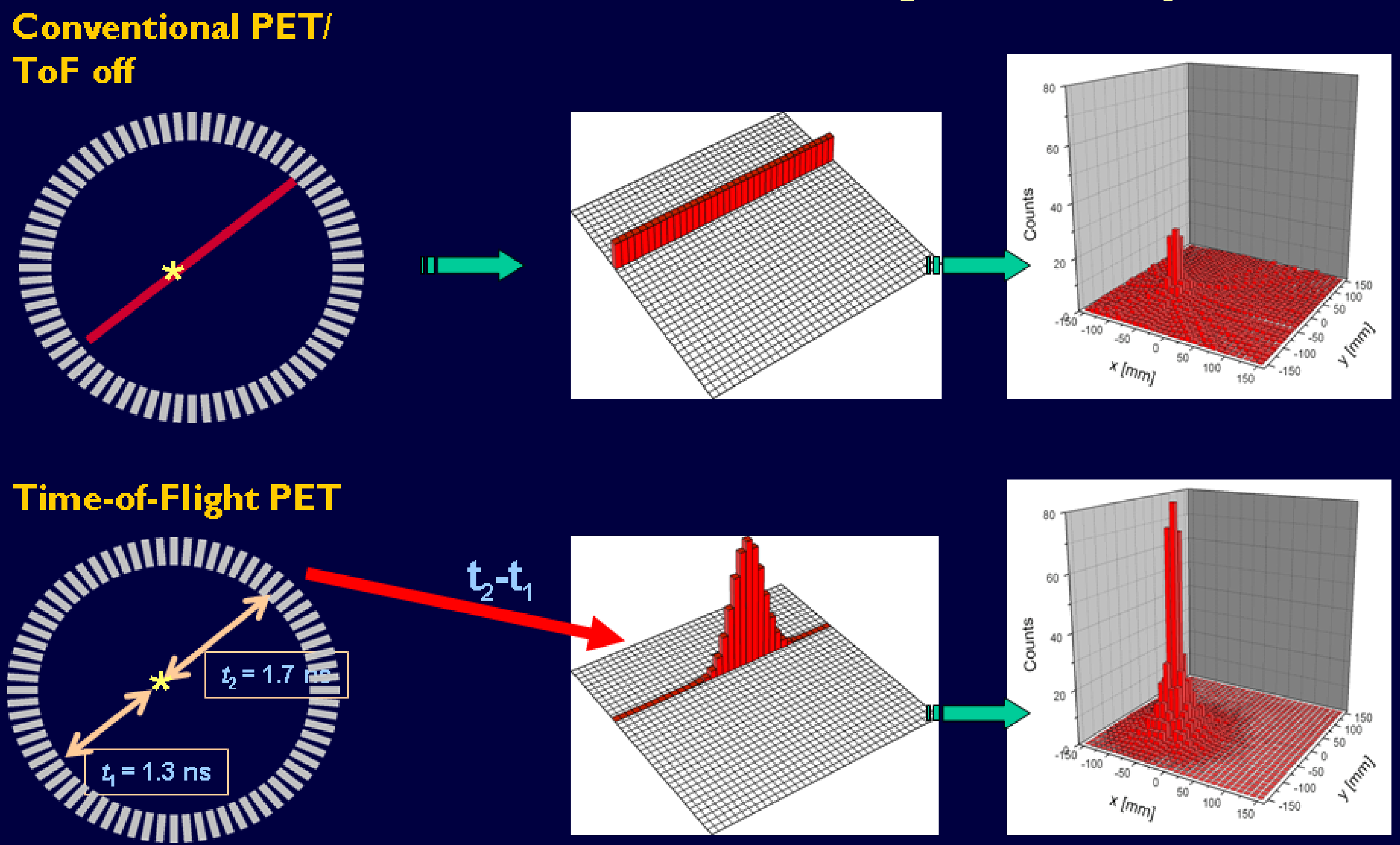

→ ToF: more signal, less noise

Dennis R. Schaart
Delft University of Technology

Time-of-flight PET

Colon cancer, left upper quadrant peritoneal node

114 kg; BMI = 32.2
13.4 mCi; 2 hr post-inj

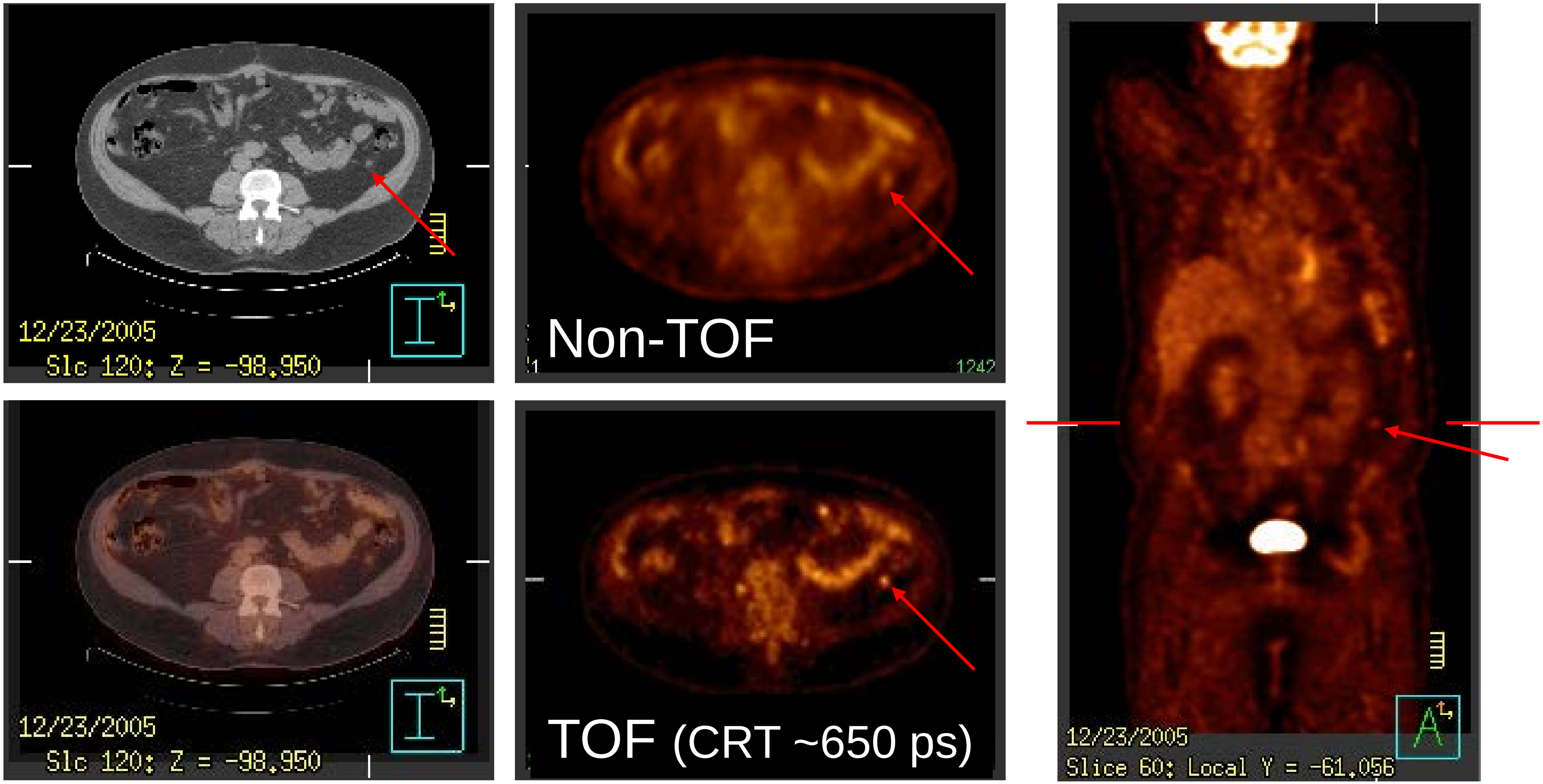

State-of-the-art clinical PET: coincidence resolving time (CRT) ≈ 500 ps

Time-of-flight PET: concept of CRT

The accuracy of source position localization along line of response depends on the *coincidence resolving time (CRT)*

Δx = uncertainty in position along LOR = c · CRT/2, where c is the speed of light.

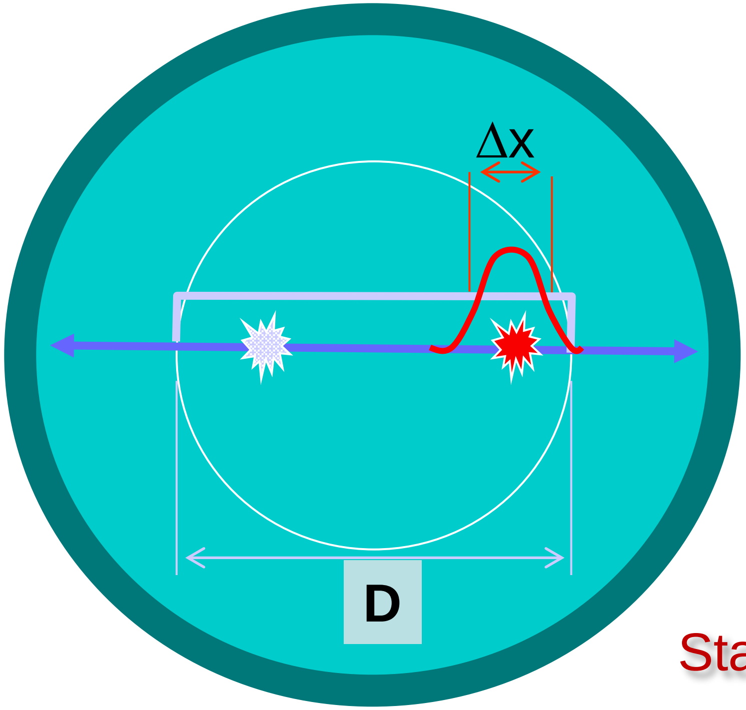

The TOF benefit is proportional to Δx/D, where D is the effective patient diameter.

=> The smaller the CRT, the better.

State-of-the-art: CRT ≈ 500 ps ⇒ Δx ≈ 7.5 cm.

PET detectors: classic “block” detector

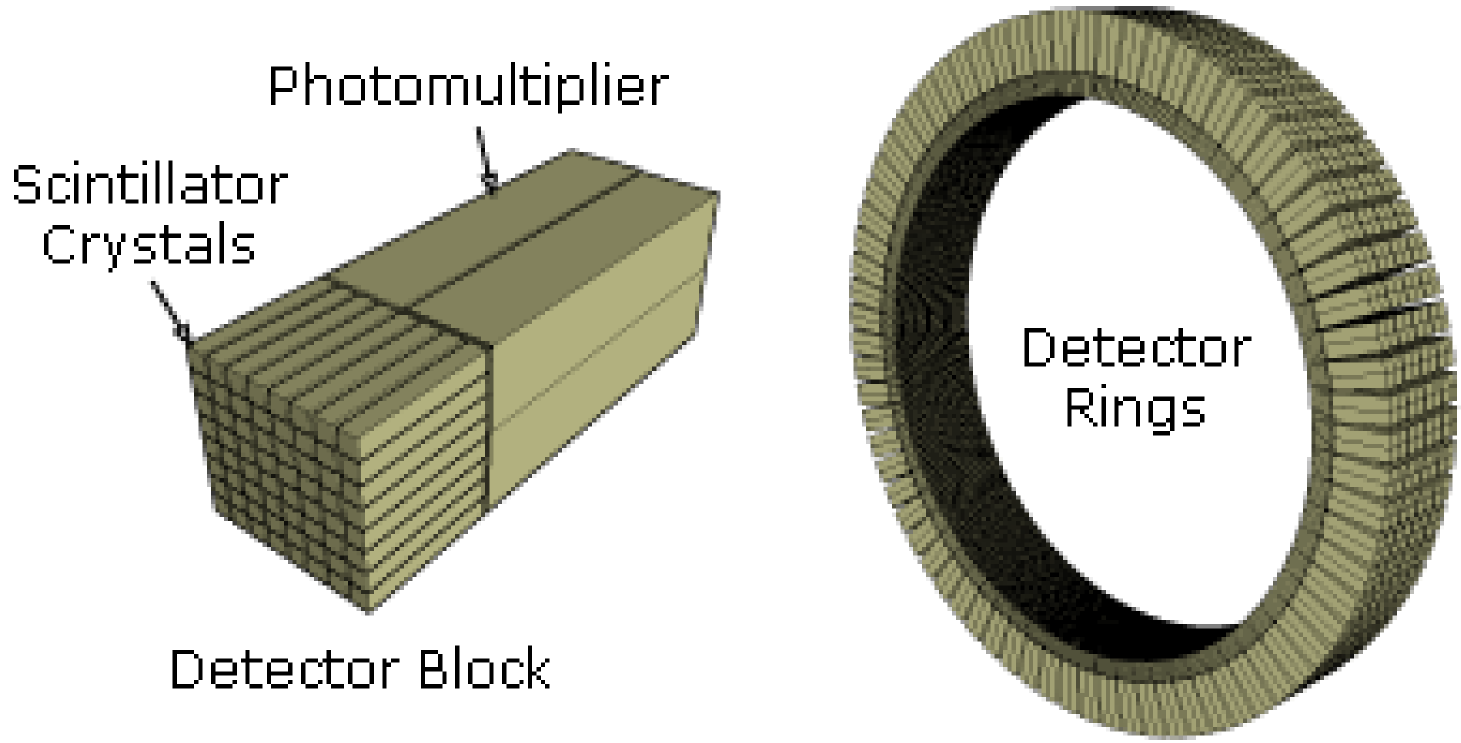

- Several block detectors are assembled into a ring
- A scanner may consist of several detector rings

Silicon Photomultiplier (SiPM)

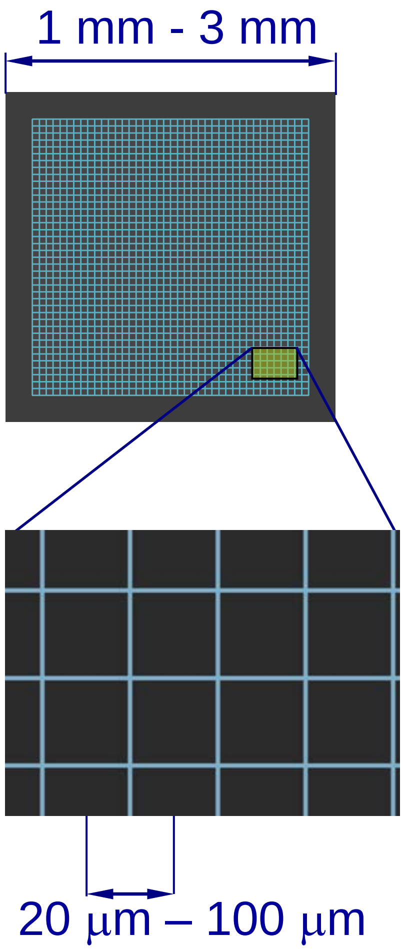

- Array of many self-quenched Geiger-mode APDs (microcells) connected in parallel

- Increasingly interesting as replacement for PMTs:
  - high gain (~10^6)
  - high PDE
  - compact and rugged
  - transparent to γ-photons
  - fast response (ns)
  - insensitive to magnetic fields

Multimodality: PET + MRI

Now: avalanche photodiodes (APDs)
Next generation systems: SiPMs

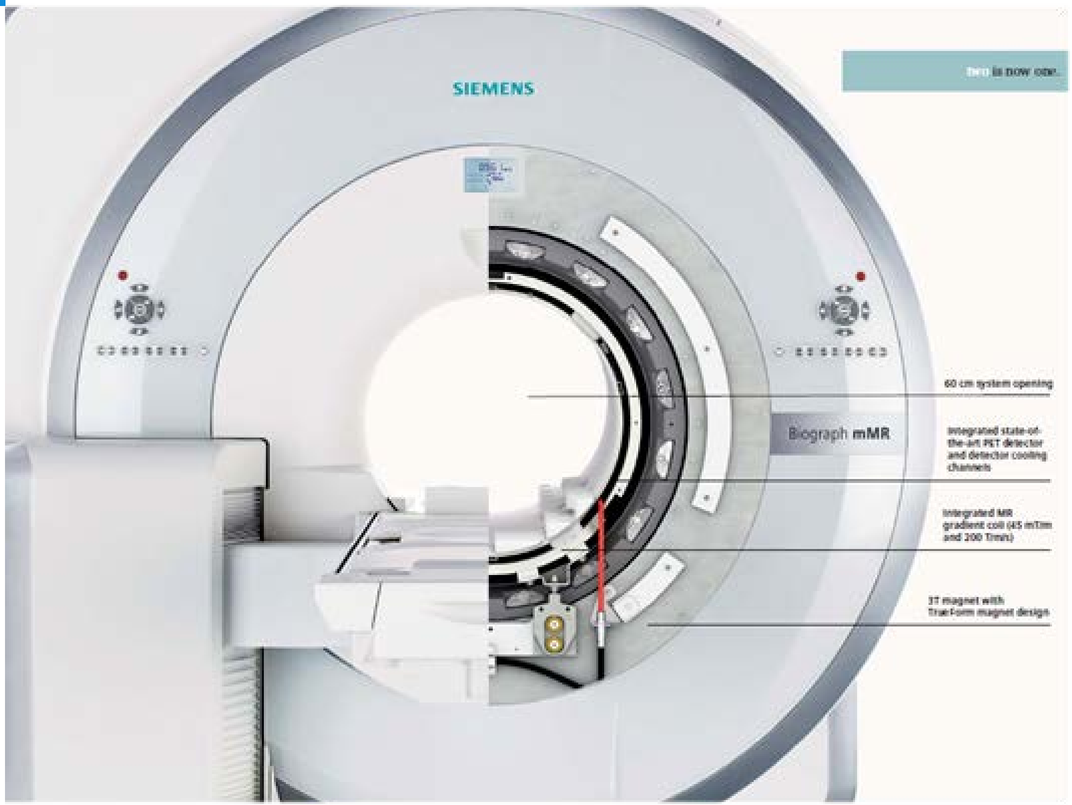

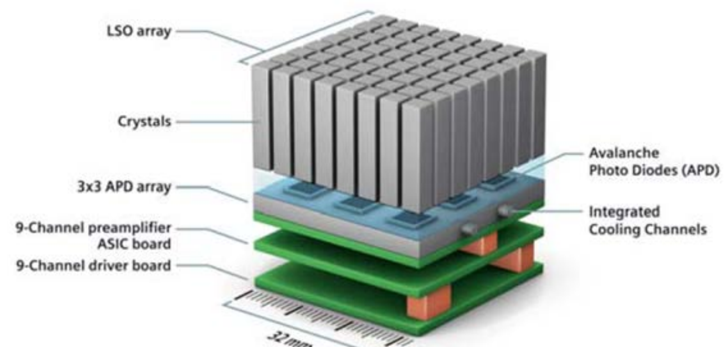

Images: Siemens

Multimodality: PET + MRI

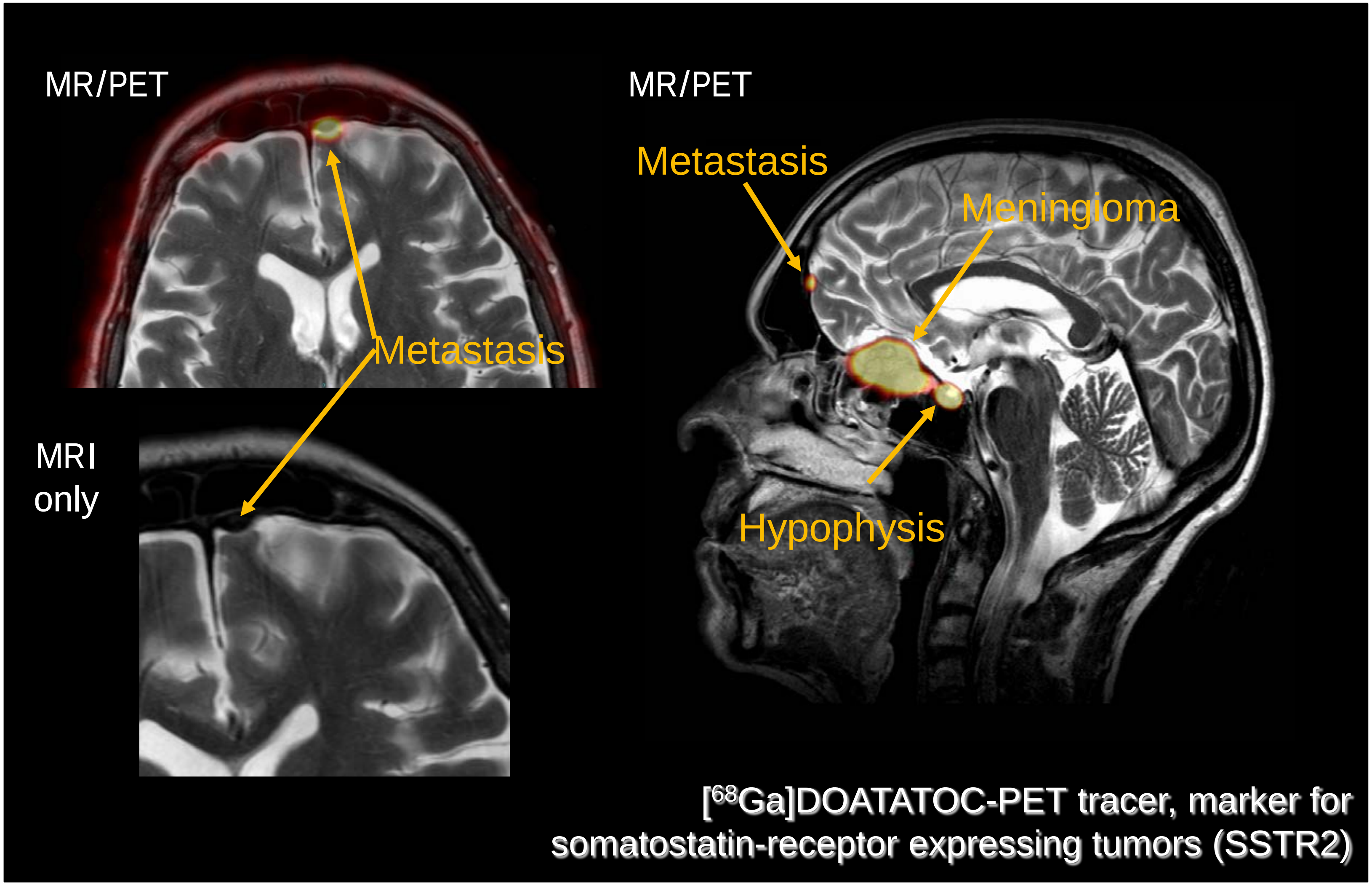

Single-photon avalanche diode (SPAD)

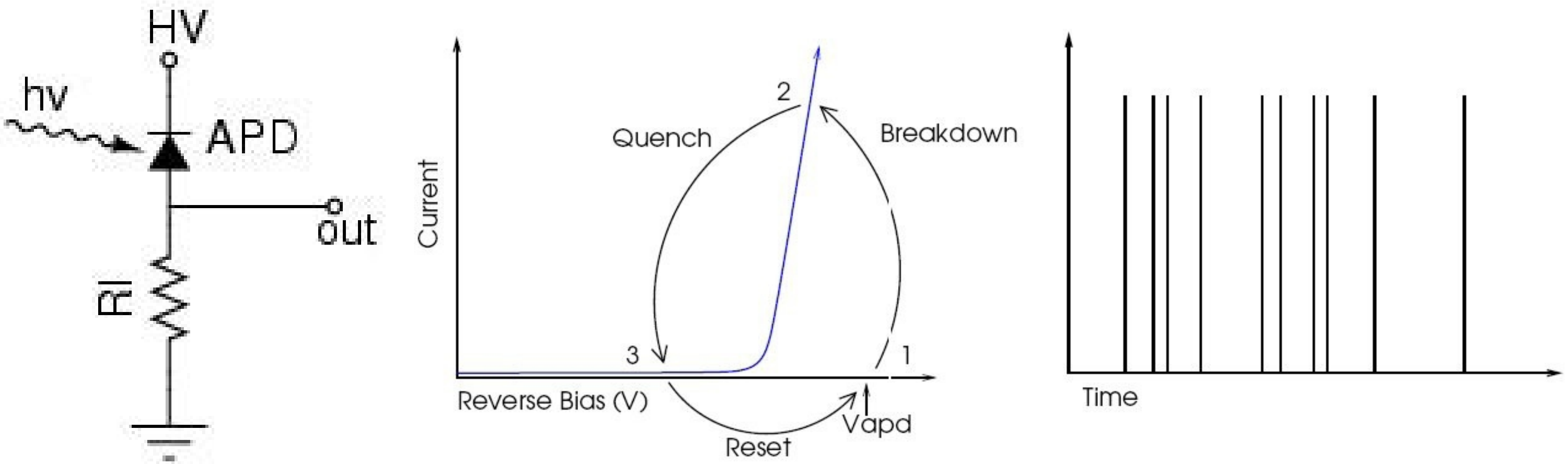

Above the breakdown voltage, electrons generate a Geiger discharge

- Quenched by a series resistor
- A binary device: “on” or “off”
- Very large gain ($\sim 10^5$ to $\sim 10^6$) => sensitive to single photons
- Fast response (time jitter ~100 ps for single photons)

Figure: J. O’Keeffe, Sensl

SiPM: parallel array of many SPADs

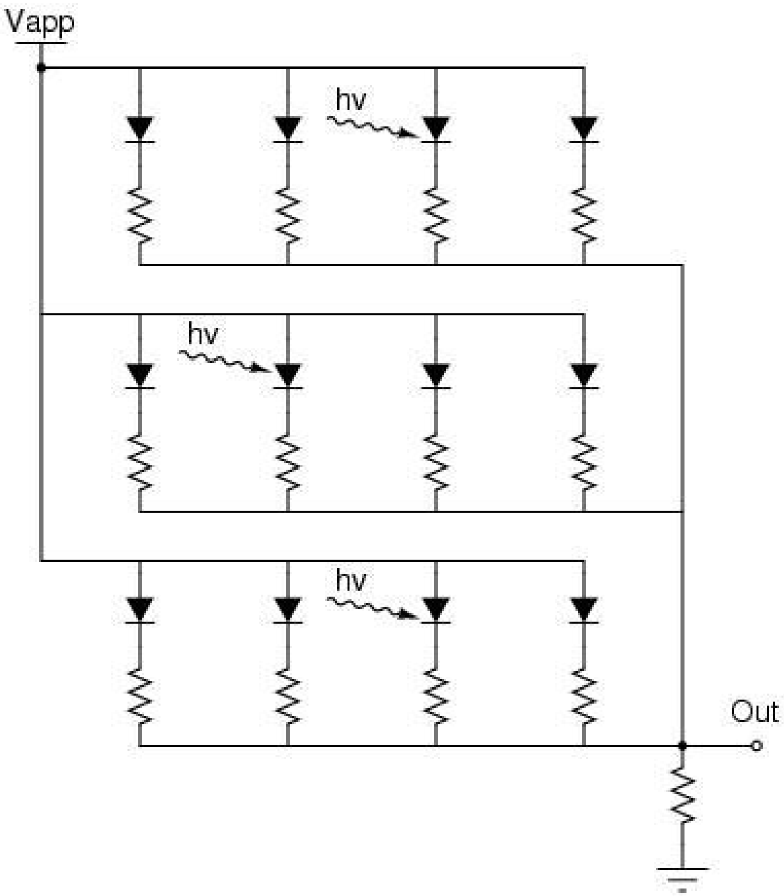

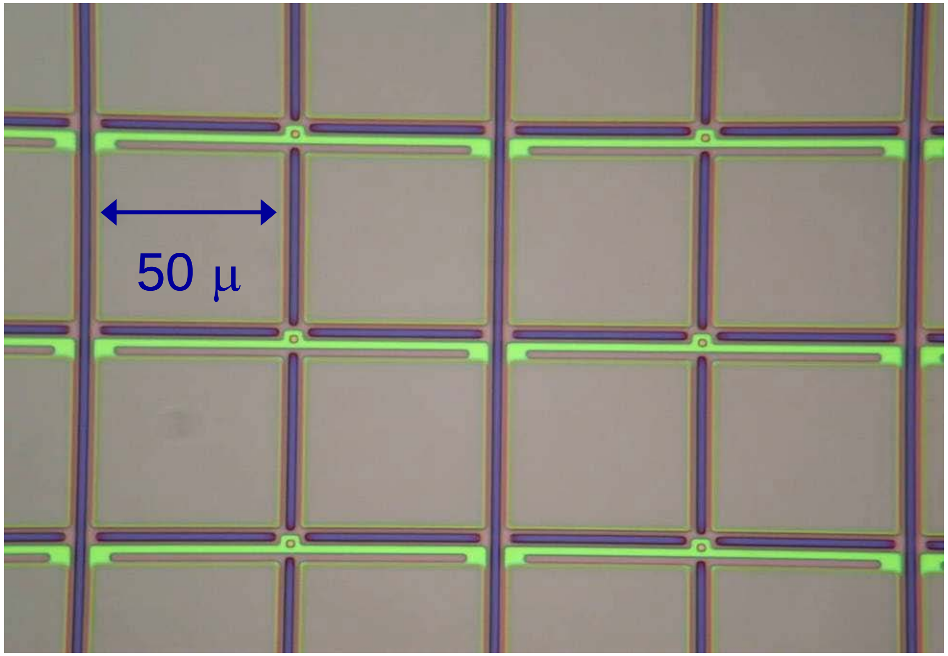

- Array of many SPADs (“microcells”) in parallel
- The combined output of all the microcells is “proportional” to the incident photon flux.

Figure: J. O’Keeffe, Sensl

100 ps barrier broken using SiPMs

Made possible by the combination of:

- Small $LaBr_3$:Ce(5%) crystals (3 mm x 3 mm x 5 mm)
- Silicon Photomultipliers (Hamamatsu MPPC-S10362-33-050C)
- Digital Signal Processing (DSP)

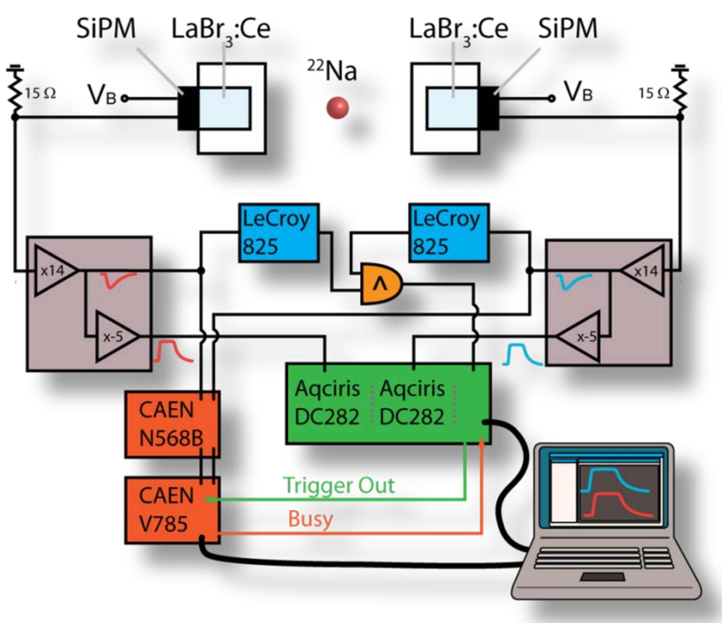

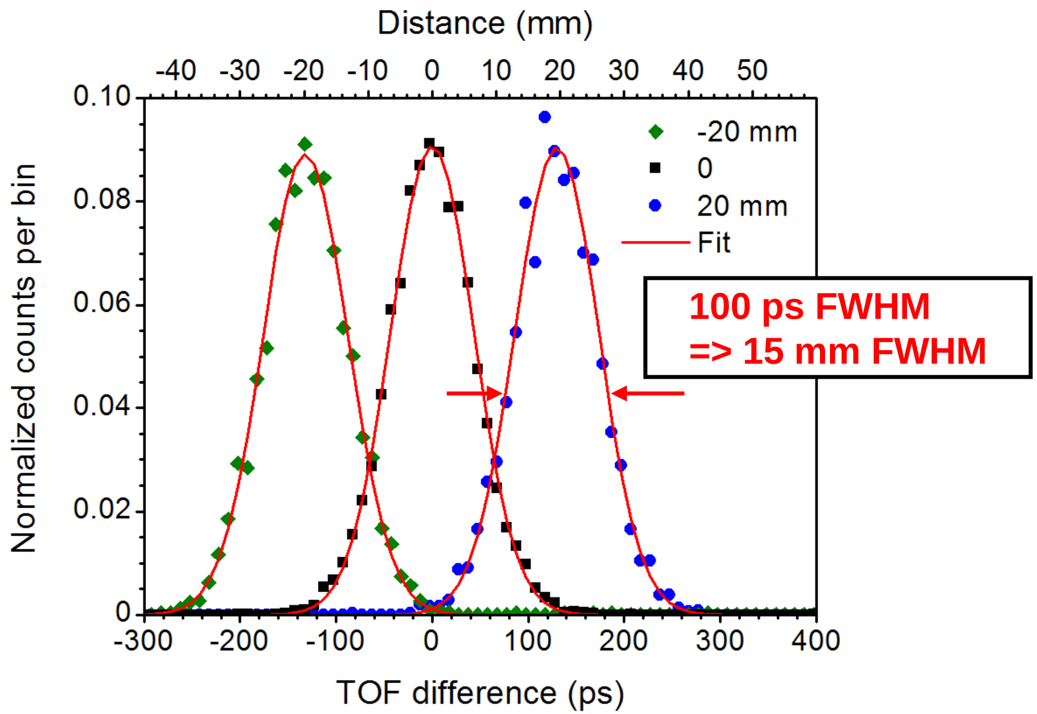

Recent measurements with LSO:Ce,Ca

S. Seifert et al, NDIP 2011

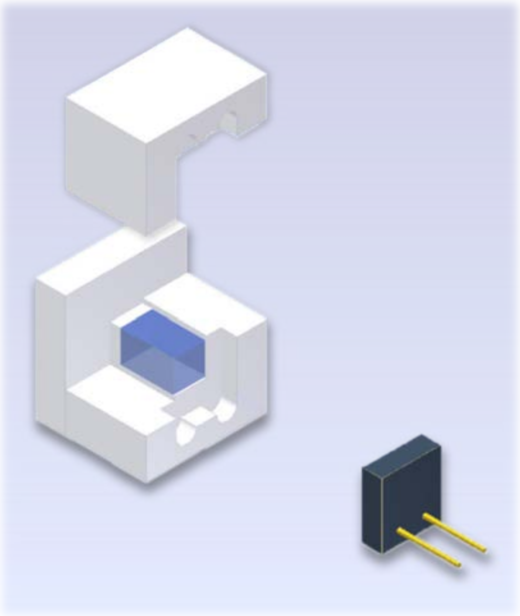

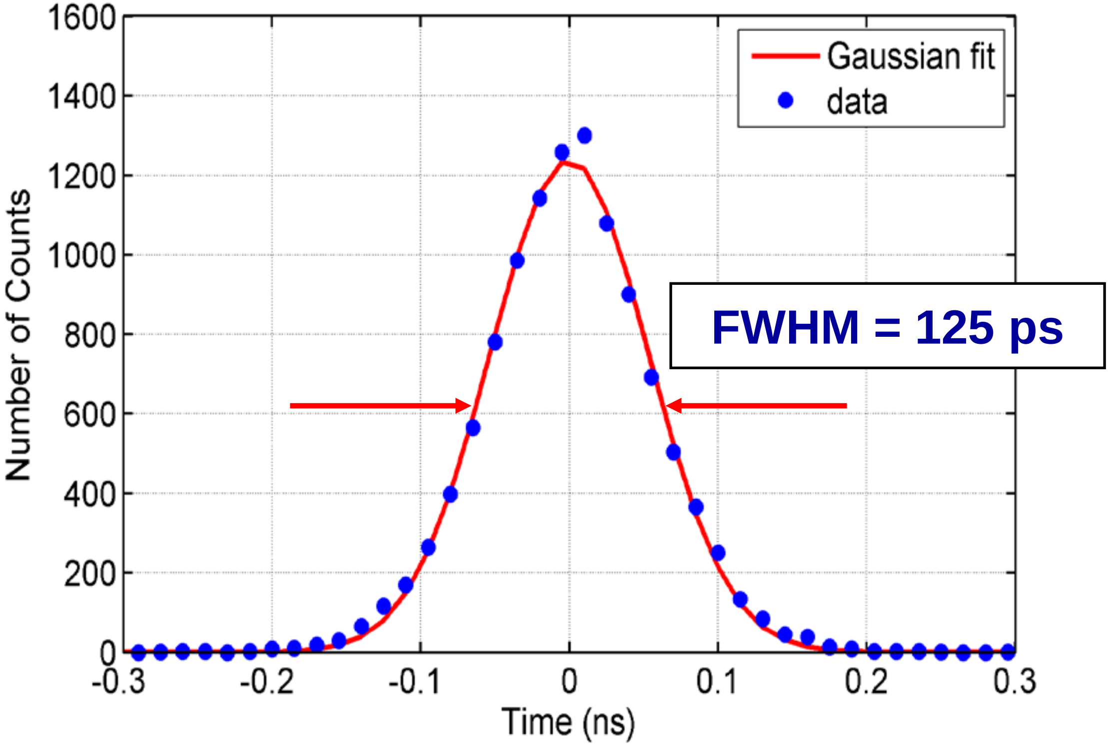

- 3 mm x 3 mm x 5 mm LSO:Ce,Ca (U Tennessee)
- 3 mm x 3 mm SiPM (MPPC-S10362-33-050C)

SiPM preamplifier

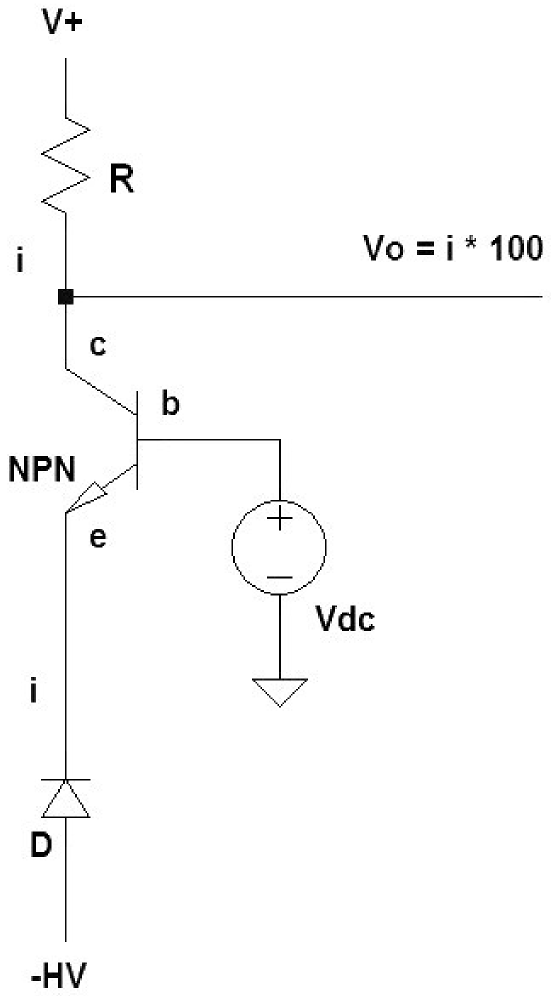

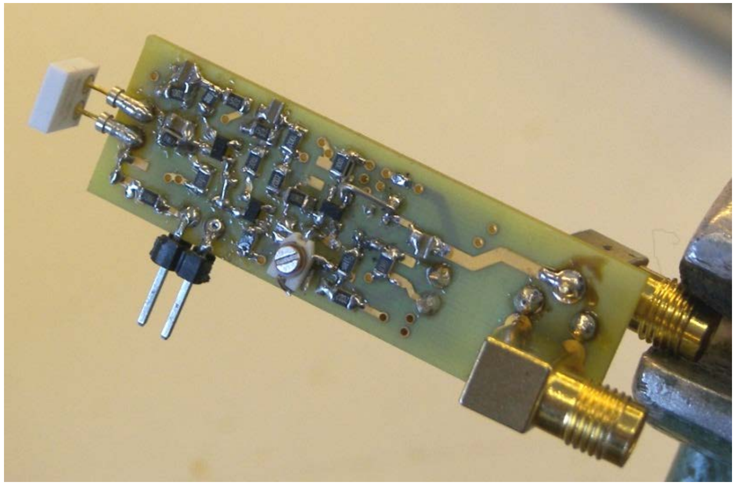

- SiPM: either a bad voltage source, or a bad current source
- Large capacitance (> 300 pF)
- Solution: common-base amplifier
- The signal current i is copied at collector and transformed into a voltage by resistor R.
- Low input impedance of the emitter isolates the detector capacitance from the rest of the circuit

J. Huizenga et al, NIMA A, http://dx.doi.org/10.1016/j.nima.2011.11.012

SiPM preamplifier

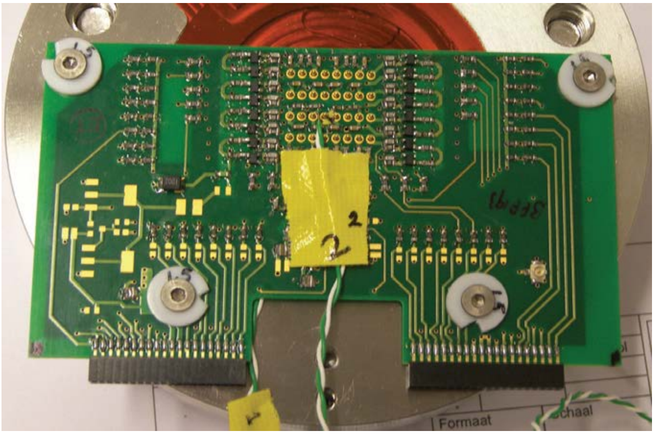

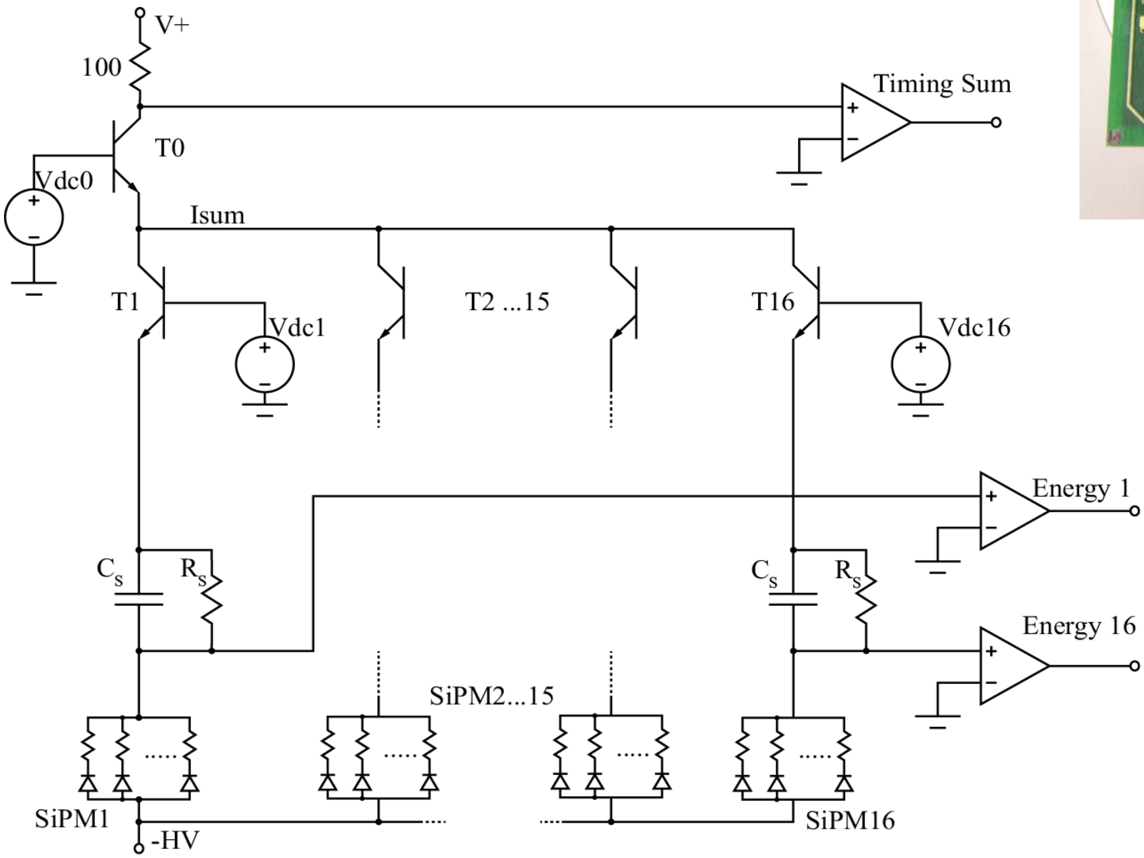

16-channel version with sum signal for timing and individual energy outputs

S. Seifert et al, "Monolithic $LaBr_3$:Ce crystals on silicon photomultiplier arrays for time-of-flight positron emission tomography", accepted for publication in Phys Med Biol 2012

SiPM-array based PET detectors

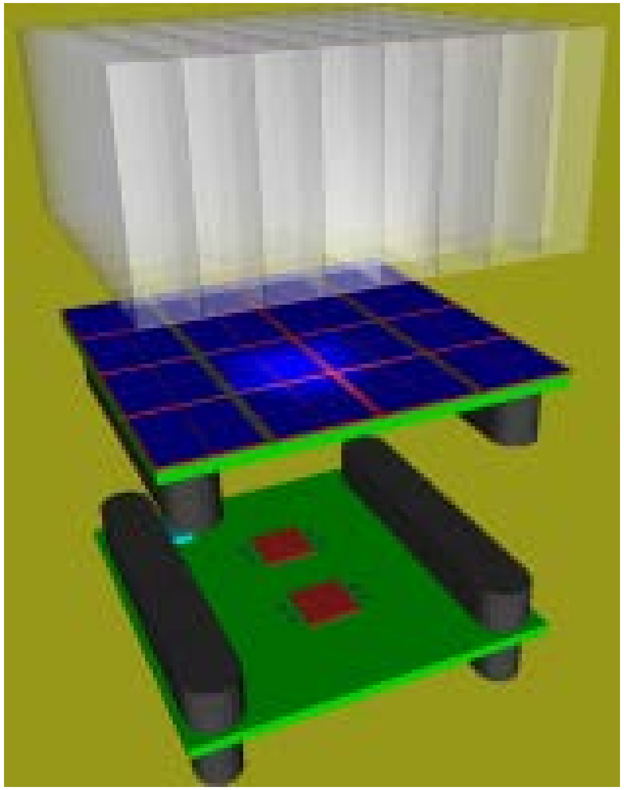

For example:

- crystal matrix composed of e.g. 4 mm x 4 mm x 20 mm crystals
- each crystal coupled 1-to-1 to an individual SiPM

=> high spatial resolution

=> high energy resolution

=> excellent timing

Image courtesy of Philips

SiPM arrays – some examples

FBKirst

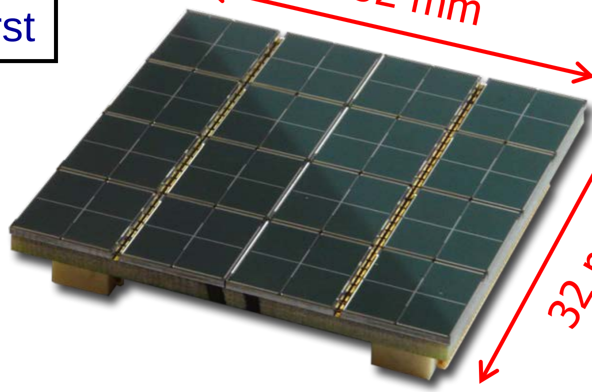

Hamamatsu

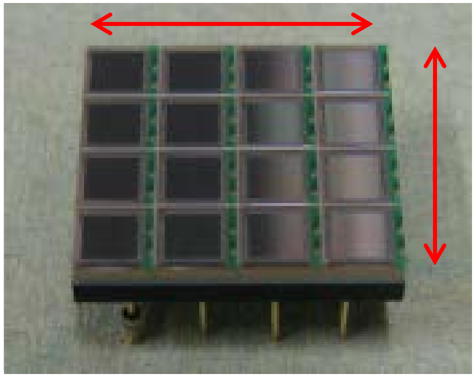

SensL

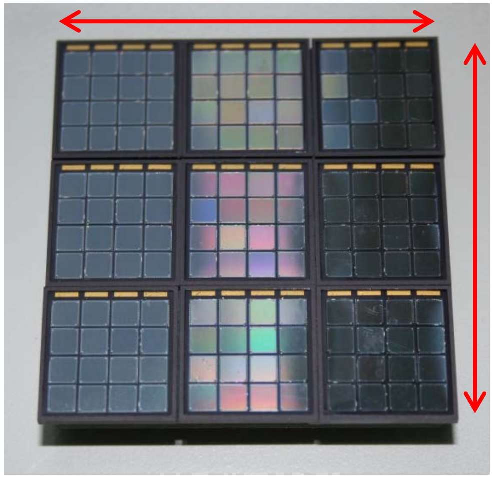

Philips Digital Photon Counting

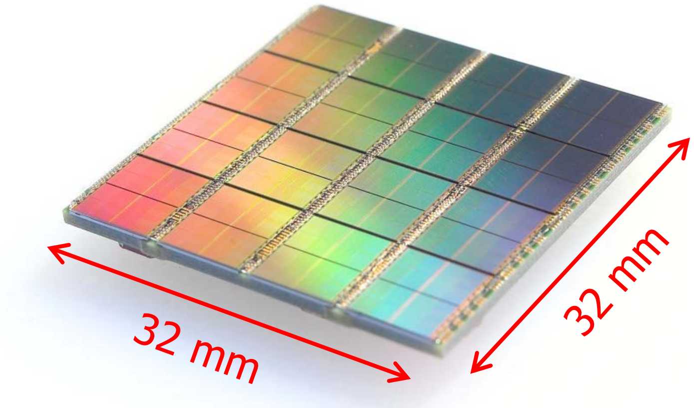

Individual readout of array elements => position-sensitive light sensor

Digital PET system

- Local position decoding and time-stamping
  - → no limit on no. of channels, no loss of (Fisher) information!
- Real-time DOI correction of spatial and timing information
- Fast, accurate & repeatable system calibration and time alignment

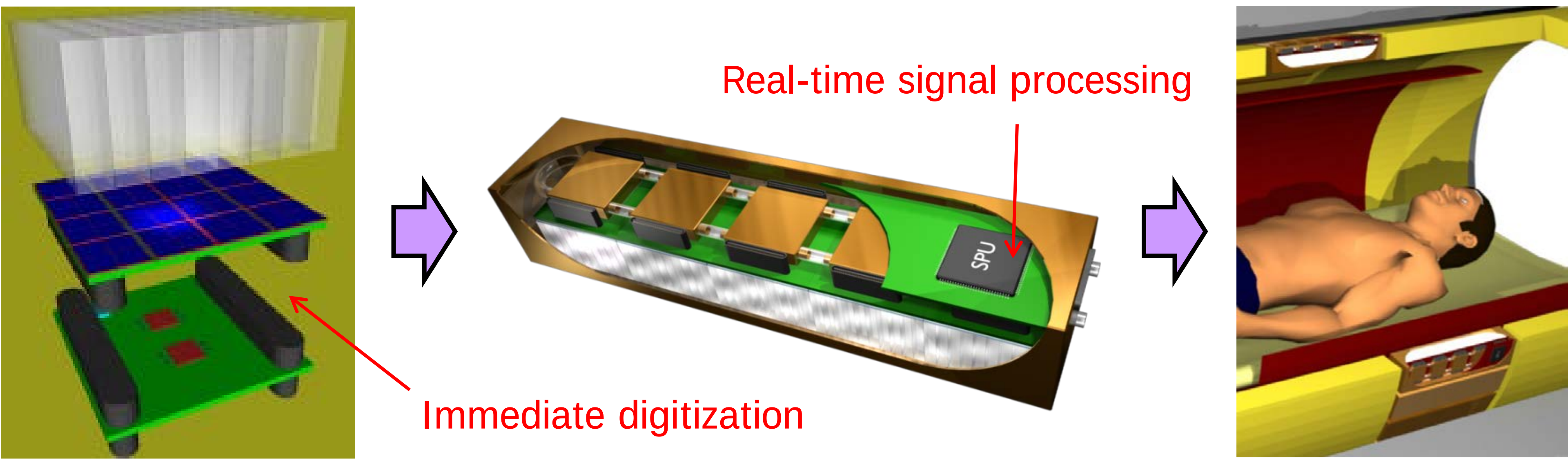

Detector Module System

SUBLIMA project

Whole-body TOF-PET / MRI

Philips Research
Delft University of Technology
Leiden University Medical Center
University of Heidelberg
University of Ghent
King's College London
Fondazione Bruno Kessler
University of Pennsylvania
Ecole Polytechnique Fédérale de Lausanne
Micro Systems Engineering GmbH
Technolution BV

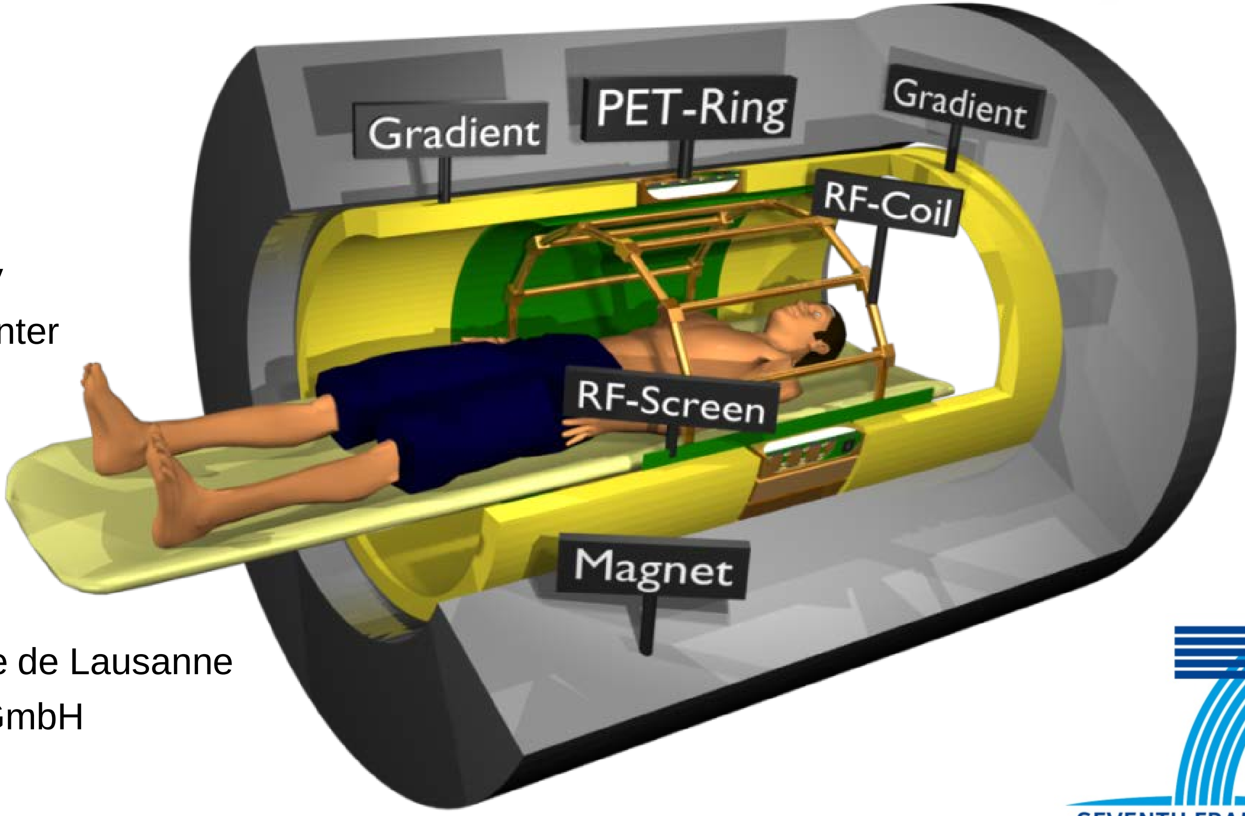

The importance of spatial resolution

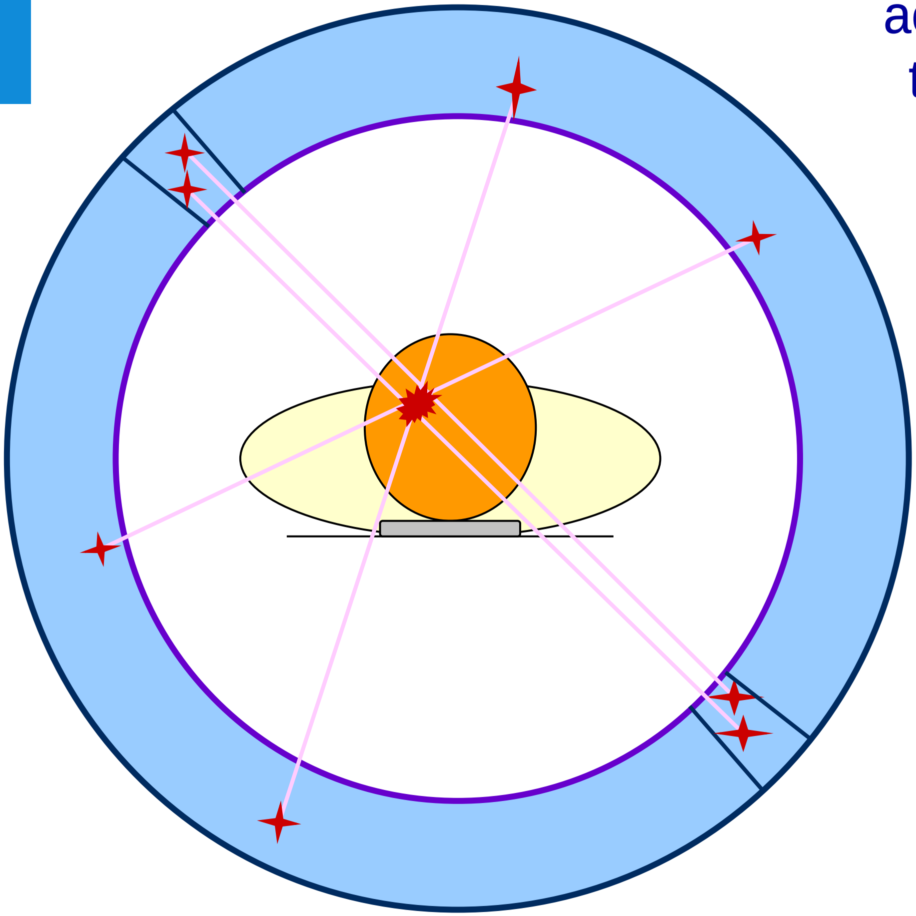

Image resolution is determined by the accuracy with which we can determine the interaction position of the gamma photon in the detector

State-of-the-art PET: 2 – 4 mm

low spatial resolution:

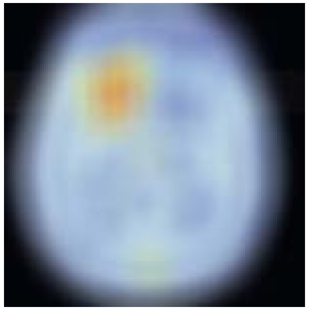

high spatial resolution:

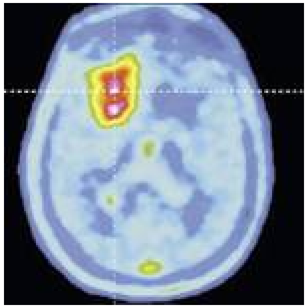

Depth of interaction errors

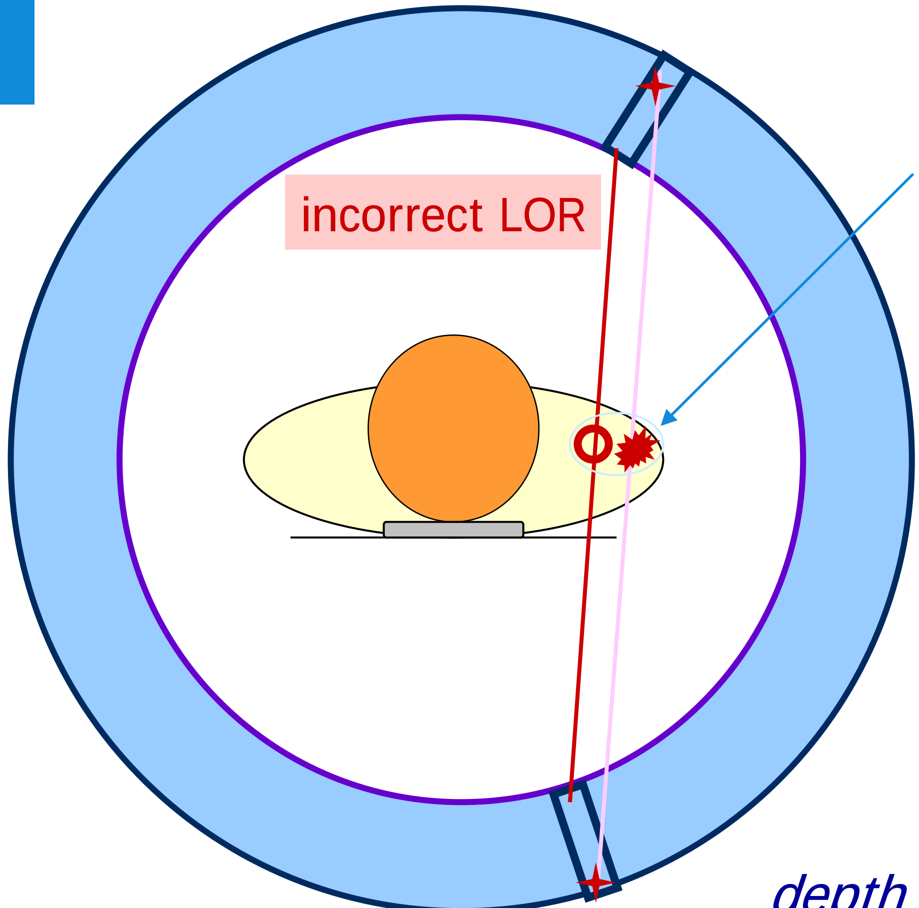

parallax error or radial elongation (at off-centre positions only)

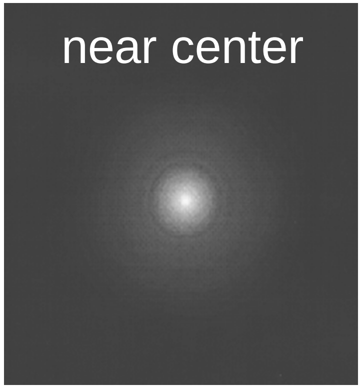

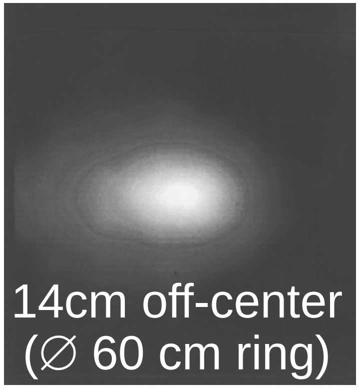

Parallax errors can be avoided by correcting for the *depth of interaction (DOI)* in the scintillator

Monolithic scintillator detectors

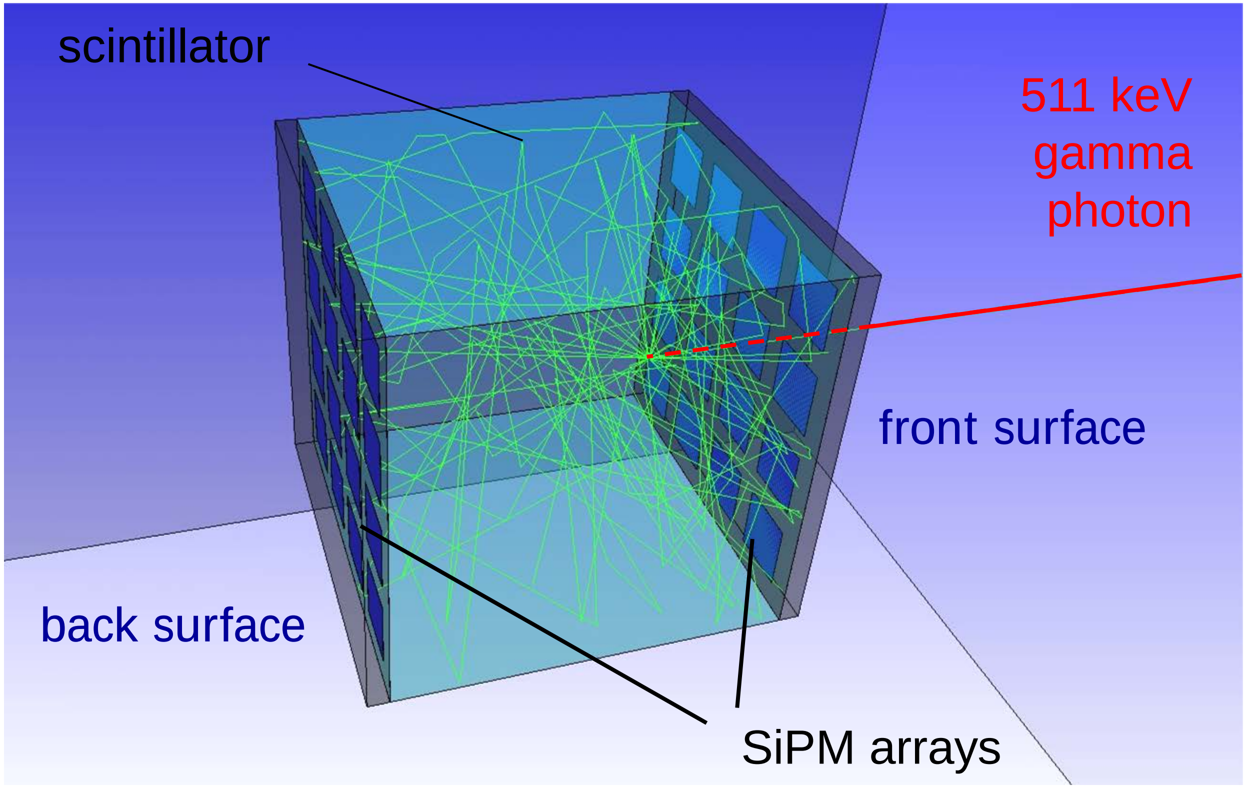

- GEANT4 simulation of monolithic scintillation crystal
- One or more (d)SiPM arrays (double-sided readout, DSR, shown here)
- Gamma *interaction position* from scintillation *light distribution*
- Intrinsic depth-of-interaction information

Monolithic scintillator detectors

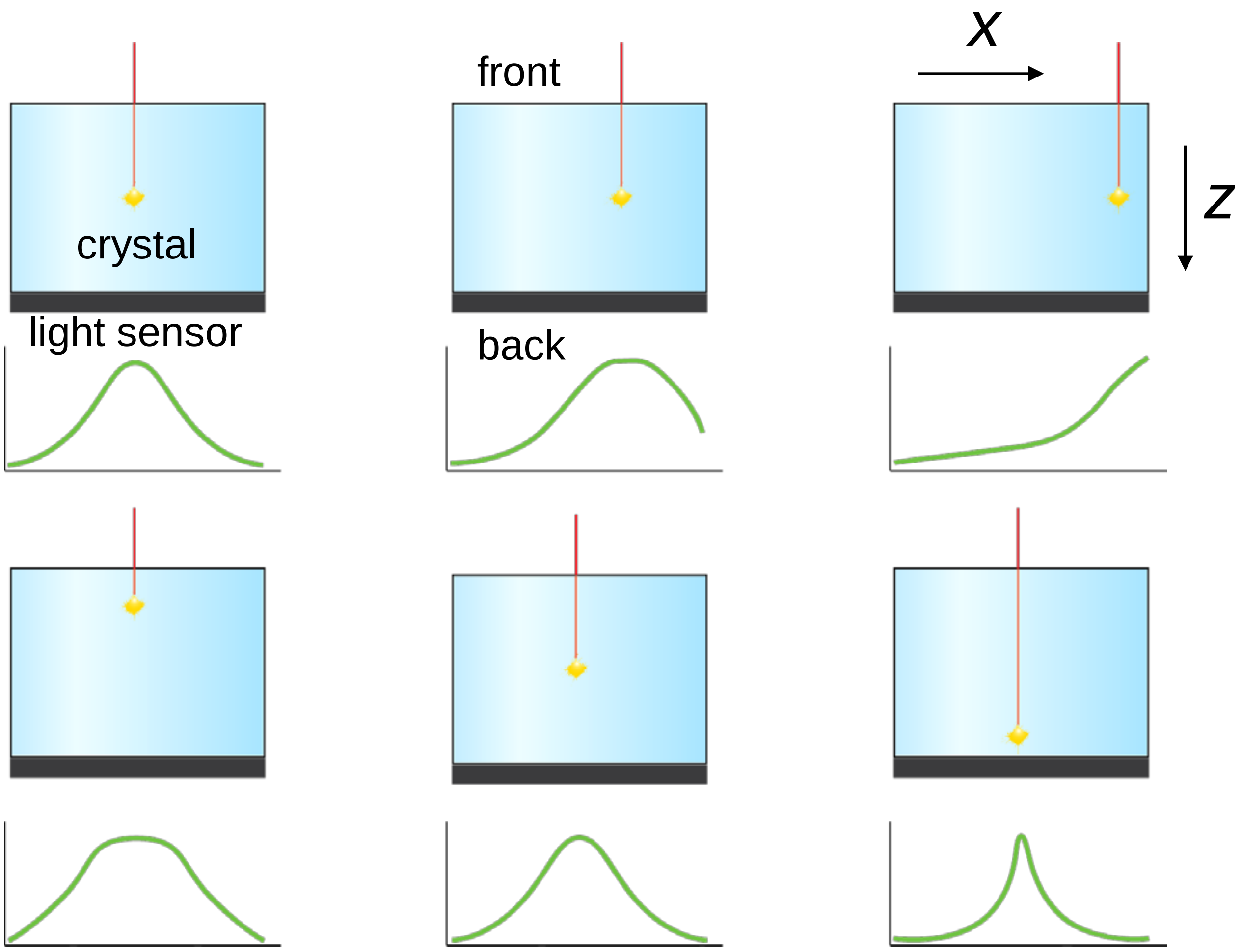

Light distribution depends on the entry point on the front surface…

and on the depth of interaction (DOI).

Digital SiPMs

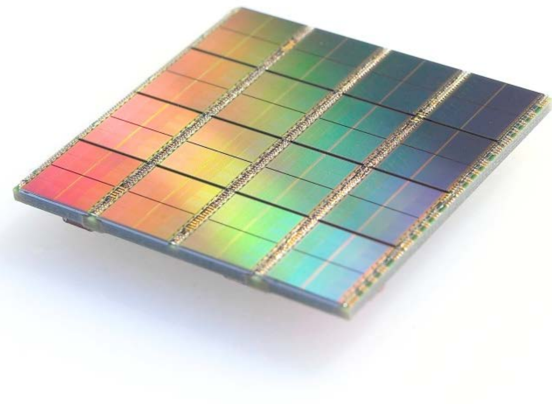

Analog Silicon Photomultiplier

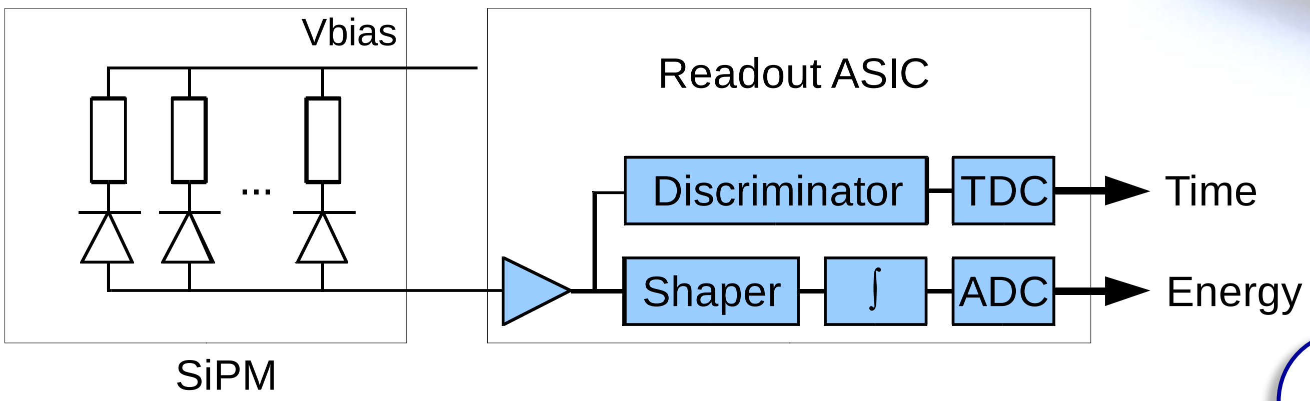

Digital Silicon Photomultiplier

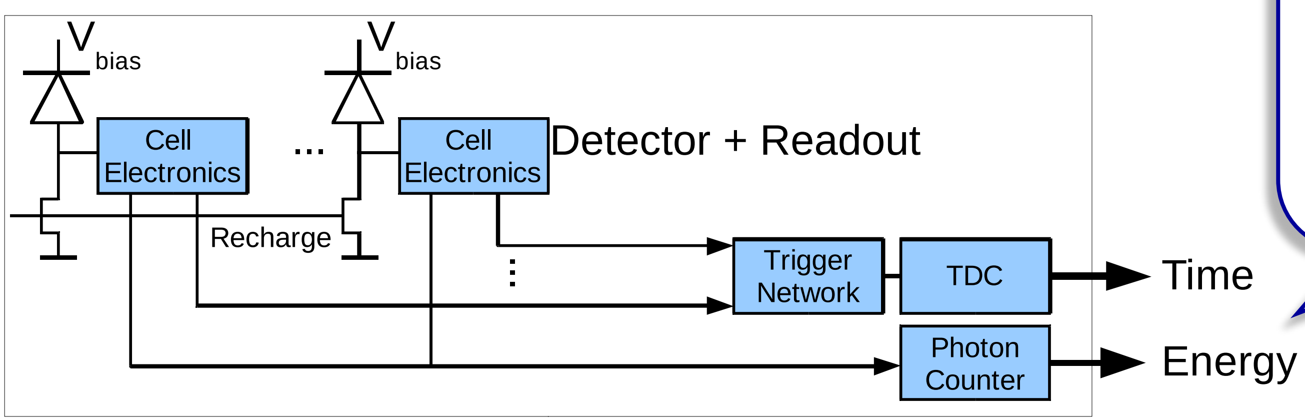

dSiPM provides a digital timestamp and the photon count for each light pulse, without need for any front-end electronics

Installation of 1st prototypes in Delft

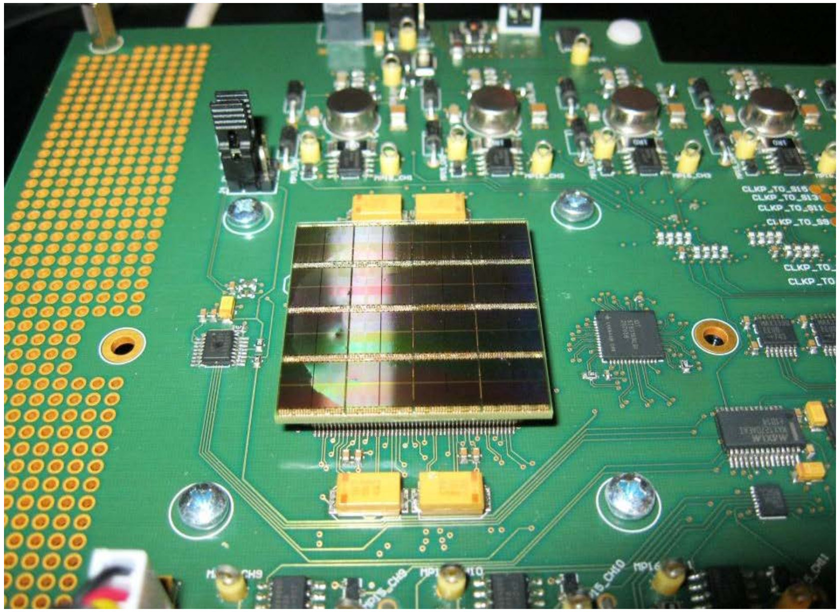

First tests in progress:

- Timing performance
- PDPC with monolithic scintillators

Test setup dSiPM-based detectors

Reference detector

X-Y stage

Collimator

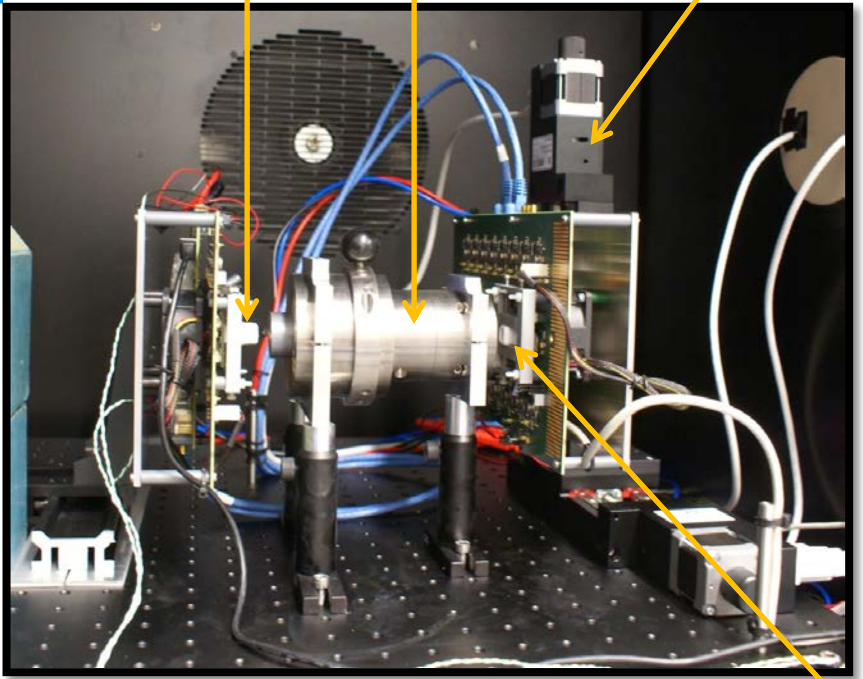

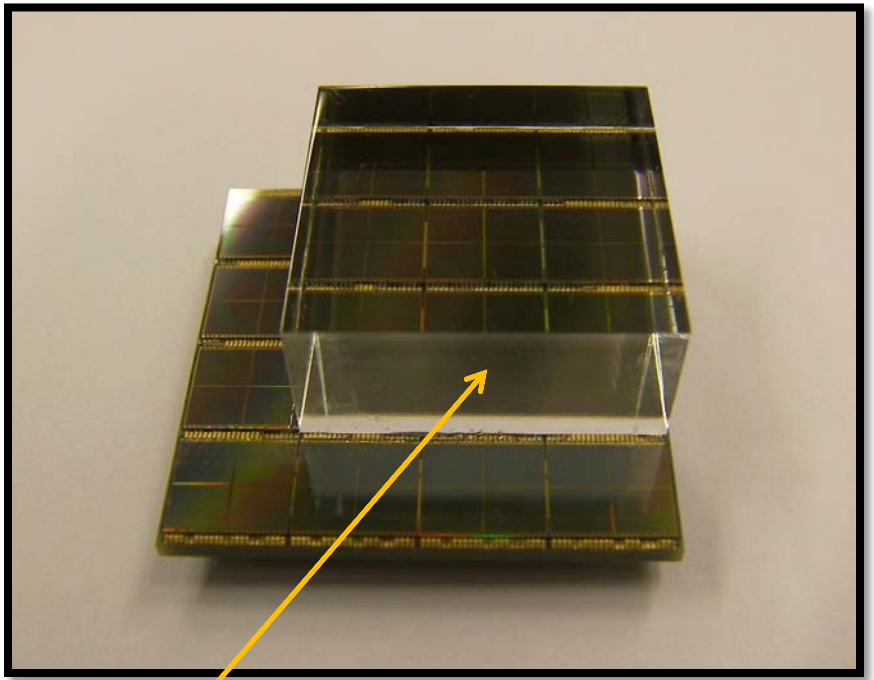

24 mm x 24 mm x 10 mm monolithic LSO:Ce,Ca on PDPC array

Sub-mm spatial resolution

0.98 mm FWHM and 2.31 mm FWTM average resolution

FWHM position resolution

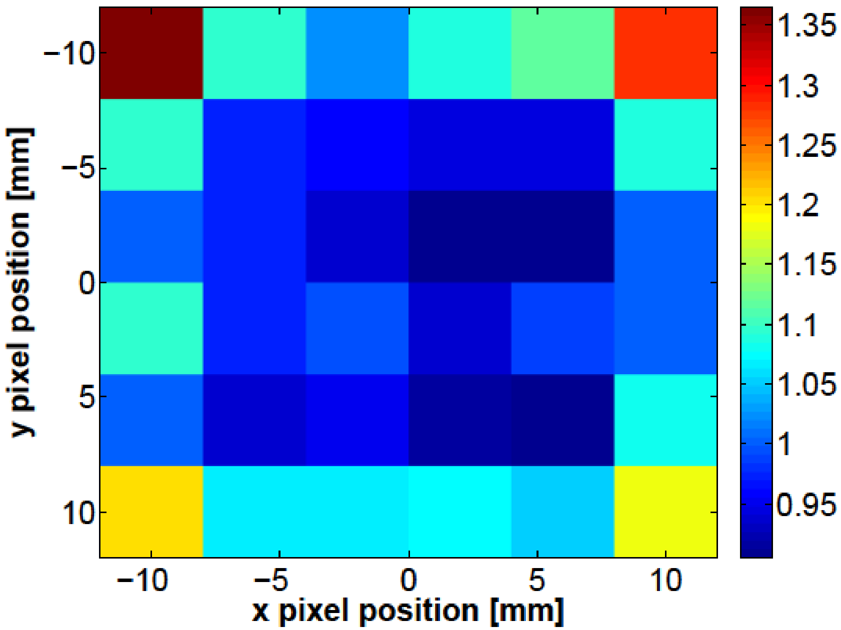

FWTM position resolution

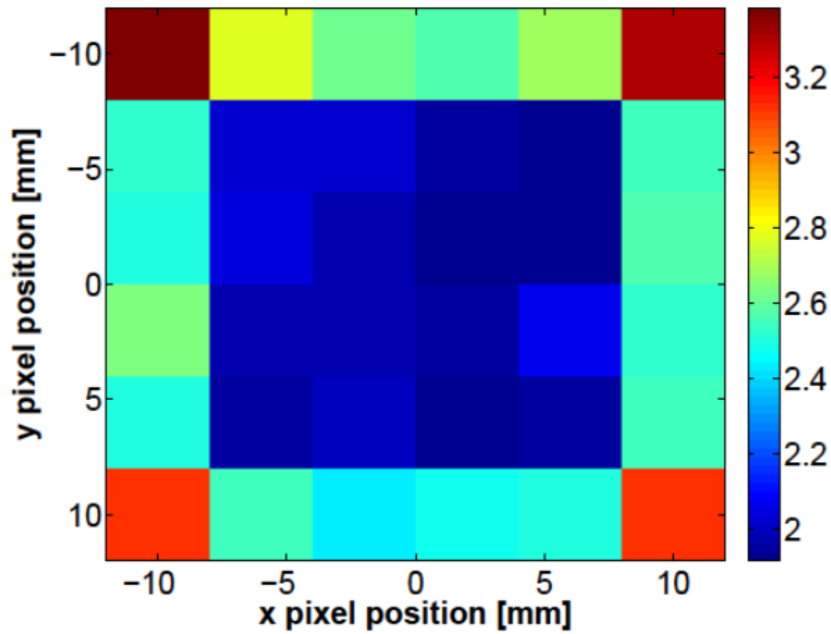

- Improved nearest neighbors method (*H.T. van Dam, IEEE Trans Nucl Sci 58, 2139-2147, 2011*), using 100 reference events per calibration position
- Measurement performed at 0 °C.

Energy resolution

- Average energy resolution: ~11.5% FWHM
- Negligible saturation

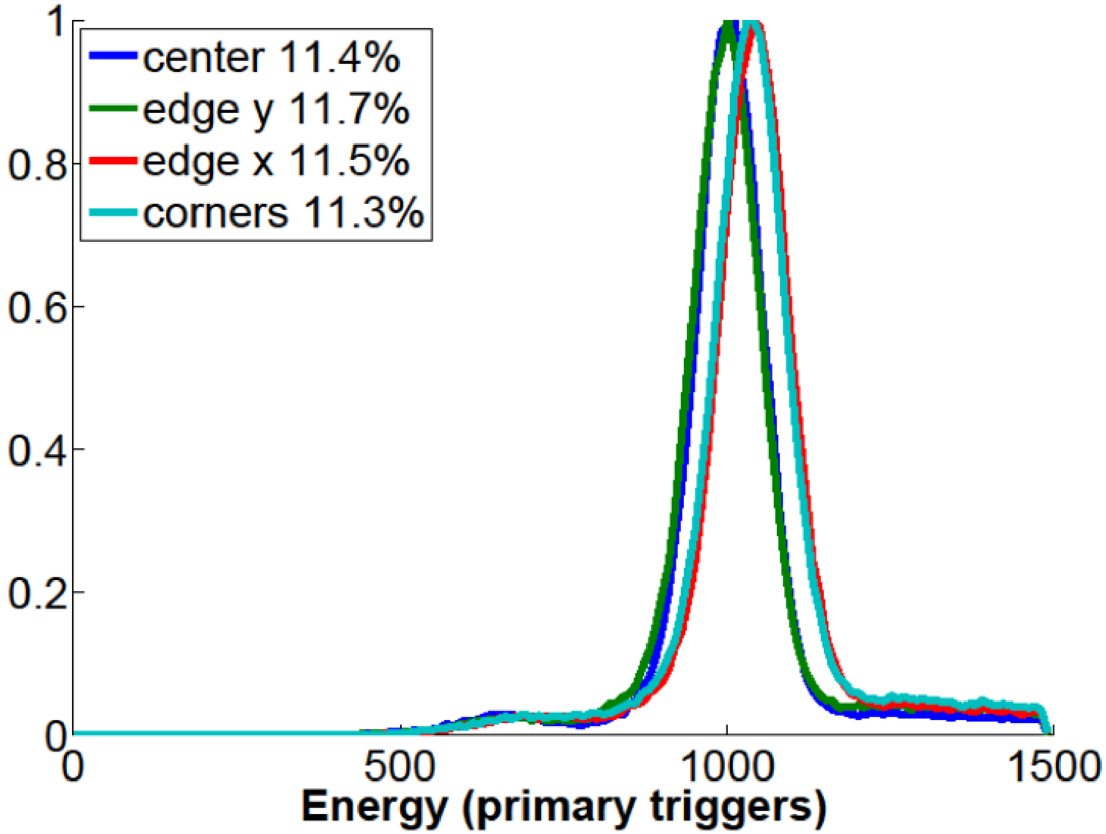

Excellent timing resolution

- Better timing using time stamps of multiple Si dies
- Coincidence resolving time for 2 detectors: < 350 ps FWHM
- Further improvement expected with version 2.0 tiles, having better photon detection efficiency and neighbor logic between dies.

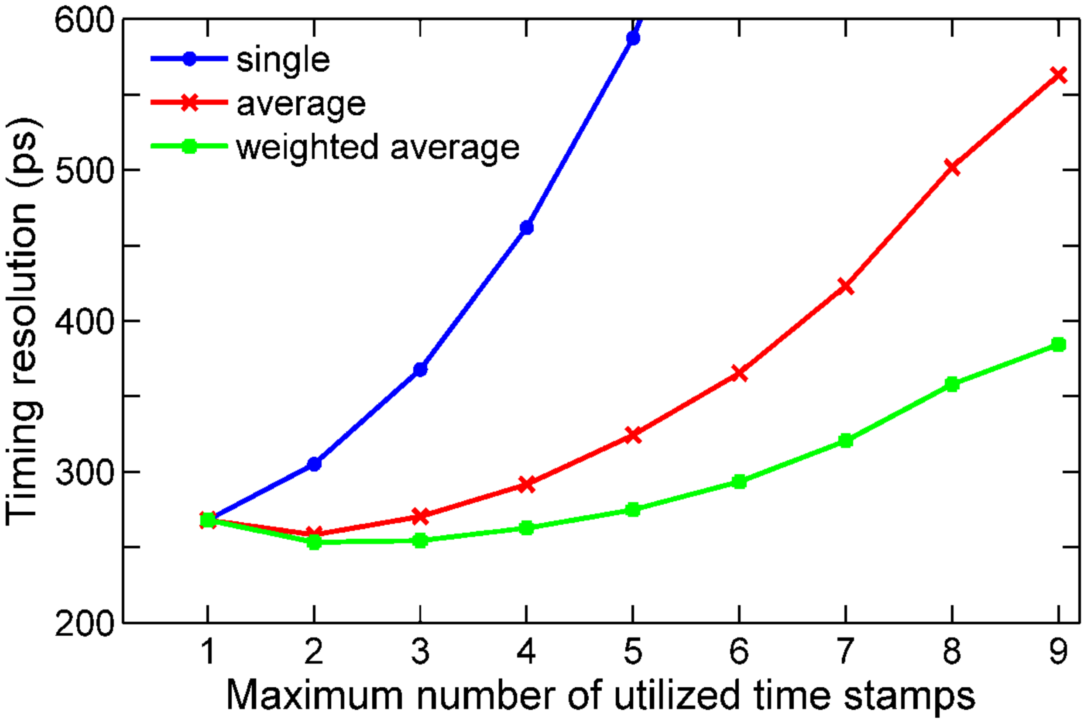

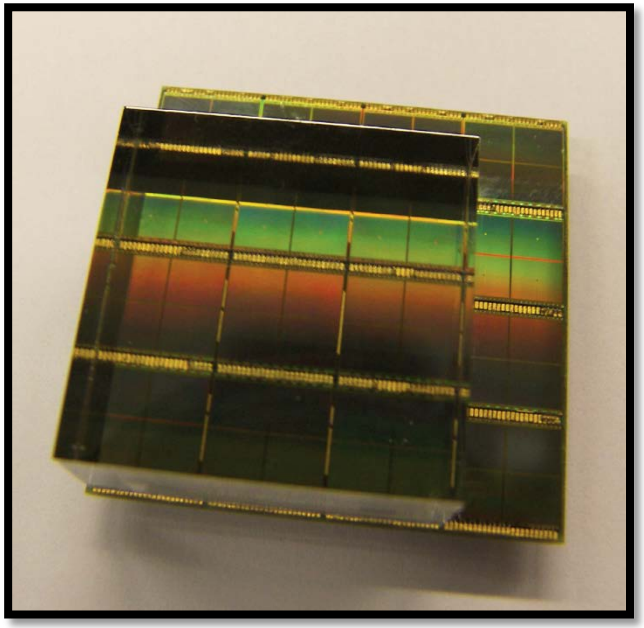

Sub-mm resolution, TOF & DOI

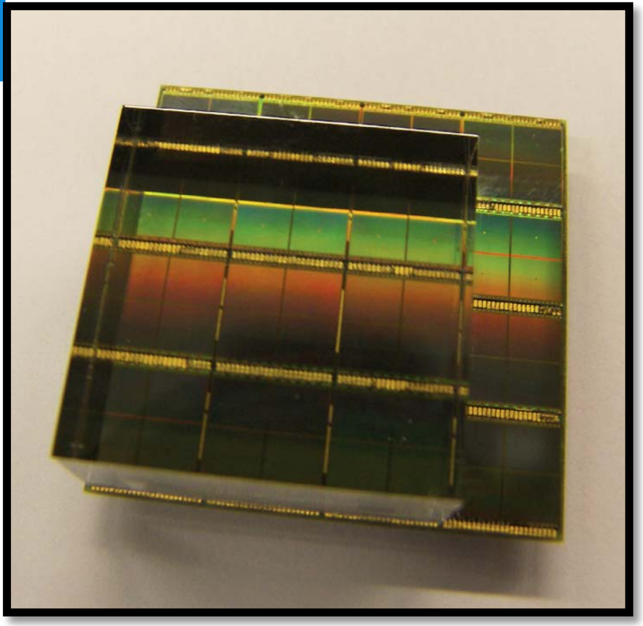

Summary of results with 24 x 24 x 10 mm^3 LSO:Ce,Ca:

- Coincidence resolving time < 350 ps FWHM
- 0.98 mm FWHM average spatial resolution
- 11.5% average energy resolution
- Intrinsic depth-of-interaction information
- Further improvement expected with version 2.0 dSiPM arrays

$\Rightarrow$ A cost-effective, high-performance detector concept for clinical PET/CT and PET/MRI?

And now for something (not) completely different...

Proton therapy initiatives in NL

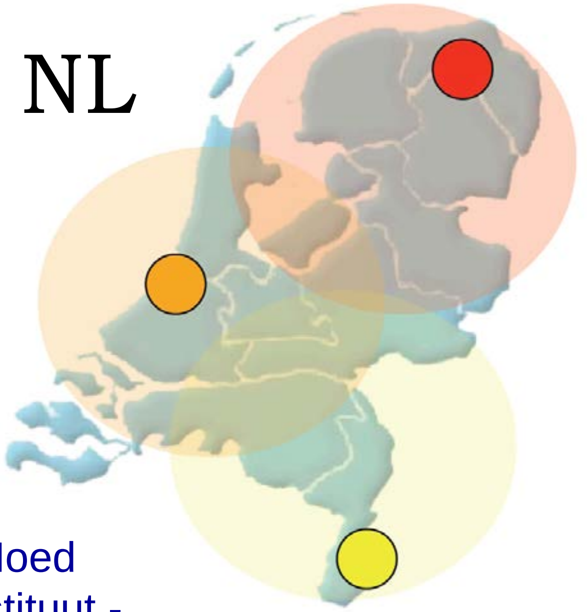

- Holland Particle Therapy Centre
  - Erasmus Universitair Medisch Centrum - Daniël den Hoed Kankercentrum (ErasmusMC), Nederlands Kanker Instituut - Antoni van Leeuwenhoek Ziekenhuis (NKI-AVL), Leids Universitair Medisch Centrum (LUMC), Technische Universiteit Delft (TU Delft)
- UMCG Protonen Therapie Centrum Noord-Nederland
  - Universitair Medisch Centrum Groningen (UMCG), Kernfysisch Versneller Instituut (KVI)
- Particle Therapy Center Euregion Meuse Rhine
  - Maastricht Radiation Oncology (MAASTRO Clinic), Maastricht Universitair Medisch Centrum (MUMC+), Universitätsklinikum Aachen (UKA), Rheinisch-Westfälische Technische Hochschule Aachen (RWTH), and others

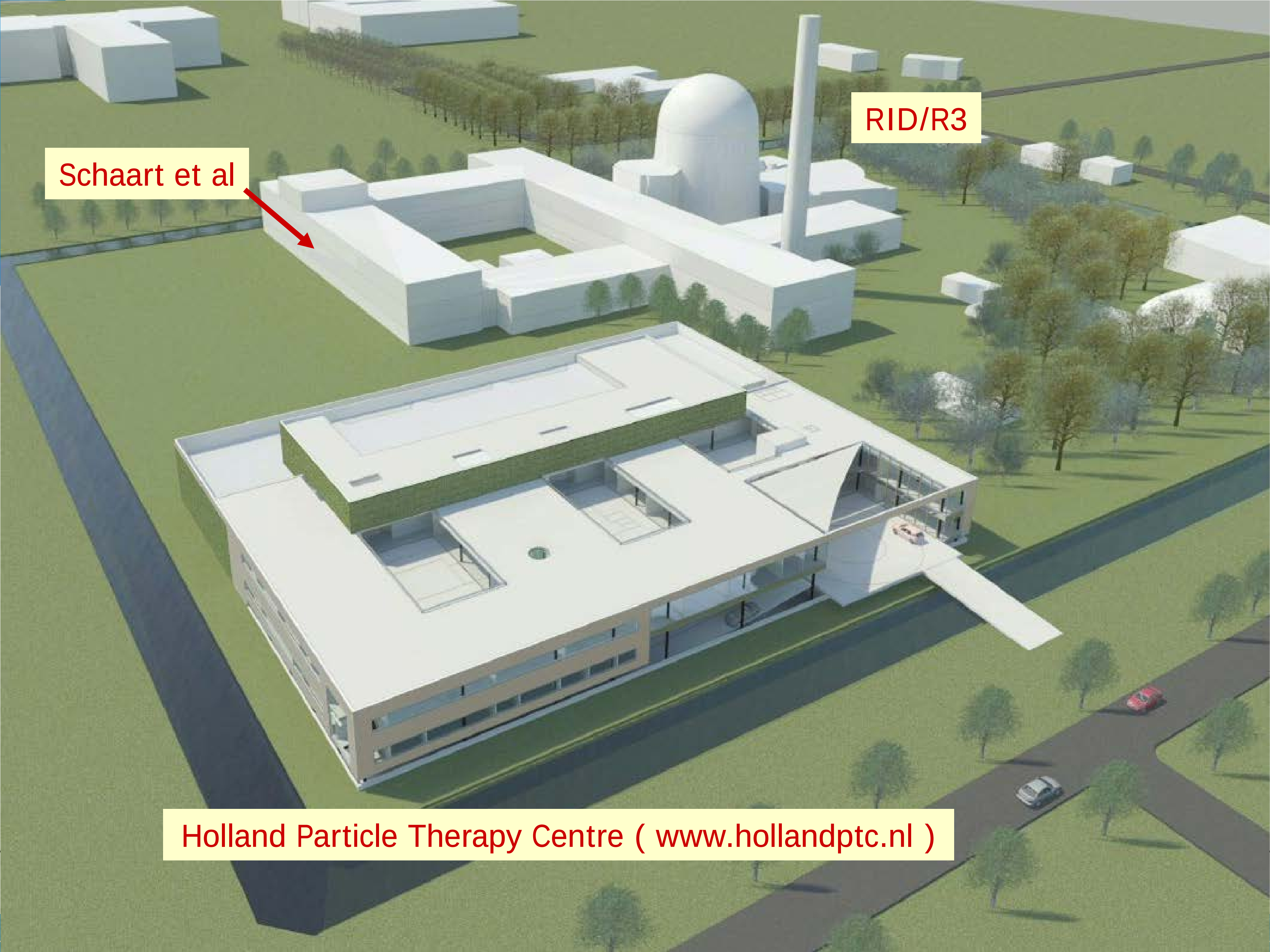
RID/R3
Schaart et al
Holland Particle Therapy Centre (www.hollandptc.nl)

Particle therapy: the promise...

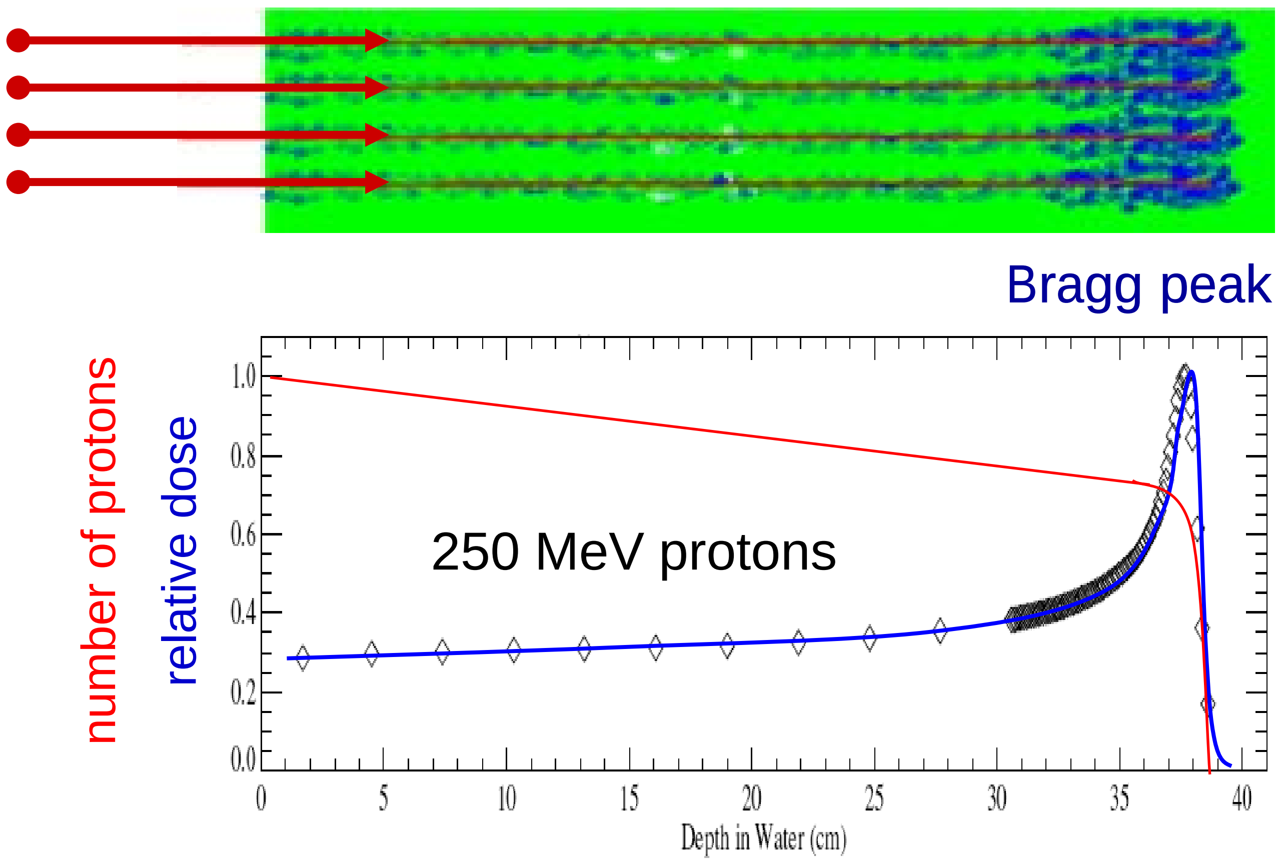

… and the problem

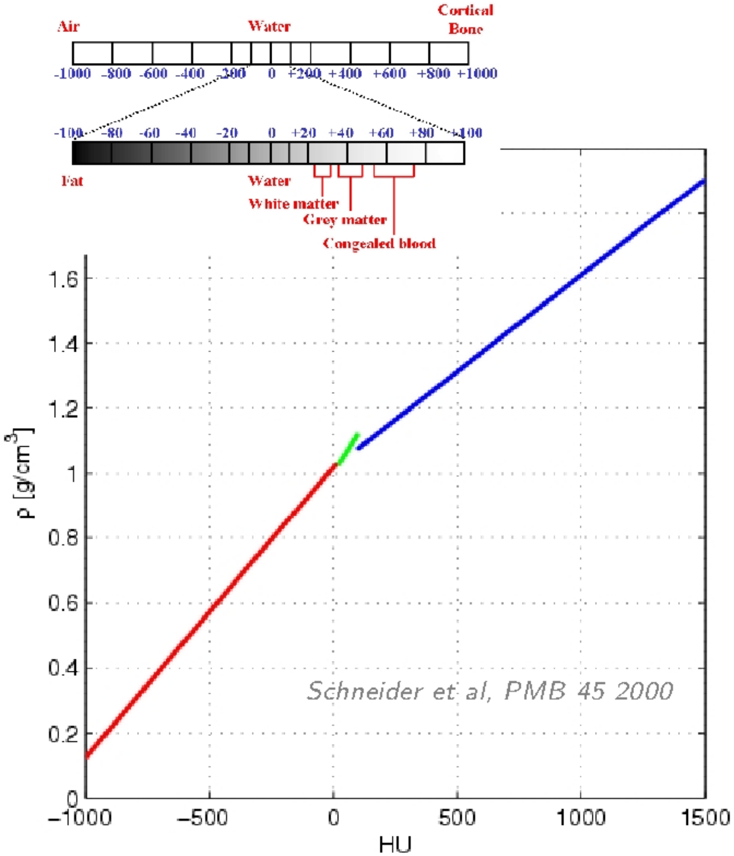

$$\rho = \begin{cases} (1.018 + 0.893 \cdot 10^{-3} HU) & HU \leq 14 \\ (1.003 + 1.169 \cdot 10^{-3} HU) & 23 \leq HU \leq 100 \\ (1.017 + 0.592 \cdot 10^{-3} HU) & HU > 100 \end{cases}$$

Water Equivalent Path Length

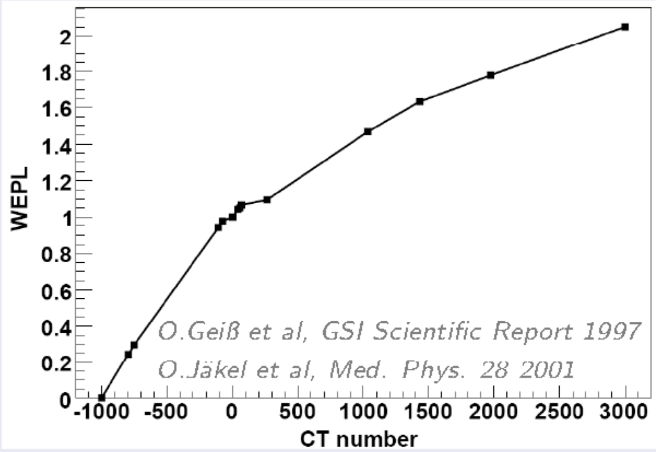

$$if \; I' \cong I_{H_2O} \quad \Rightarrow$$

$$z_{wepl} = \int_0^z \frac{\rho(z')}{\rho_{H_2O}} \, dz'$$

Effect of density variation

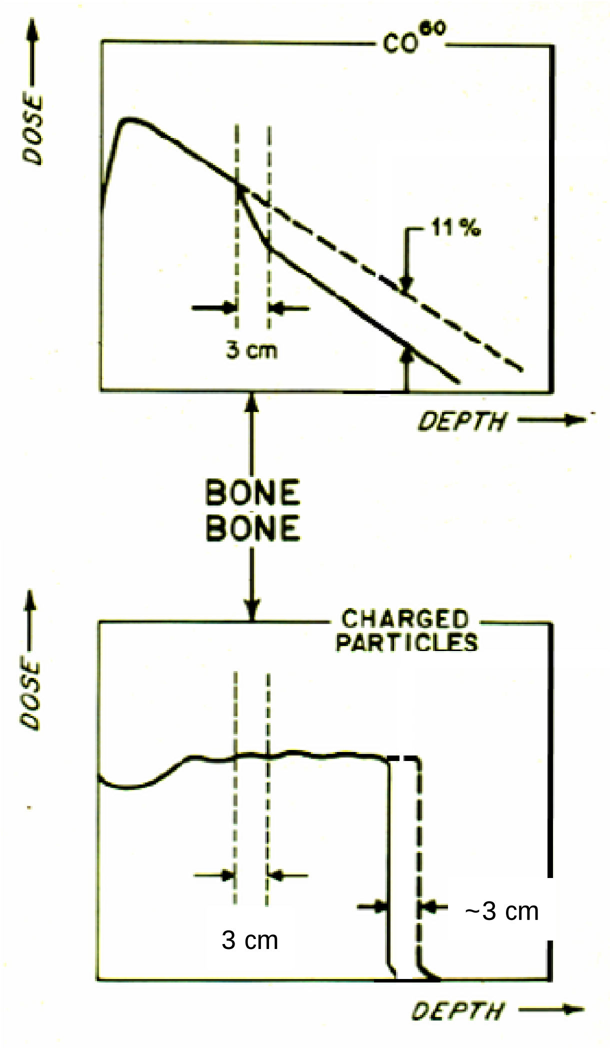

X-rays:

Dose drops

11%

protons:

Range

~3 cm less

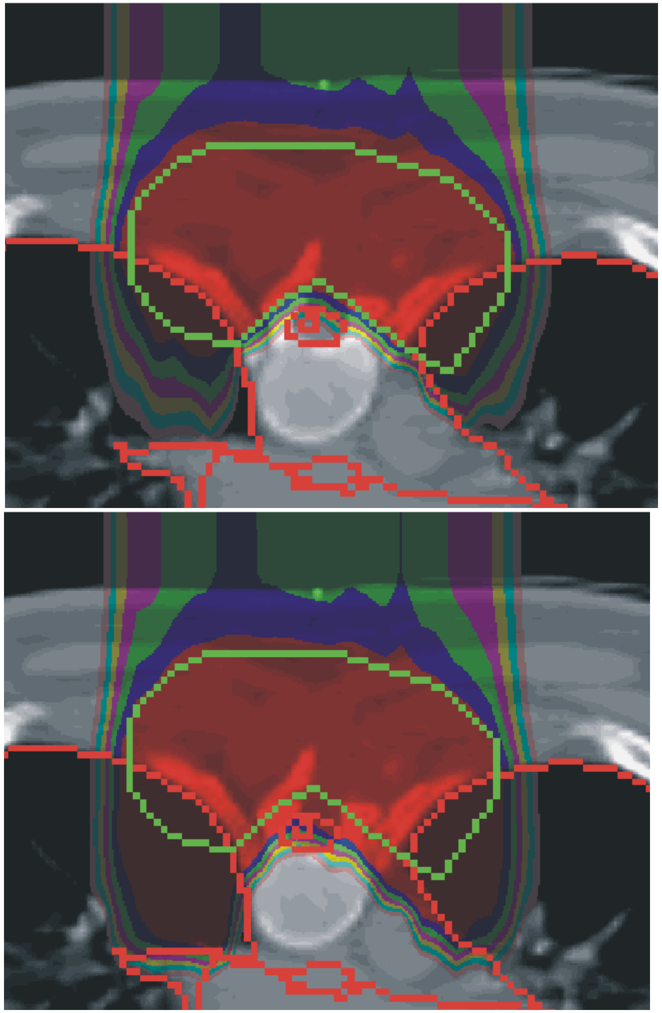

Tissue activation by protons

Radionuclide production by protons in tissue

Activation process	E_{th} (MeV)	τ_d (min^{-1})	E_{max} (MeV)
$p + {}^{16}O \rightarrow {}^{15}O + (p, n)$	16.6	0.341	1.73
$p + {}^{16}O \rightarrow {}^{13}N + \alpha, 2(p, n)$	5.5	0.07	1.19
$p + {}^{16}O \rightarrow {}^{11}C + 3(p, n)$	14.3	0.034	0.96
$p + {}^{14}N \rightarrow {}^{13}N + (p, n)$	11.2	0.07	1.19
$p + {}^{14}N \rightarrow {}^{11}C + \alpha, 2(p, n)$	3.1	0.034	0.96
$p + {}^{12}C \rightarrow {}^{11}C + (p, n)$	20.1	0.034	0.96

In-beam PET

Verification of dose delivery accuracy through imaging of positron emitters created by therapeutic charged particles in tissue

Proof-of-concept
K. Parodi, P. Crespo, et al
GSI Darmstadt / FZ Dresden-Rossendorf

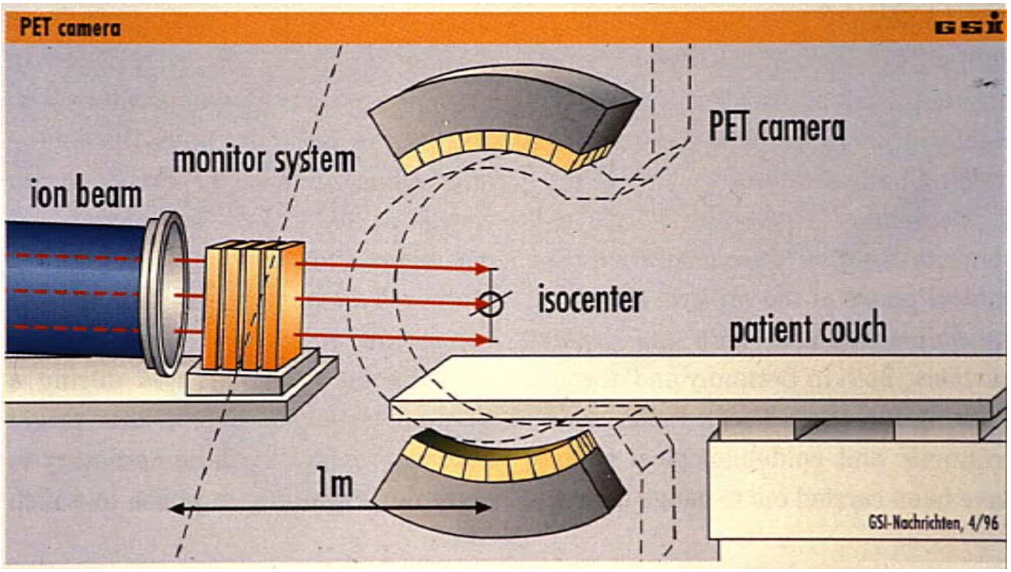

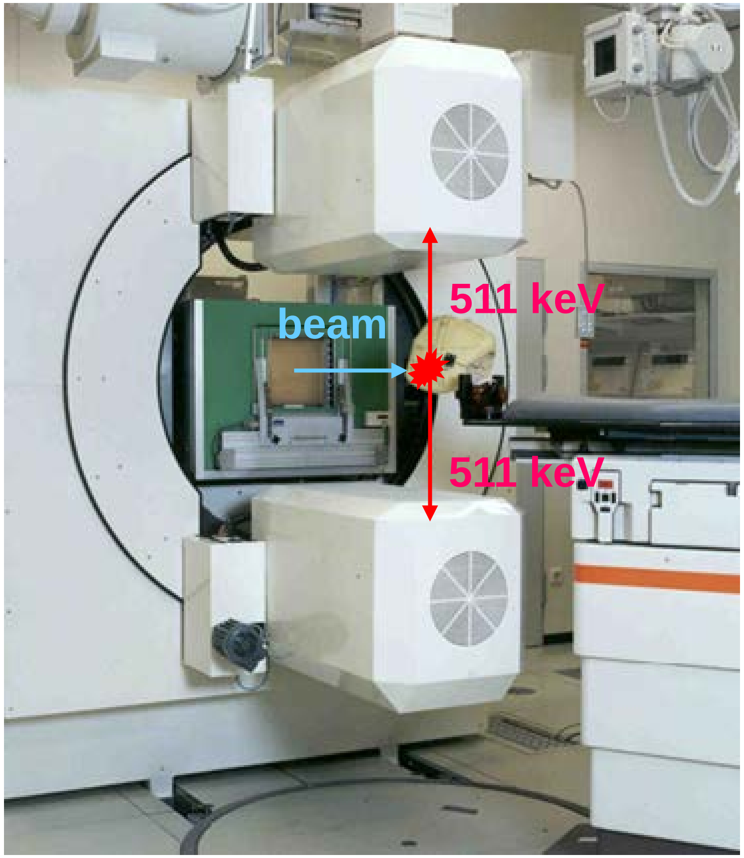

Proof of principle

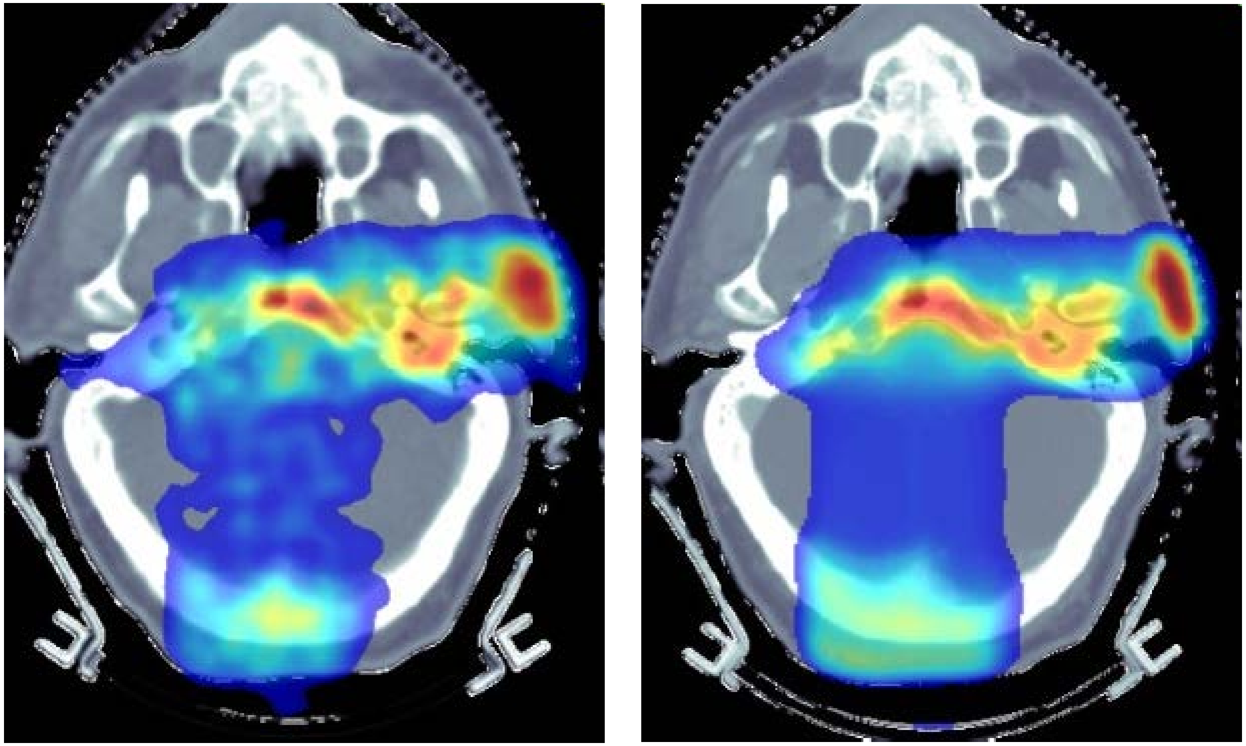

Measured and predicted activity distribution after proton irradiation of a clivus chordoma patient at Massachusetts General Hospital, Boston.

In-beam TOF-PET: early work at GSI

Problem: low angular coverage => insufficient counts & image artefacts

Solution: better system design & TOF

Proof-of-concept
K. Parodi, P. Crespo, et al
GSI Darmstadt / FZ Dresden-Rossendorf

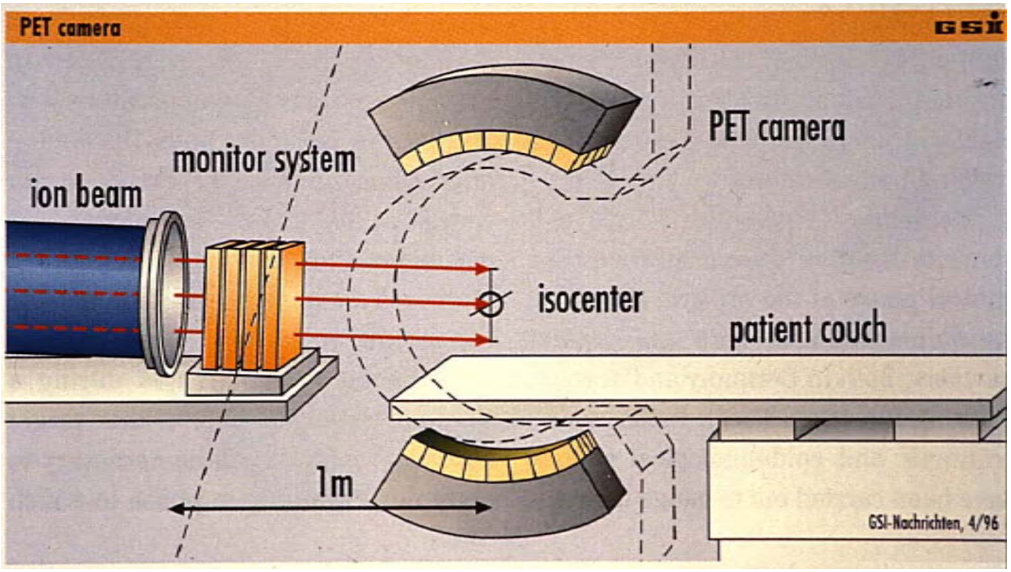

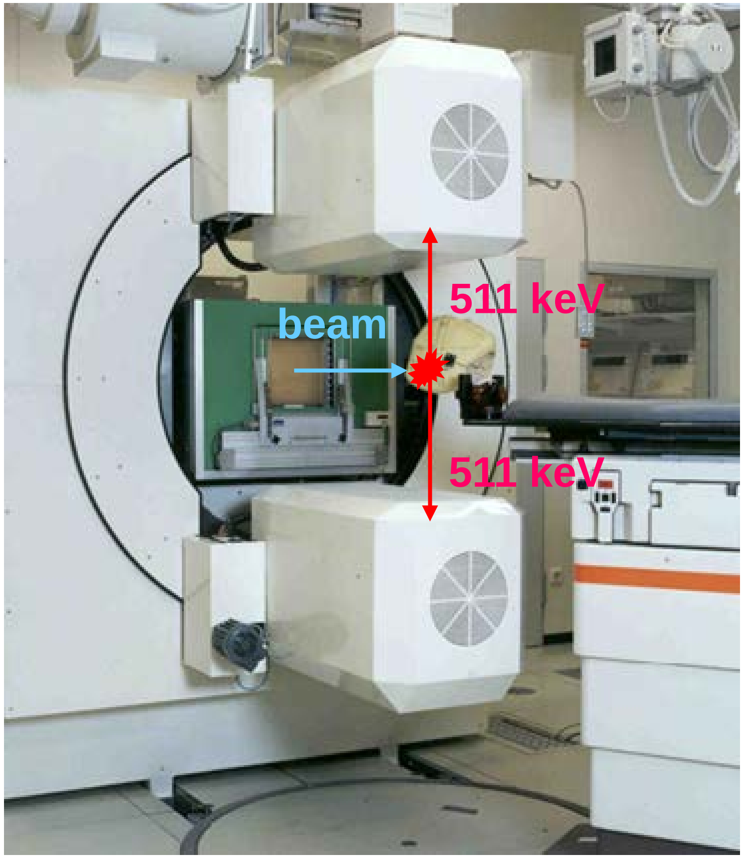

In-beam TOF-PET

⇒ How to implement PET in a particle gantry?

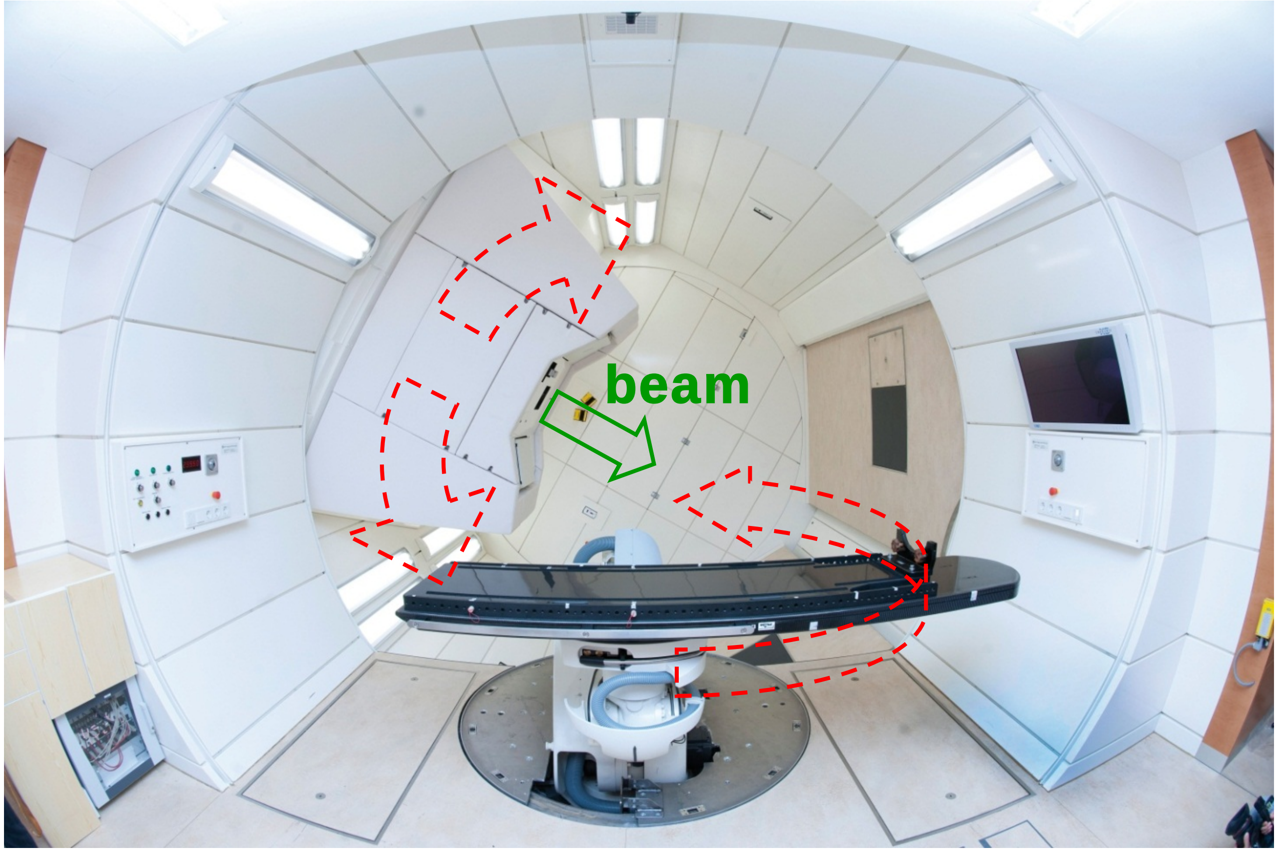

Gantry of Heidelberger Ionenstrahl-Therapiezentrum (HIT)

In-beam TOF-PET

⇒ How to implement in gantry?

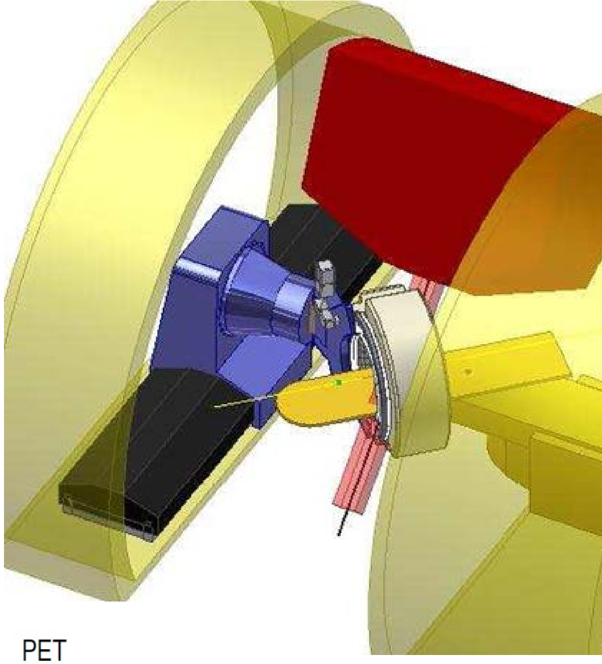

Sliding PET geometry,
Paulo Crespo

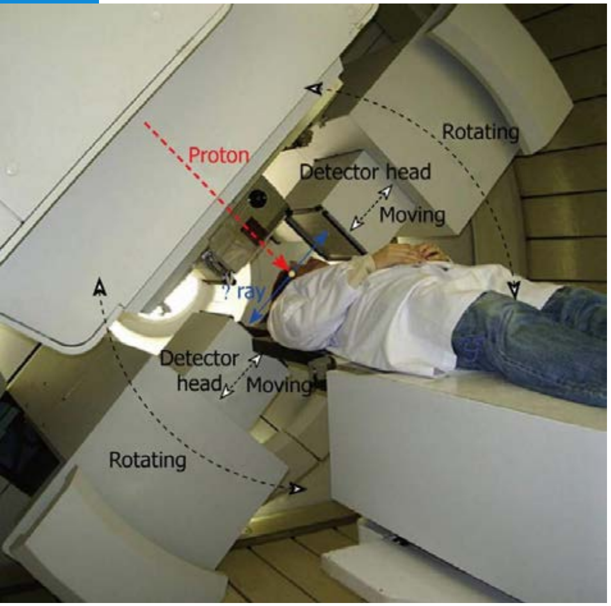

Gantry-mounted PET geometry,
National Cancer Center,
Kashiwa, Japan

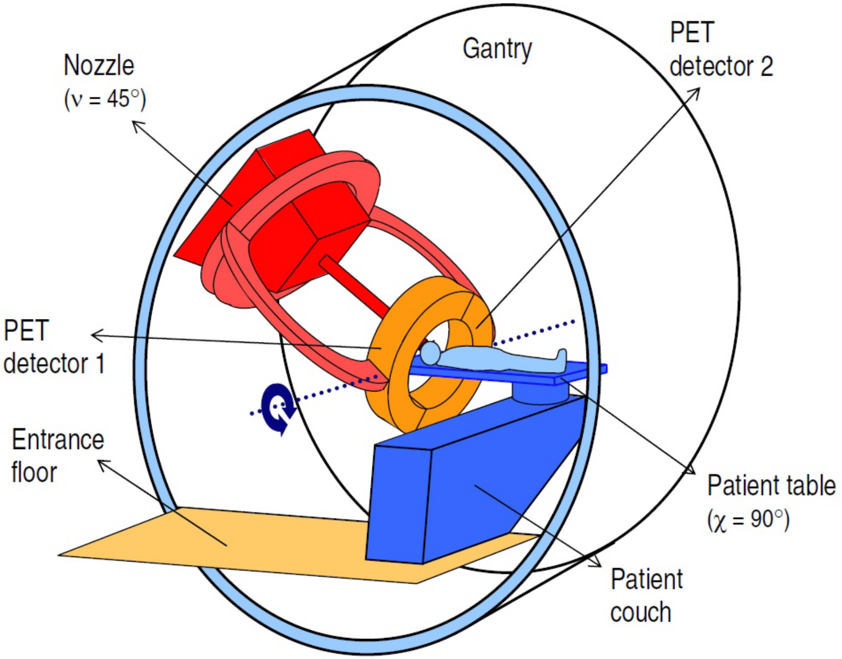

Nozzle-mounted
PET geometry,
Paulo Crespo

In-beam TOF-PET

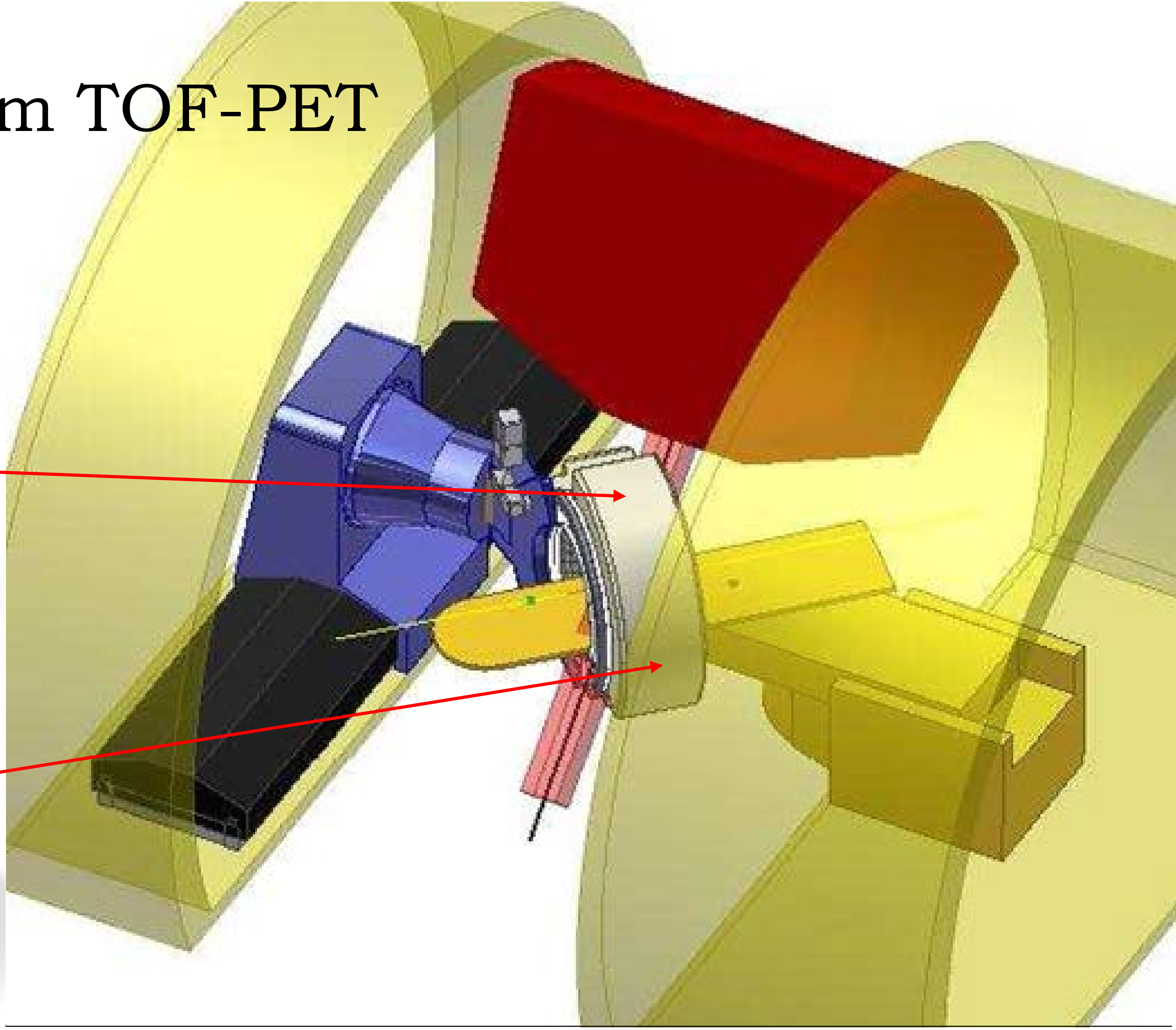

Images: Paulo Crespo et al; Philips

TOF detection of prompt gamma's

GEANT4 Monte Carlo simulation geometry

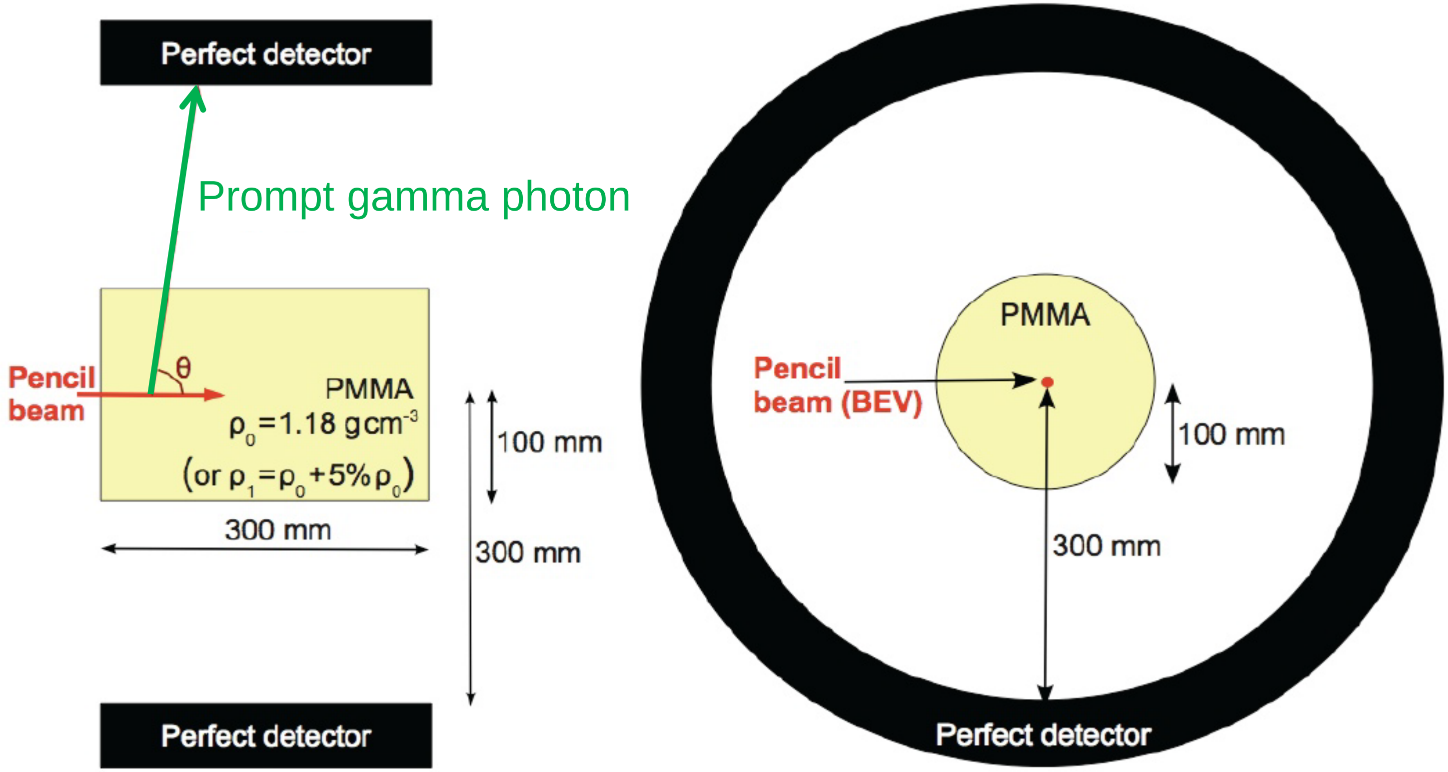

- Prompt-gamma's created by proton interactions escape from phantom
- Escaped gamma photons measured perpendicularly to the beam

TOF neutron rejection

GEANT4 Monte Carlo simulation

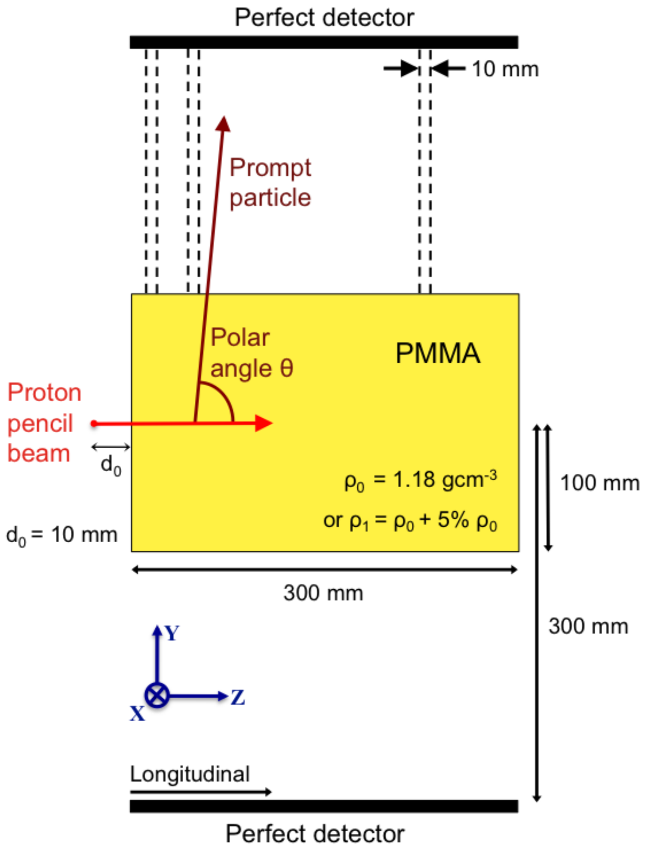

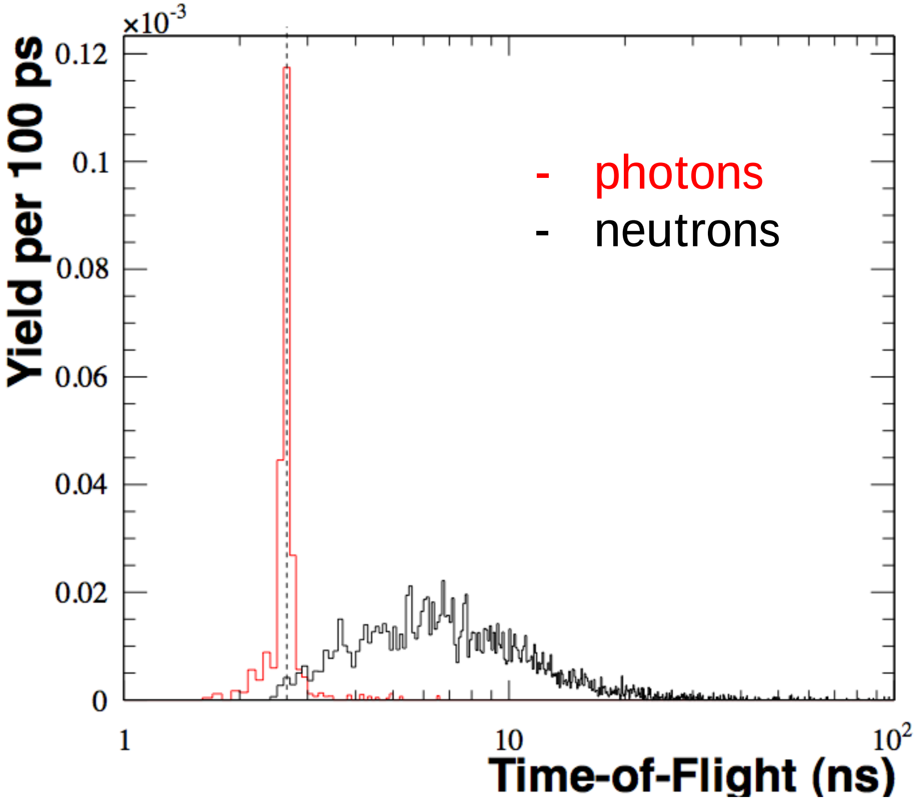

TOF neutron rejection

TOF shift for different energies

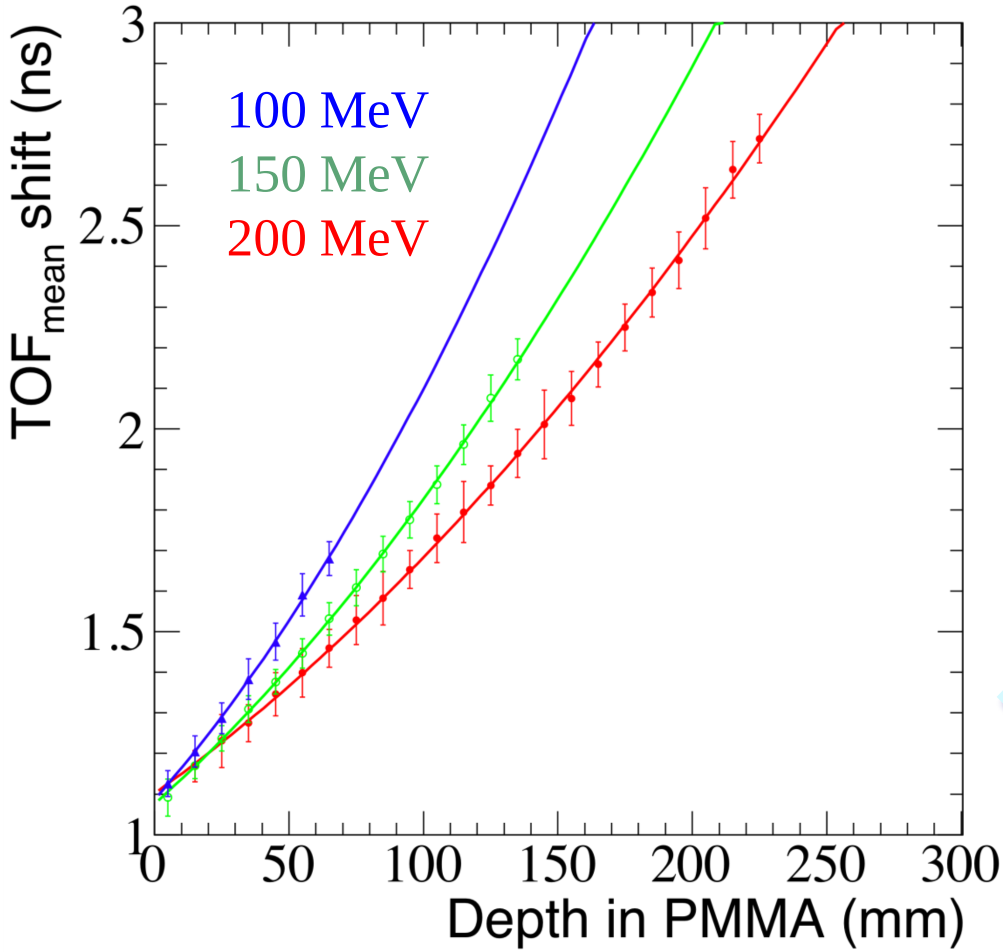

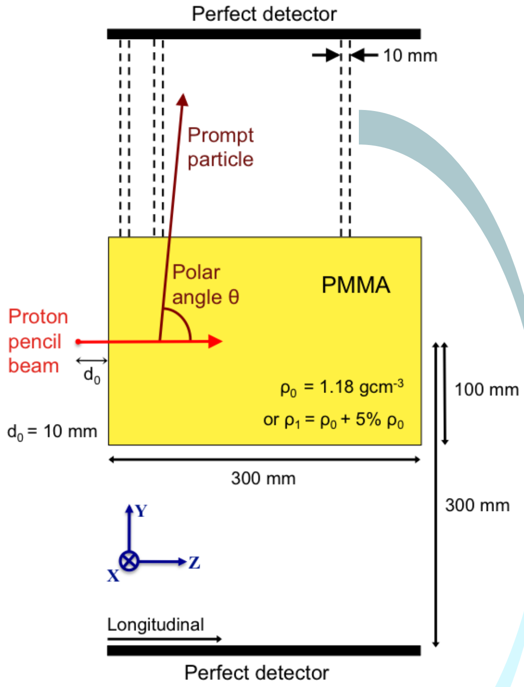

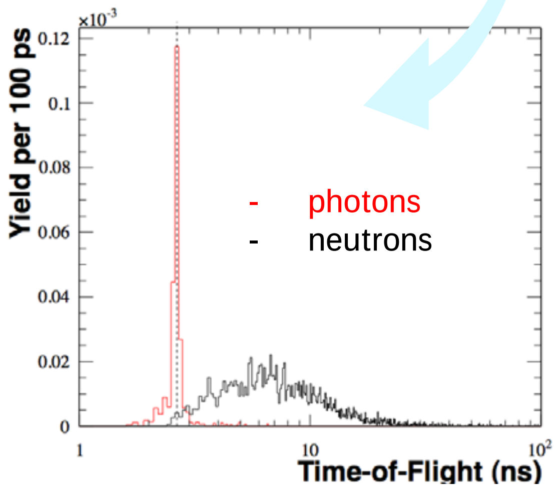

TOF neutron rejection

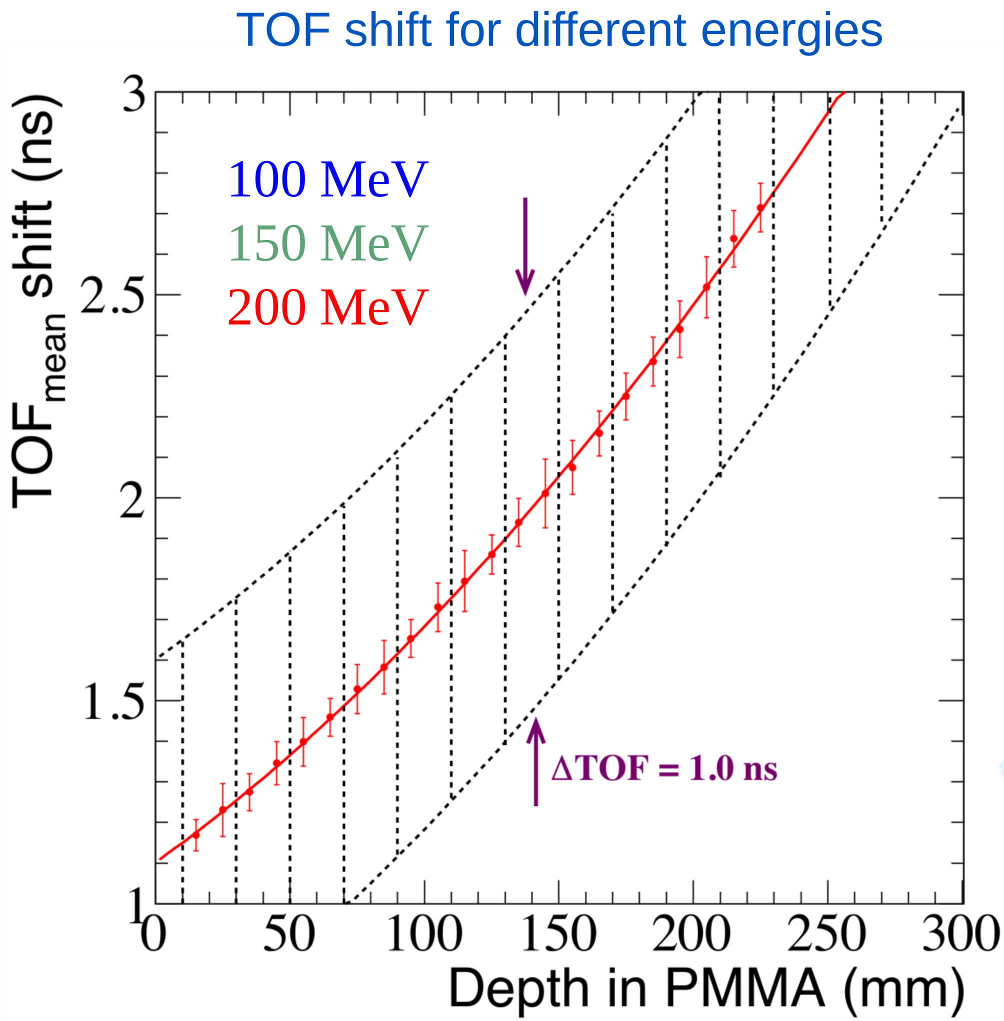

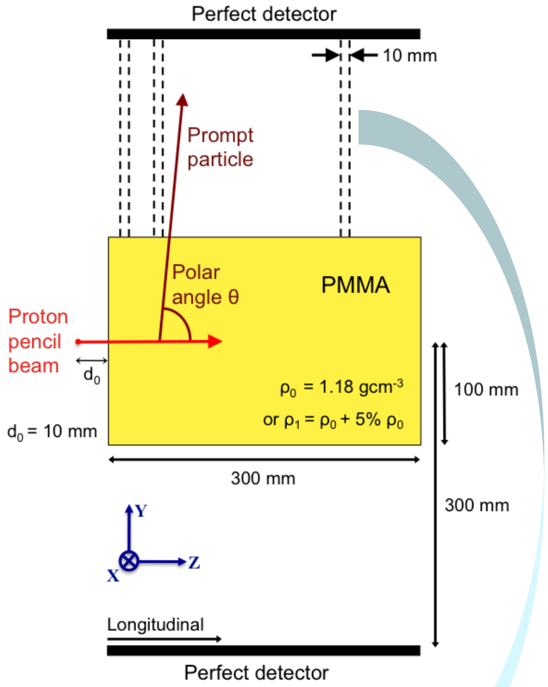

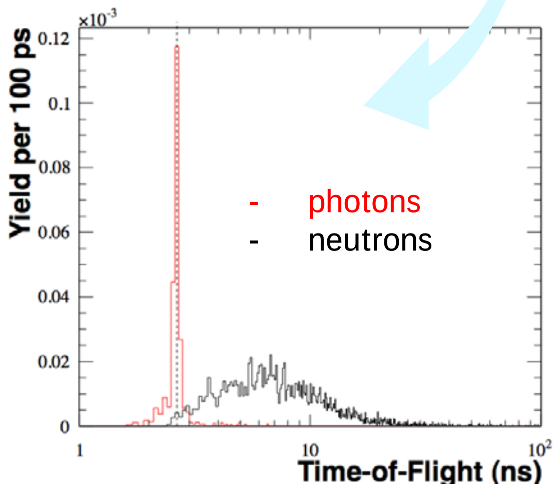

TOF neutron rejection

GEANT4 Monte Carlo simulation

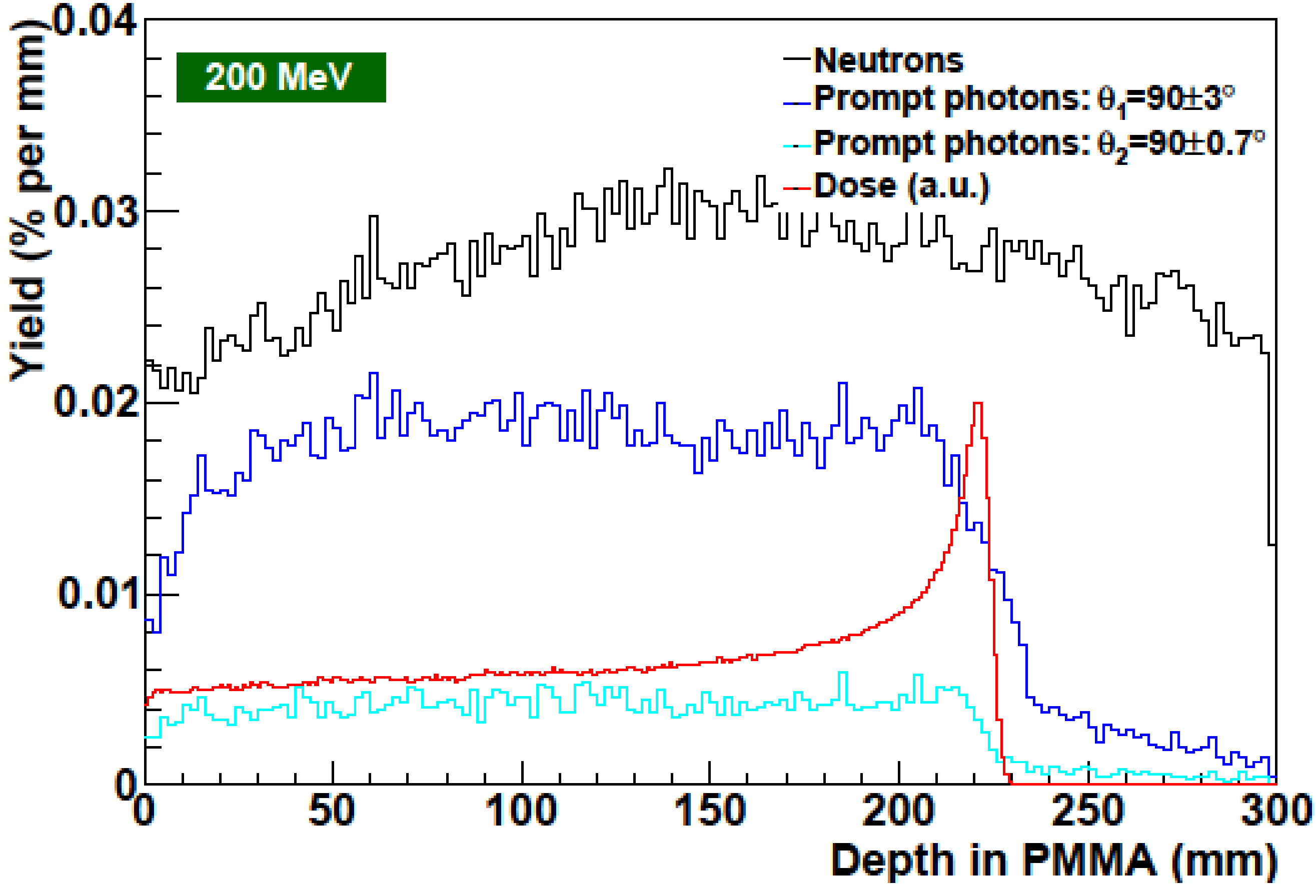

BEFORE

TOF neutron rejection

GEANT4 Monte Carlo simulation

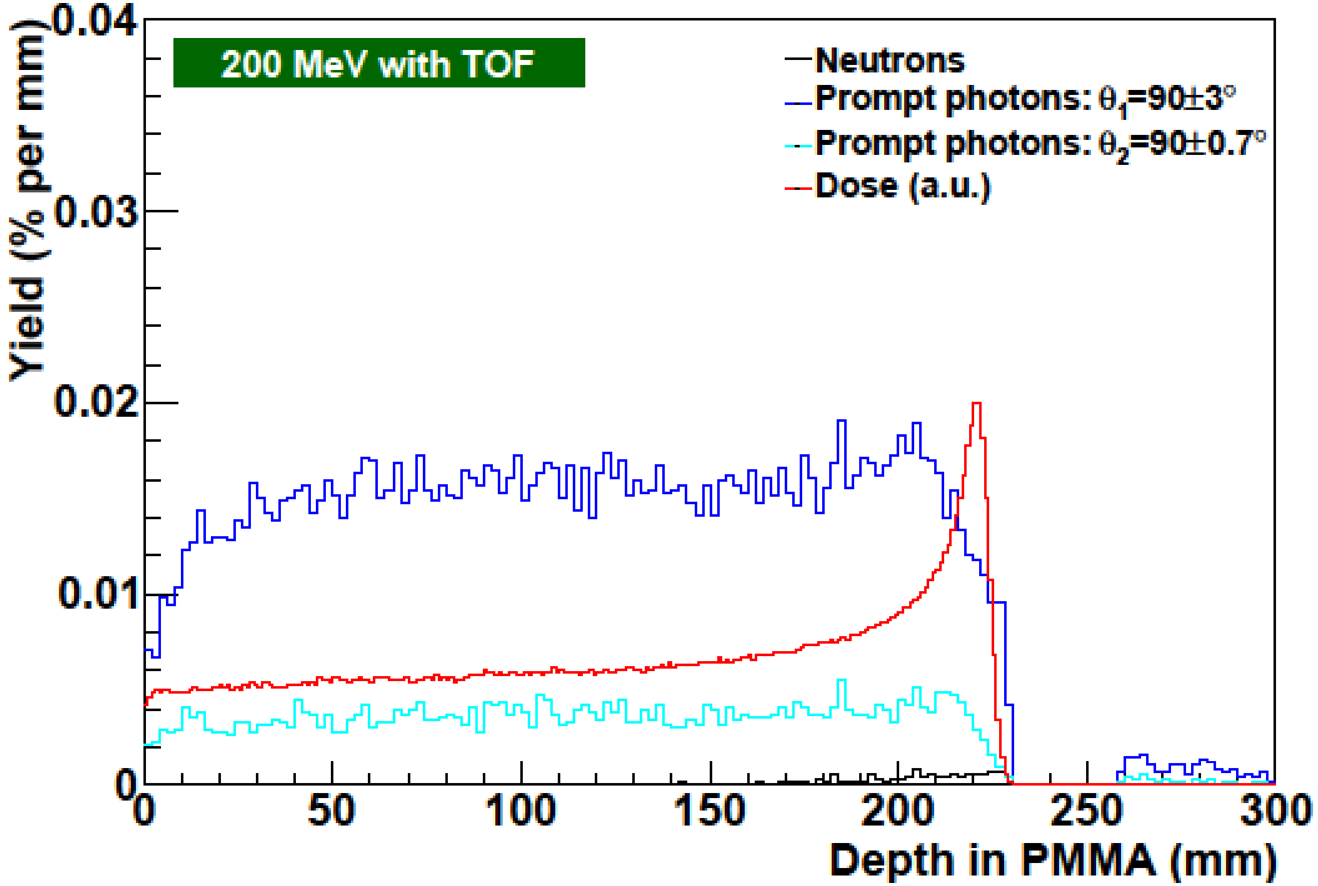

AFTER

TOF-PET detectors for PG imaging

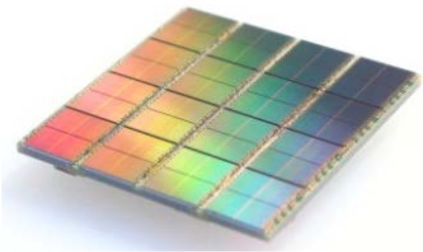

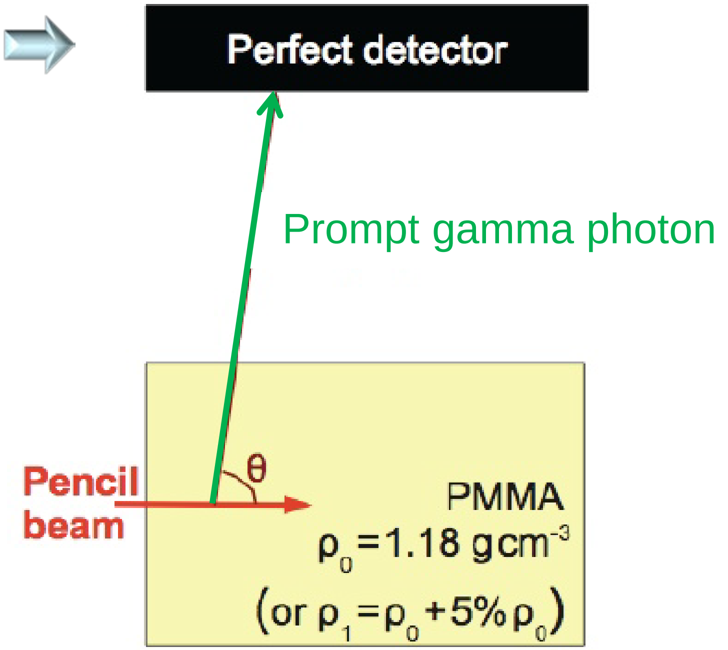

- High spatial resolution
- High count rate capability
- Time-of-flight ready
- Magnetic-field compatible
- Compact
- Scalable

Goals

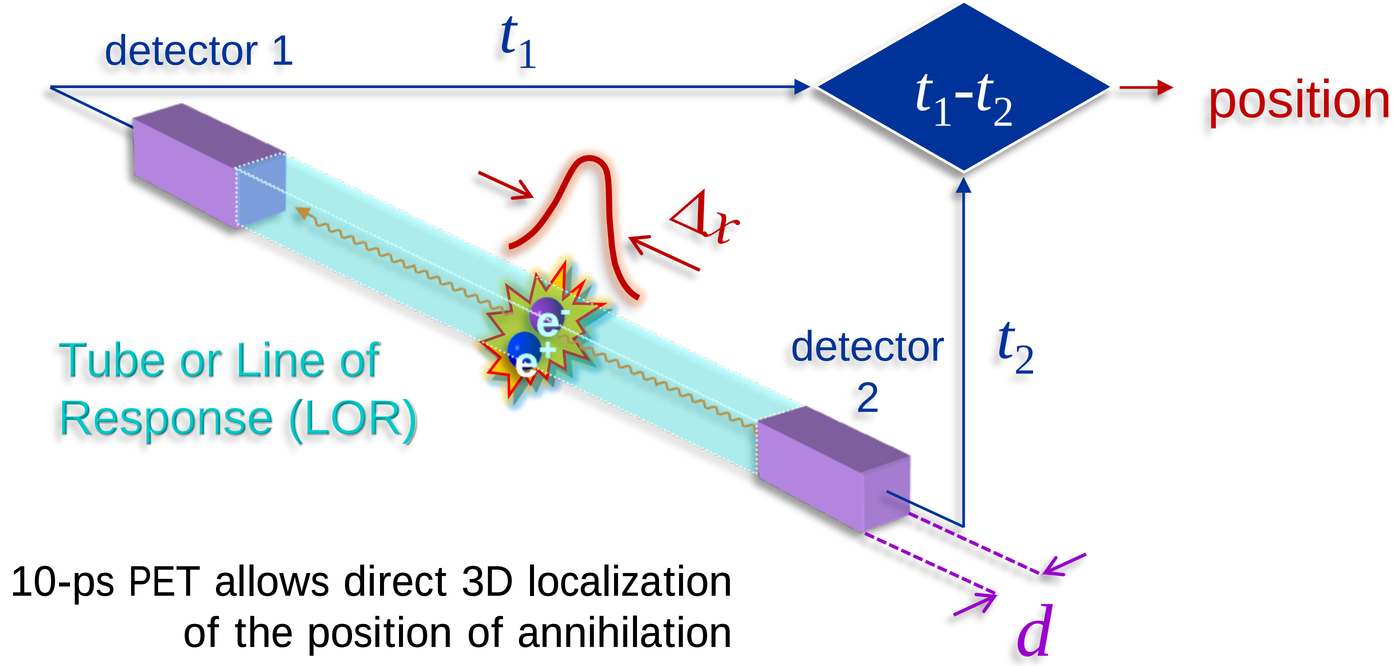

- Bring high-performance SiPM-based detectors from the lab to clinical TOF-PET and PET/MRI systems
- Apply TOF technology in hadron therapy applications
- Keep on pushing the limits in time-of-flight resolution, ultimately towards “10-picosecond PET”

Acknowledgements

PhD Students
- Stefan Seifert
- Herman van Dam
- Patricia Lopes
- Giacomo Borghi
- Valerio Tabacchini

Postdocs
- David Oxley
- Alekesandra Biegun

MSc and BSc Students
- Gerben vd Lei
- Thom de Rijk
- Joop Meijlink
- Astrid Garretsen

Engineers
- Jan Huizenga
- William van Goozen
- Jeroen Koning
- Martijn de Boer
- Folkert Geurink
- Johan de Haas

Secretaries
- Jose Buurman
- Thea Miedema

This work is supported by:
- EU FP7 grant no. 241711
- Eureka grant no. IS055019
- COST action TD1007
- NIG-FOM project 09NIG18
- FCT doctoral grant P Lopes

Backup slides

Detector signal processing algorithms

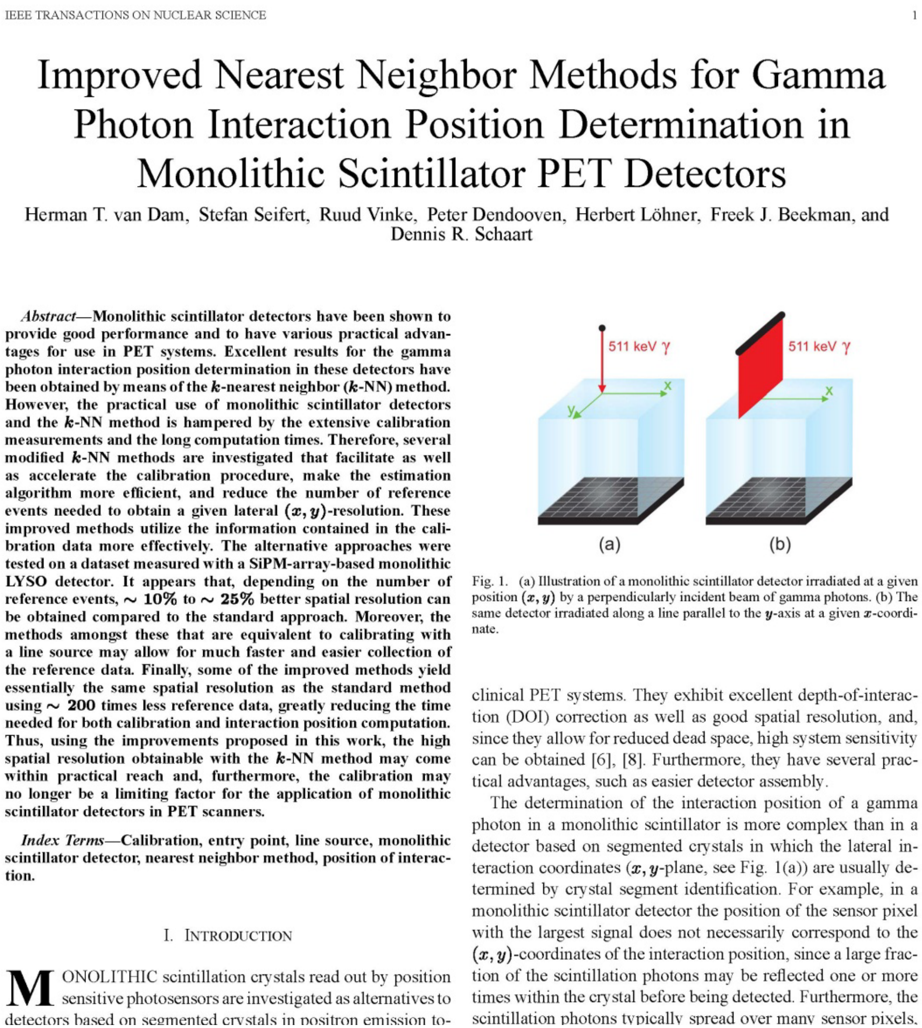

Improved Nearest Neighbor Methods for Gamma Photon Interaction Position Determination in Monolithic Scintillator PET Detectors

Herman T. van Dam, Stefan Seifert, Ruud Vinke, Peter Dendooven, Herbert Löhner, Freek J. Beekman, and Dennis R. Schaart

***Abstract*—Monolithic scintillator detectors have been shown to provide good performance and to have various practical advantages for use in PET systems. Excellent results for the gamma photon interaction position determination in these detectors have been obtained by means of the k-nearest neighbor (k-NN) method. However, the practical use of monolithic scintillator detectors and the k-NN method is hampered by the extensive calibration measurements and the long computation times. Therefore, several modified k-NN methods are investigated that facilitate as well as accelerate the calibration procedure, make the estimation algorithm more efficient, and reduce the number of reference events needed to obtain a given lateral (x, y)-resolution. These improved methods utilize the information contained in the calibration data more effectively. The alternative approaches were tested on a dataset measured with a SiPM-array-based monolithic LYSO detector. It appears that, depending on the number of reference events, $\sim 10\%$ to $\sim 25\%$ better spatial resolution can be obtained compared to the standard approach. Moreover, the methods amongst these that are equivalent to calibrating with a line source may allow for much faster and easier collection of the reference data. Finally, some of the improved methods yield essentially the same spatial resolution as the standard method using ~ 200 times less reference data, greatly reducing the time needed for both calibration and interaction position computation. Thus, using the improvements proposed in this work, the high spatial resolution obtainable with the k-NN method may come within practical reach and, furthermore, the calibration may no longer be a limiting factor for the application of monolithic scintillator detectors in PET scanners.**

***Index Terms*—Calibration, entry point, line source, monolithic scintillator detector, nearest neighbor method, position of interaction.**

I. Introduction

MONOLITHIC scintillation crystals read out by position sensitive photosensors are investigated as alternatives to detectors based on segmented crystals in positron emission to-

511 keV γ

511 keV γ

(a) (b)

Fig. 1. (a) Illustration of a monolithic scintillator detector irradiated at a given position (x, y) by a perpendicularly incident beam of gamma photons. (b) The same detector irradiated along a line parallel to the y-axis at a given x-coordinate.

clinical PET systems. They exhibit excellent depth-of-interaction (DOI) correction as well as good spatial resolution, and, since they allow for reduced dead space, high system sensitivity can be obtained [6], [8]. Furthermore, they have several practical advantages, such as easier detector assembly.

The determination of the interaction position of a gamma photon in a monolithic scintillator is more complex than in a detector based on segmented crystals in which the lateral interaction coordinates (x, y-plane, see Fig. 1(a)) are usually determined by crystal segment identification. For example, in a monolithic scintillator detector the position of the sensor pixel with the largest signal does not necessarily correspond to the (x, y)-coordinates of the interaction position, since a large fraction of the scintillation photons may be reflected one or more times within the crystal before being detected. Furthermore, the scintillation photons typically spread over many sensor pixels,

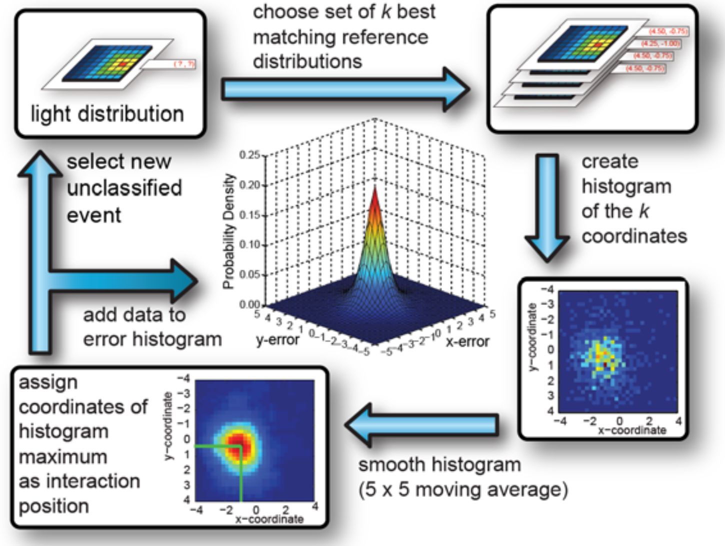

Same spatial resolution as standard method using ~200 times less reference data, speeding up calibration and interaction position computation by a similar factor

Can make use of line source calibration, allowing for much faster and easier calibration

Detector signal processing algorithms

IOP PUBLISHING PHYSICS IN MEDICINE AND BIOLOGY

Phys. Med. Biol. **56** (2011) 4135–4145 doi:10.1088/0031-9155/56/13/025

A practical method for depth of interaction determination in monolithic scintillator PET detectors

Herman T van Dam[1], Stefan Seifert[1], Ruud Vinke[2], Peter Dendooven[2], Herbert Löhner[2], Freek J Beekman[1] and Dennis R Schaart[1]

[1] Delft University of Technology, Radiation Detection and Medical Imaging, Mekelweg 15, 2629 JB Delft, The Netherlands

[2] Kernfysisch Versneller Instituut, University of Groningen, Zernikelaan 25, 9747 AA Groningen, The Netherlands

E-mail: h.t.vandam@tudelft.nl

Received 9 February 2011, in final form 24 May 2011
Published 21 June 2011
Online at stacks.iop.org/PMB/56/4135

Abstract

Several new methods for determining the depth of interaction (DOI) of annihilation photons in monolithic scintillator detectors with single-sided, multi-pixel readout are investigated. The aim is to develop a DOI decoding method that allows for practical implementation in a positron emission tomography system. Specifically, calibration data, obtained with perpendicularly incident gamma photons only, are being used. Furthermore, neither detector modifications nor *a priori* knowledge of the light transport and/or signal variances is required. For this purpose, a clustering approach is utilized in combination with different parameters correlated with the DOI, such as the degree of similarity to a set of reference light distributions, the measured intensity on the sensor pixel(s) closest to the interaction position and the peak intensity of the measured light distribution. The proposed methods were tested

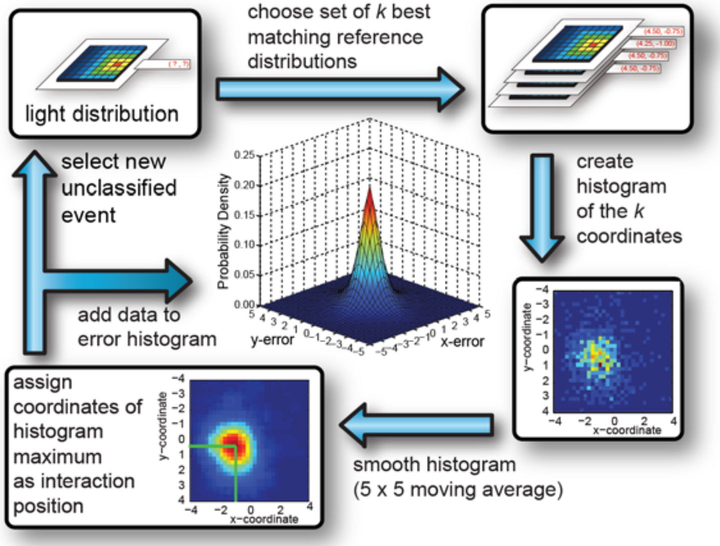

DOI resolutions of ~1 mm to ~4 mm feasible using perpendicular calibration data only.

No detector modifications nor models of the light transport and/or signal variances are required.

PET scintillators

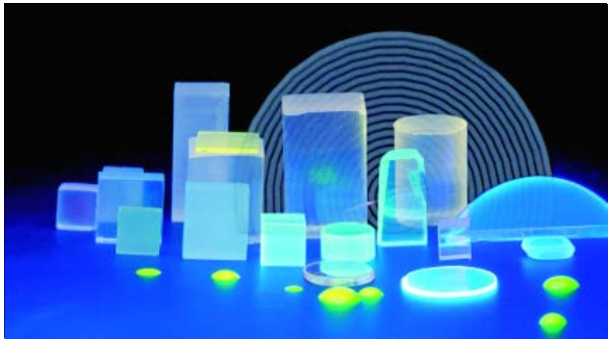

	NaI:Tl	BGO	LSO:Ce	LSO:Ce,Ca	$LaBr_3$:Ce
Density (g/cm^3)	3.67	7.13	7.4	7.4	5.1
Effective Z	51	75	66	66	47
Atten. l. 511 keV (mm)	29.1	10.4	11.4	11.4	21.3
Decay time (ns)	230	300	40-45	30-35	16
# photons /MeV	40,000	8,500	30,000	30,000	70,000
Emission max. (nm)	410	480	[illegible]	420	380
Hygroscopic	yes	no	no	no	yes

Good for TOF!

$LaBr_3:Ce^{3+}$

World-record energy resolution, extremely fast, and very bright. Discovered at TU Delft.

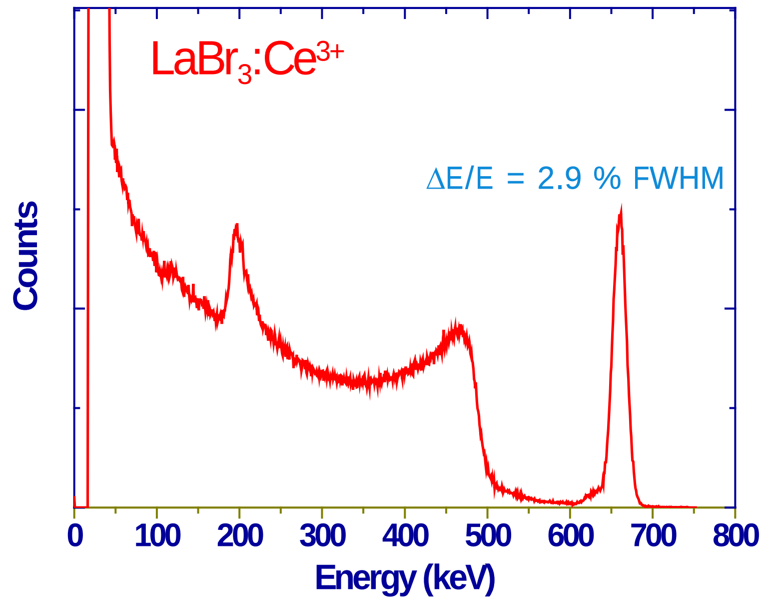

662 keV pulse-height spectrum

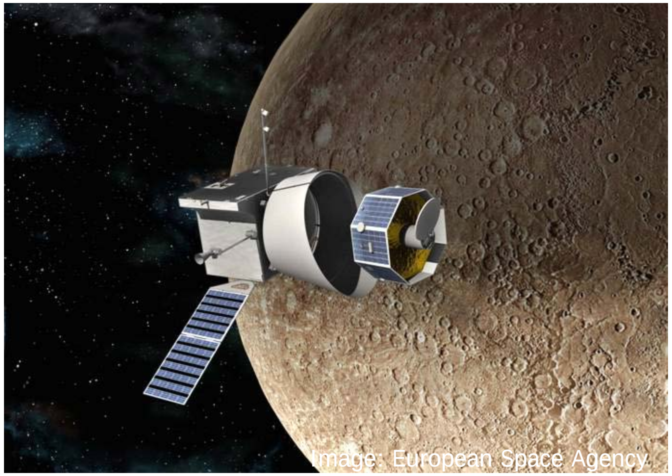

ESA 2013 BepiColombo mission

First prototype $LaBr_3:Ce$ time-of-flight PET scanner

$LaBr_3:Ce^{3+}$

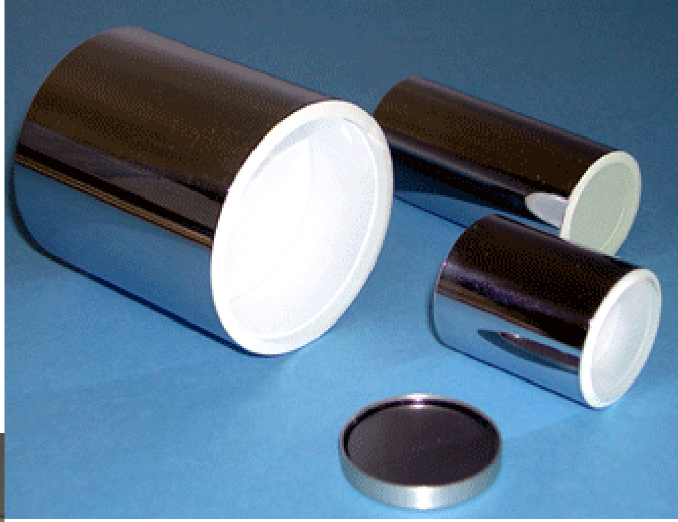

sealed detectors with windows

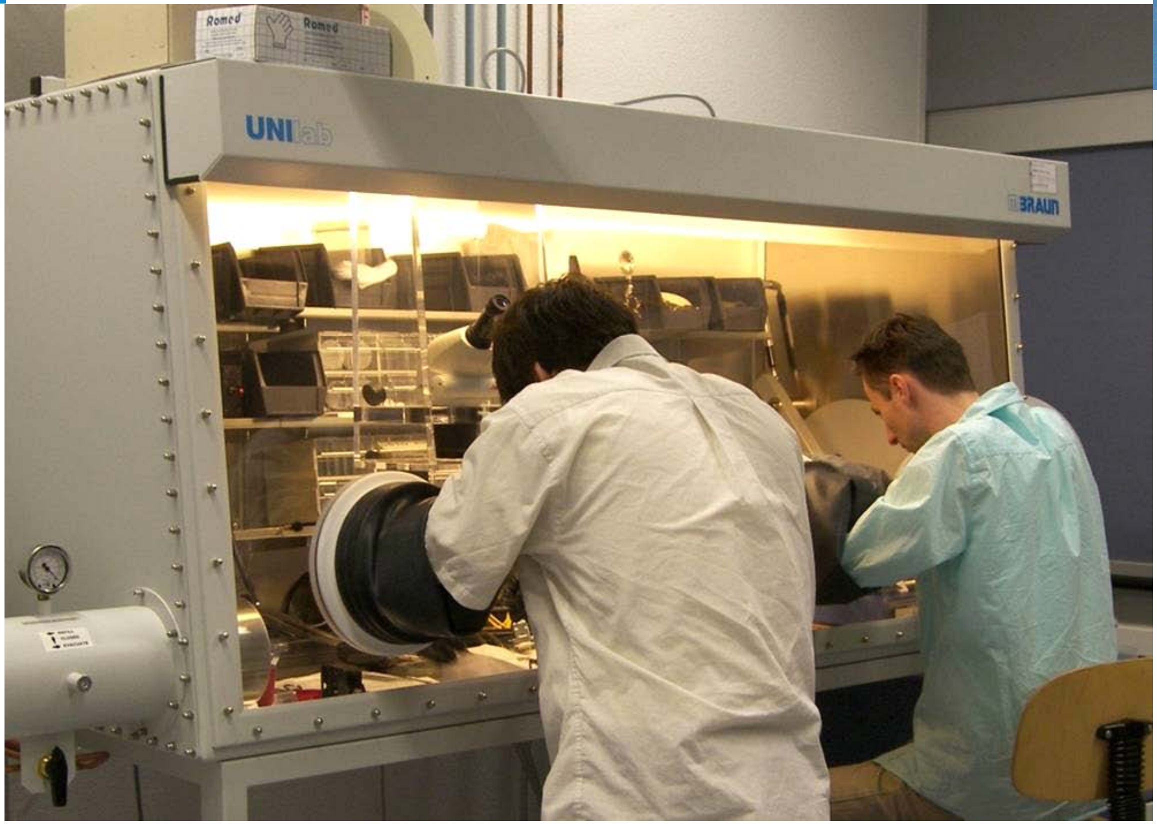

$LaBr_3:Ce^{3+}$ hygroscopic and must be handled within a dry box
$\Rightarrow$ detectors must be sealed, like NaI(Tl)

Signal from timing branch

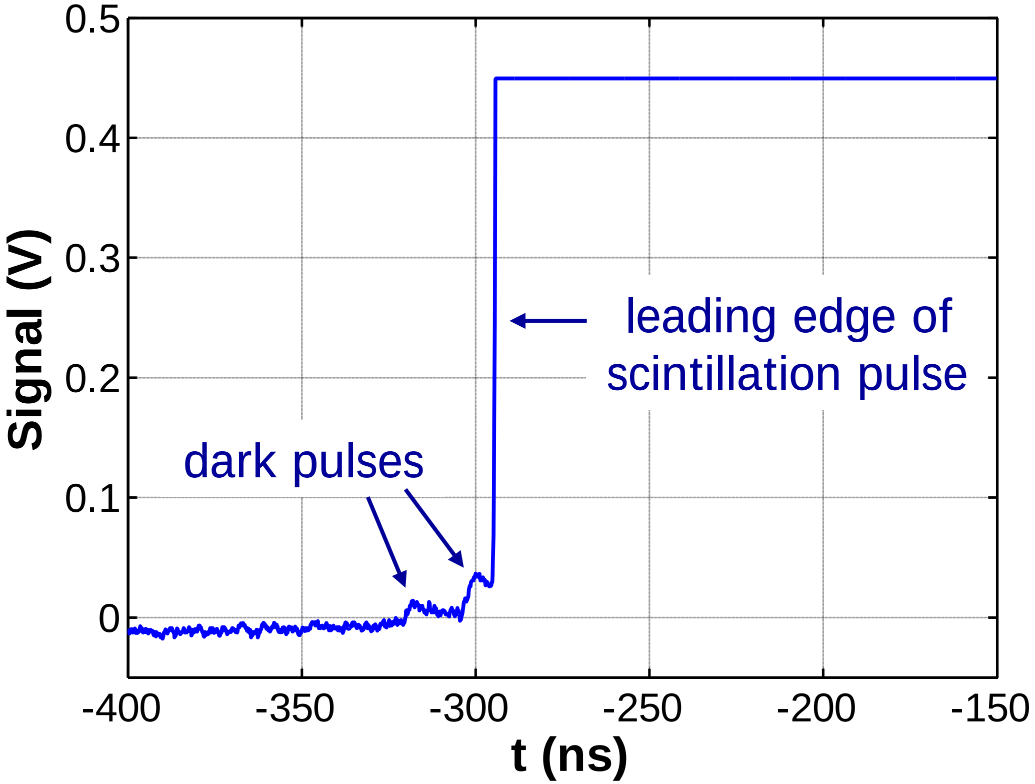

Creating a Time Stamp

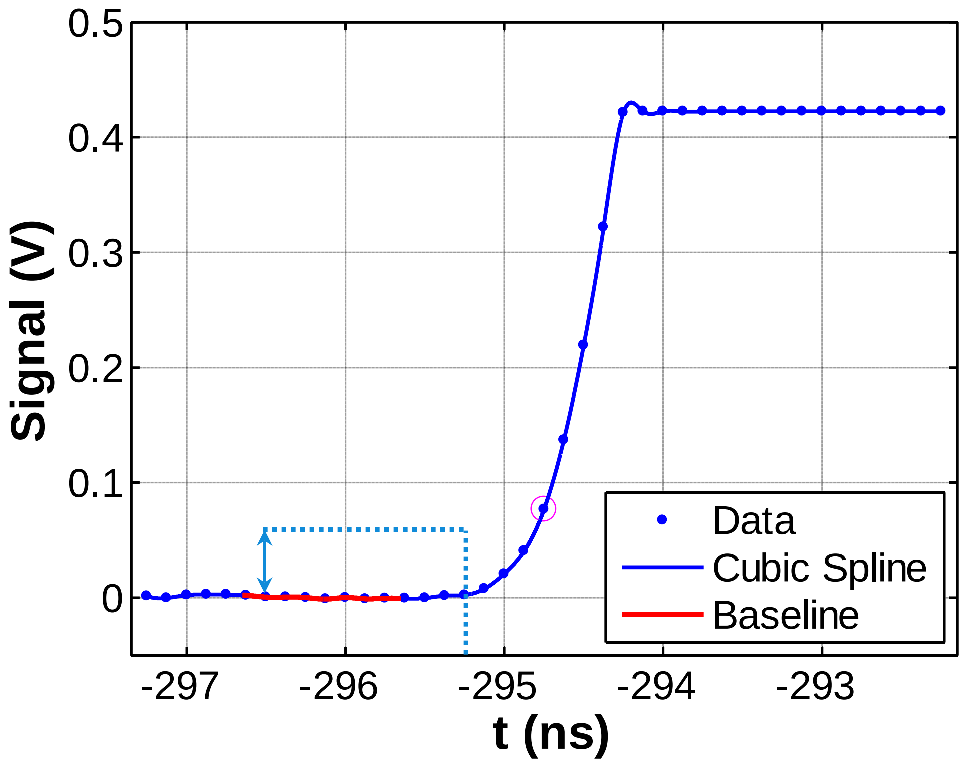

- Pick leading edge
- Interpolation with full cubic spline
- Determine baseline (averaging) directly prior to onset
- Determine intersection with constant level threshold

Monolithic $LaBr_3$:Ce detector

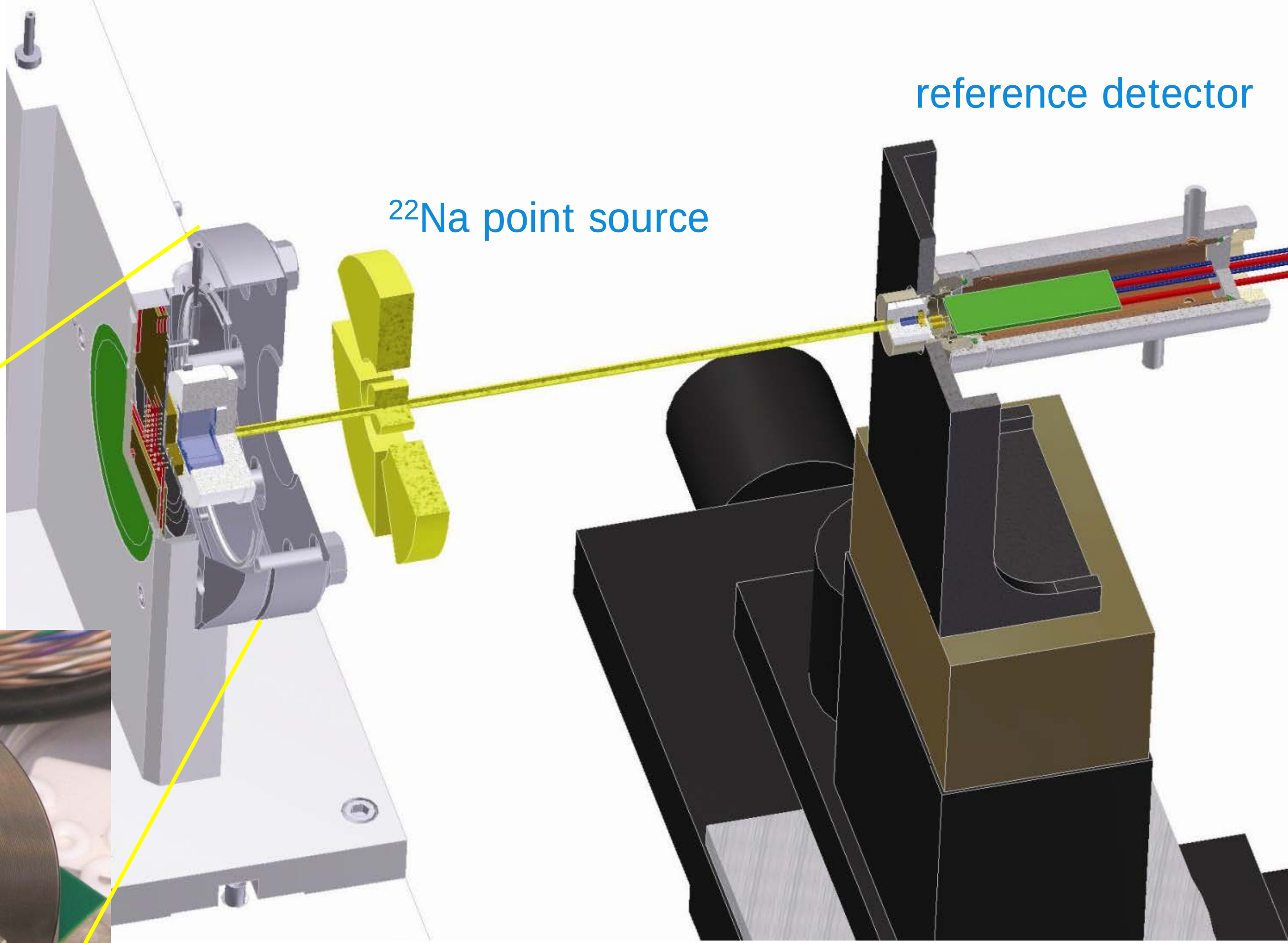

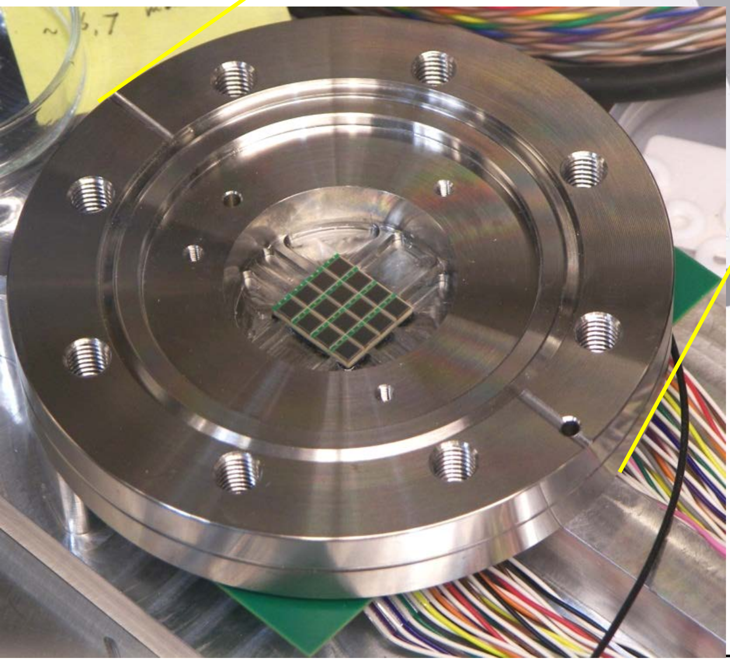

- Hamamatsu SiPM array S11064-050P(X1)
- $LaBr_3$:Ce(5%) 16.2 mm x 18 mm x 10 mm
- Front-side readout (FSR)
- Sealed, temperature-regulated detector box

S. Seifert et al, accepted, Phys Med Biol 2012

Monolithic $LaBr_3$:Ce detector

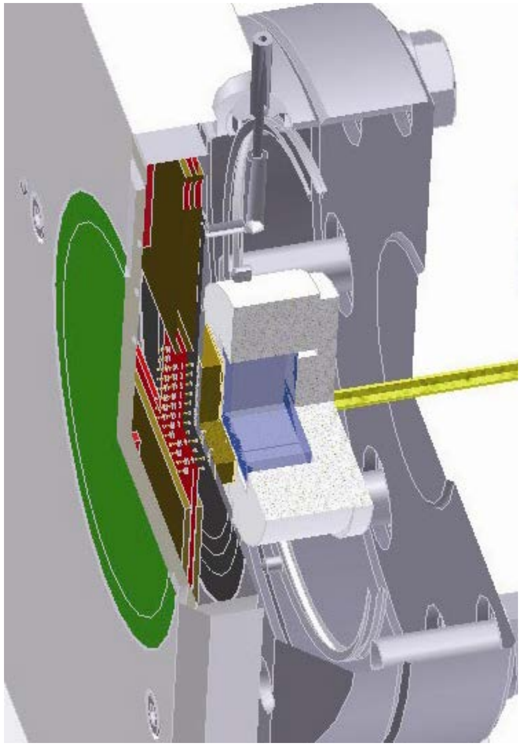

Timing against ~65 ps reference detector

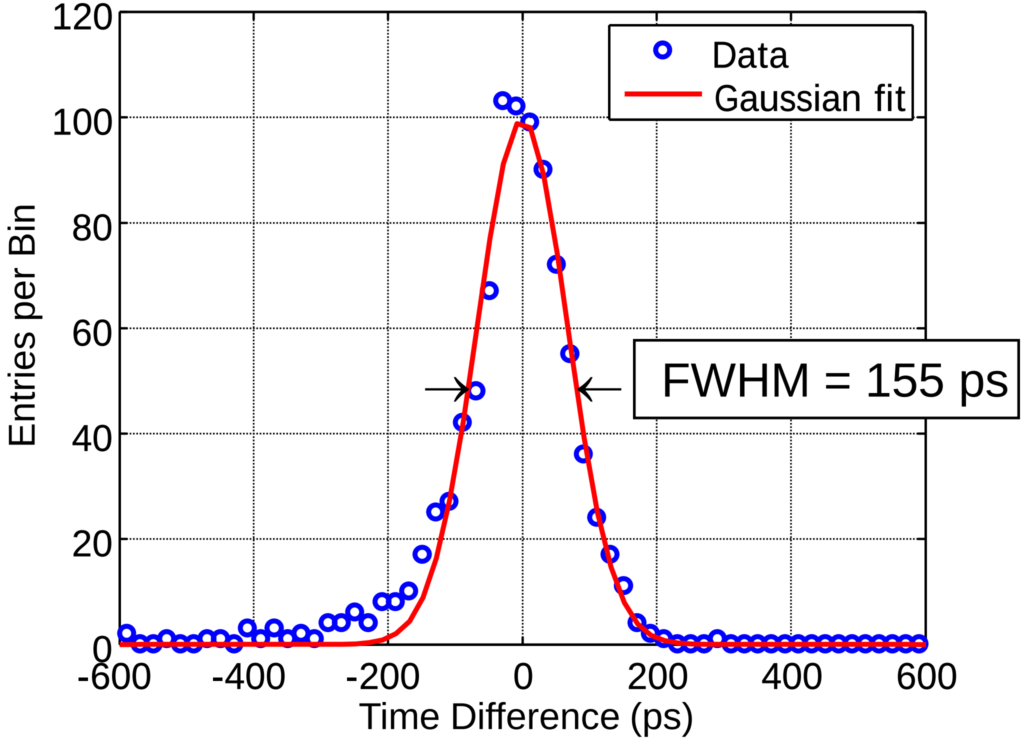

- Detector spatial resolution ~ 1.6 mm FWHM (averaged over entire detector)
- Coincidence resolving time (CRT) for 2 detectors in coincidence 198 ps FWHM
- Observed energy resolution 6.4% FWHM

DOI-dependent signal delay in crystal

Depth-of-interaction (DOI) variations deteriorate timing resolution

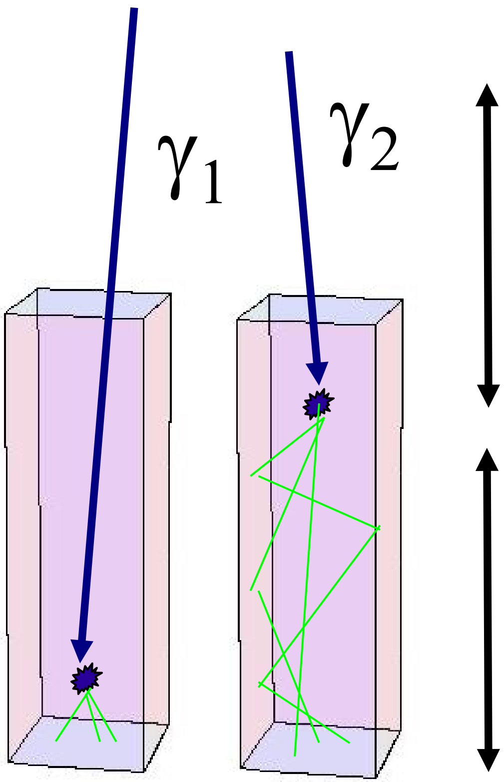

gamma photon speed: c

scintillation photon speed: $c/\hat{n}$

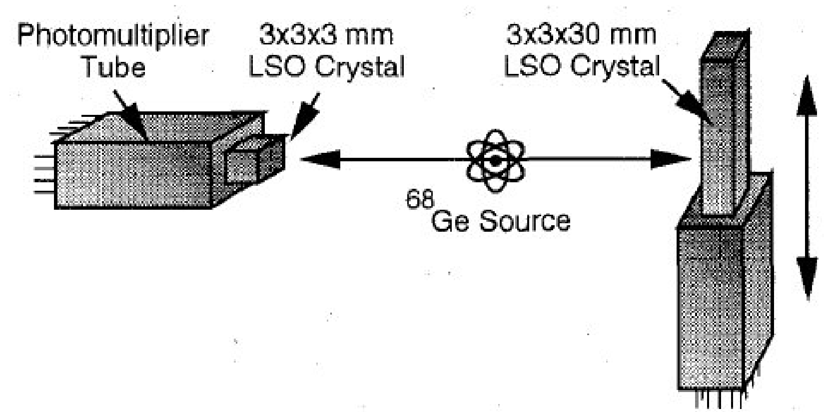

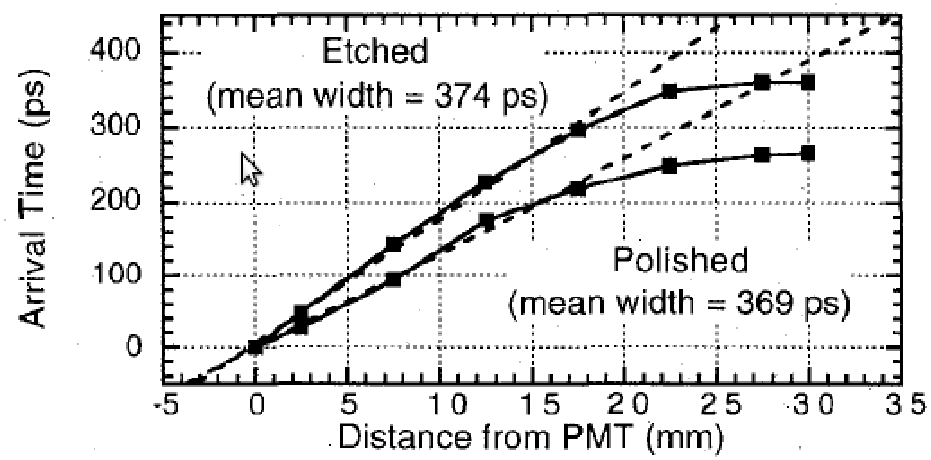

WW Moses and SE Derenzo

IEEE Trans. Nucl. Sci. 46, 474-478 (1999)

Depth-of-interaction determination

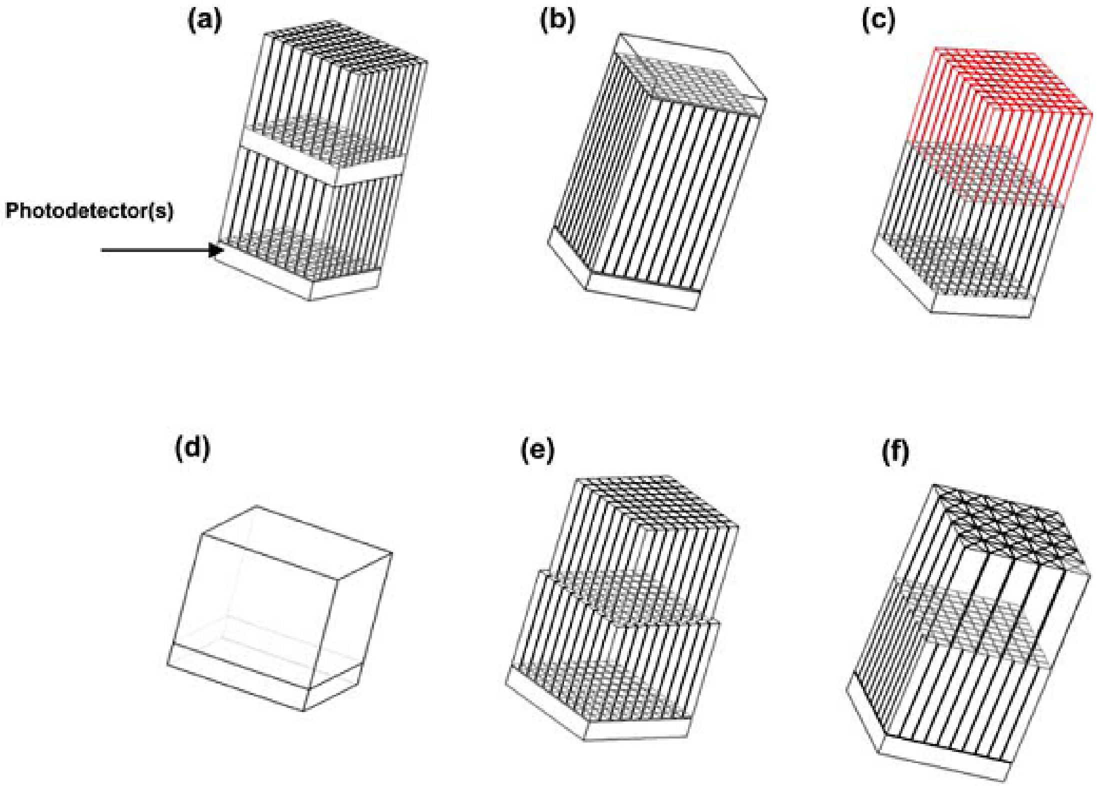

Methods to determine DOI: (a) layered design, (b) single crystals with dual-sided readout, (c) phoswich design, (d) monolithic scintillator, (e) dual layer with offset, (f) dual layer with mixed shapes

dSiPM timing performance

3 mm x 3 mm x 5 mm Ca co-doped LSO:Ce on PDPC demonstrator chip

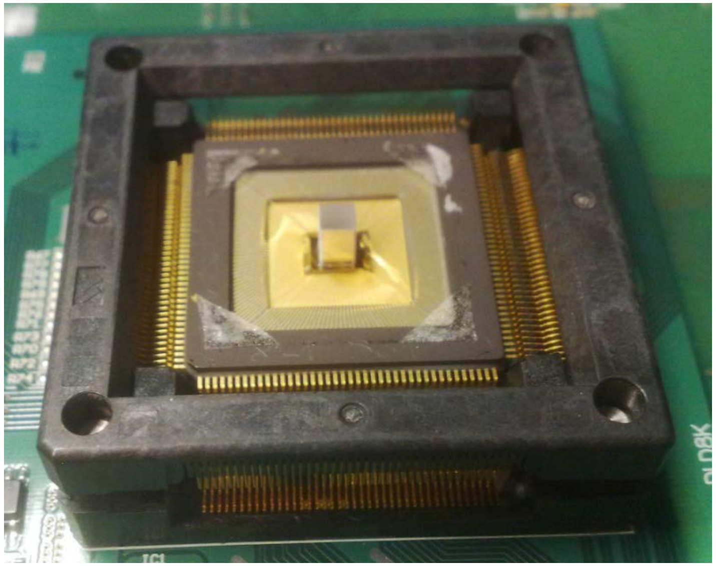

Photograph of Ca co-doped LSO:Ce crystal mounted on dSiPM demonstrator chip

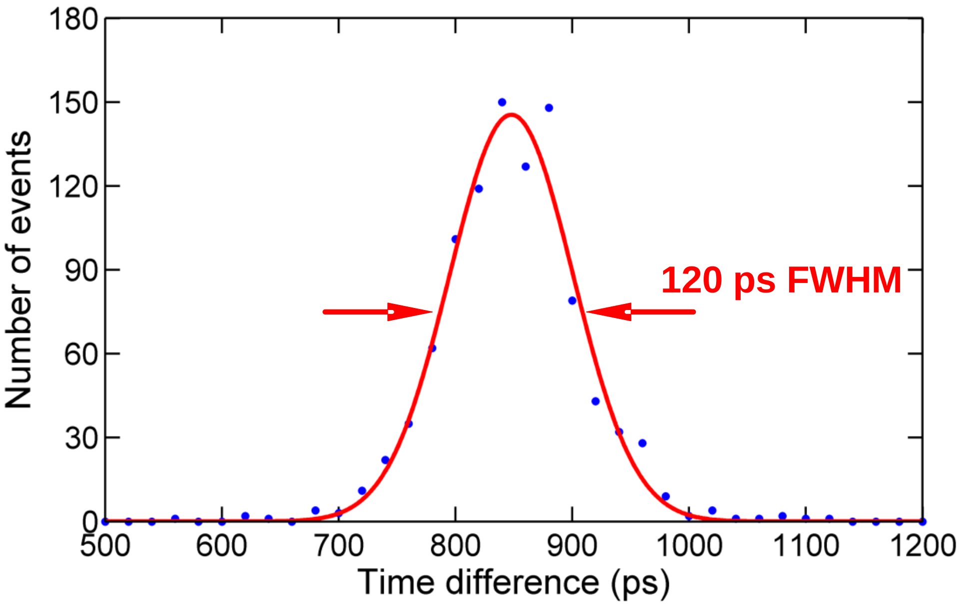

- Time difference spectrum measured with a Na-22 point source
- CRT = 120 ps FWHM (for two detectors in coincidence) at room temperature

Energy resolution

3 mm x 3 mm x 5 mm Ca co-doped LSO:Ce on PDPC demonstrator chip

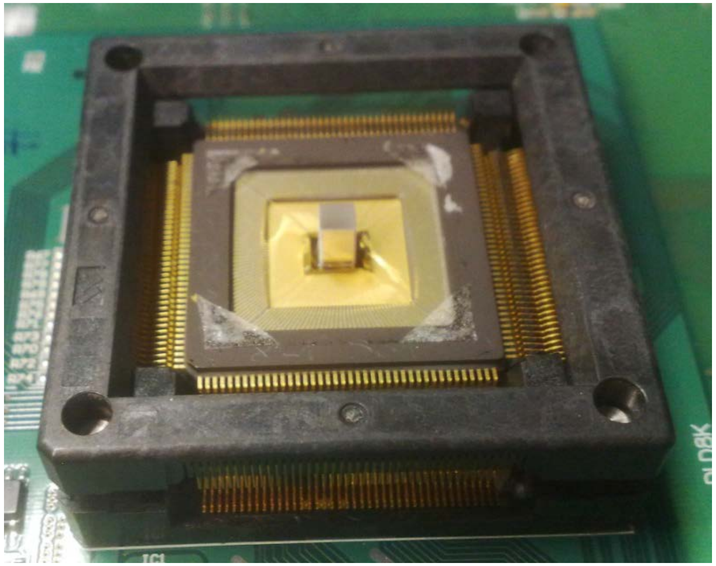

Photograph of Ca co-doped LSO:Ce crystal mounted on dSiPM demonstrator chip

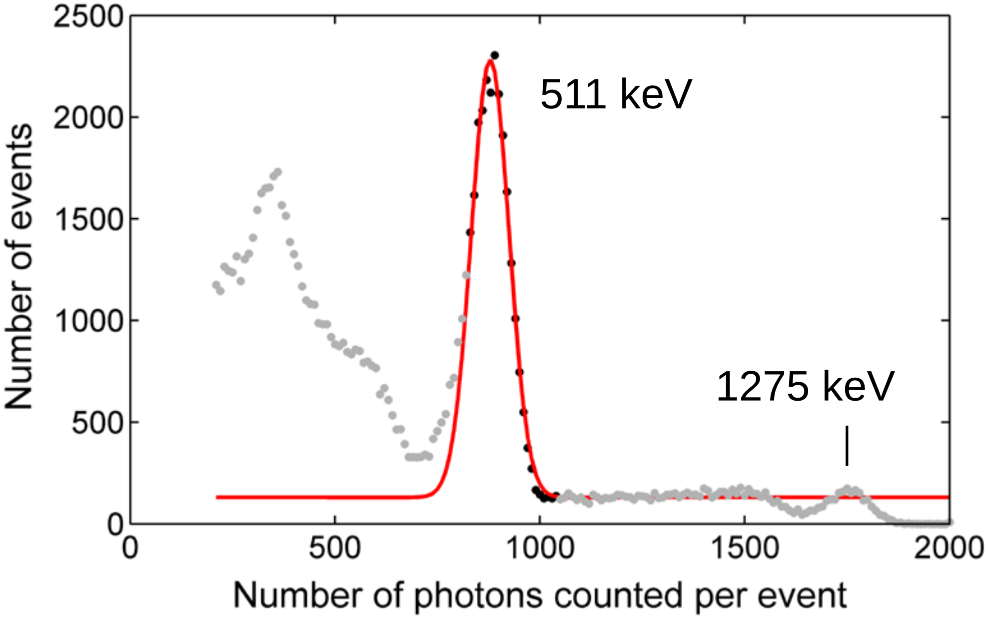

- Pulse height spectrum measured with a Na-22 point source at room temperature
- Energy resolution ≈ 10% FWHM (after saturation correction)

D.R. Schaart et al, NSS-MIC 2011, MIC15.S-137

Order Statistics

Timestamp for the n^{th} detected scintillation photon

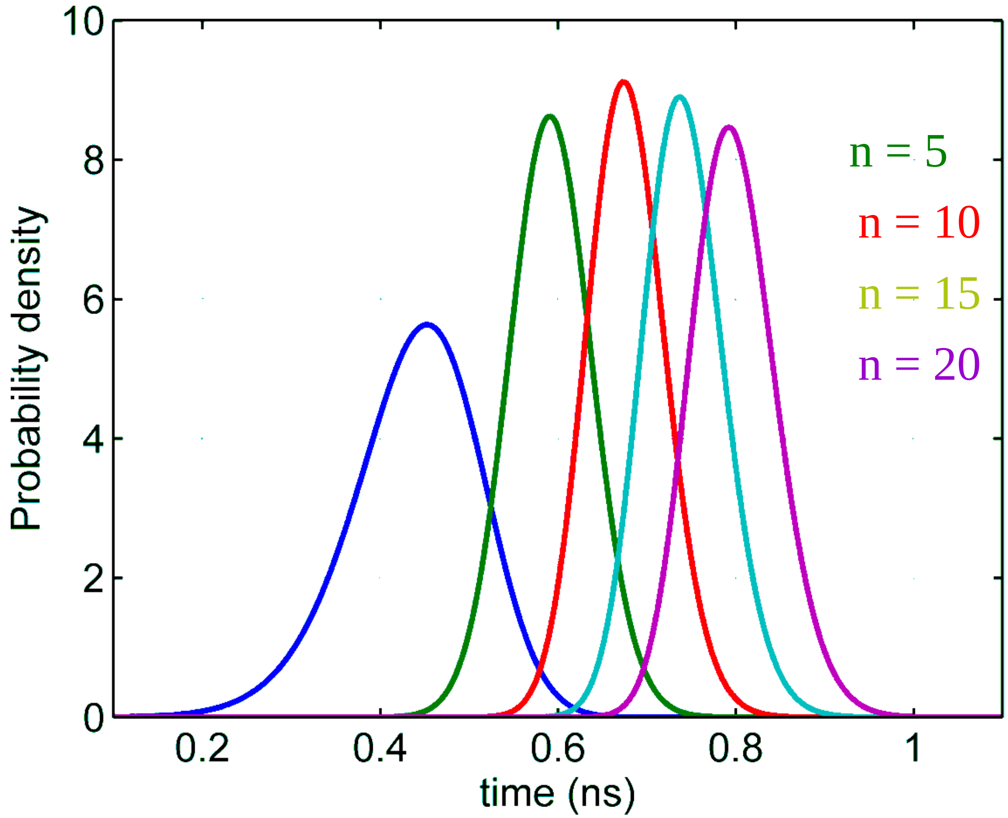

Exemplary probability density functions for the n^{th} order statistic for LYSO:Ce on MPPC-S10362-33-050C

Lower bound for LYSO:Ce

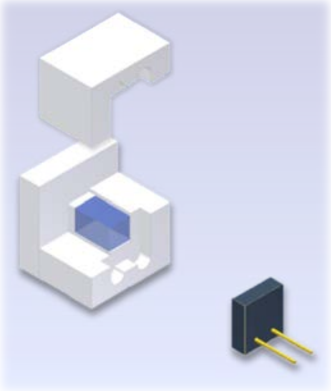

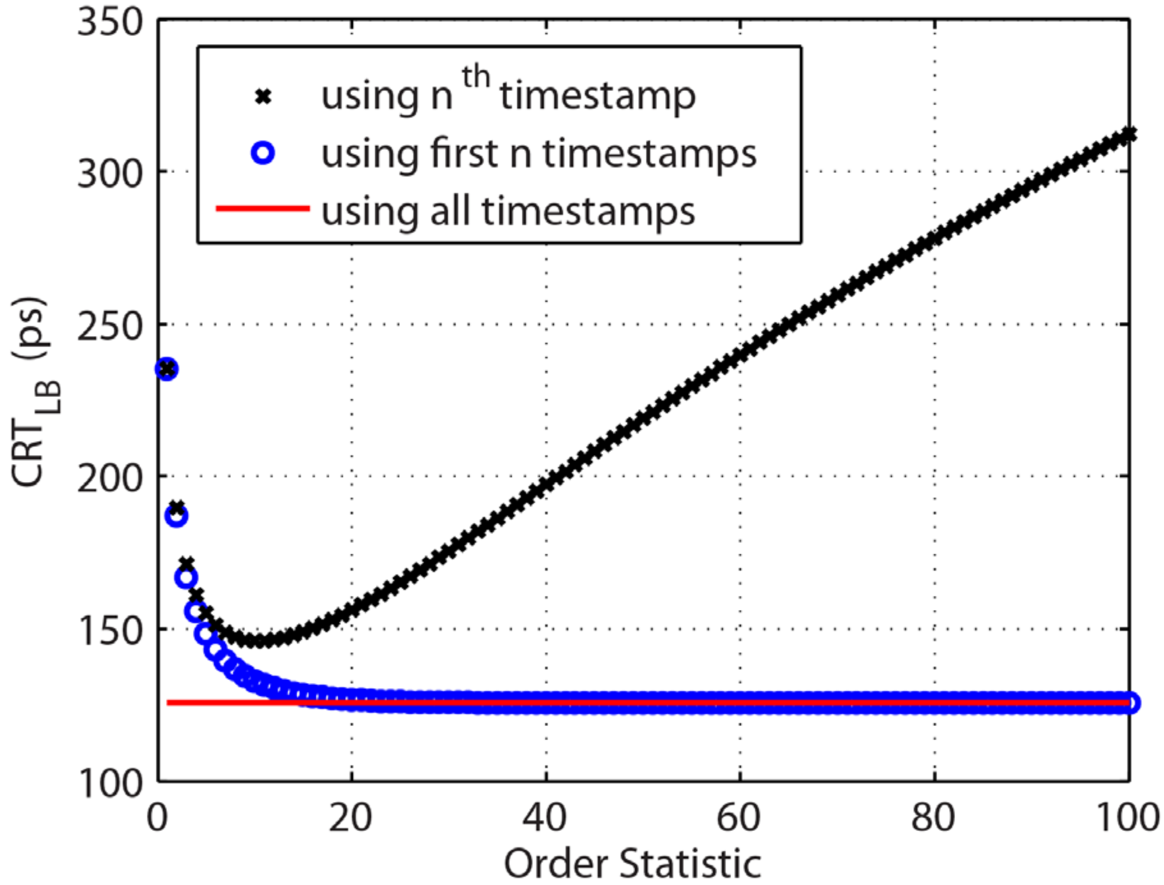

Parameters:

$\tau_r = 90$ ps

$\tau_d = 44$ ns

$\sigma = 120$ ps

$N_{det} = 4700$

Lower bound on the CRT for LYSO:Ce on MPPC-S10362-33-050C, using the n^{th}, the first n, or all detected photons ("order statistics") for timing

S. Seifert et al, "The lower bound on the timing resolution of scintillation detectors," accepted, Phys Med Biol 2012

Lower bound for LYSO:Ce

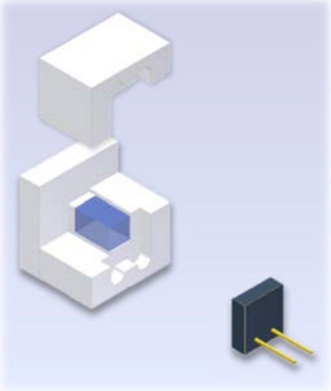

It appears possible to closely approach the CR lower bound using a leading edge trigger set at the optimum threshold level

Calculated lower bound

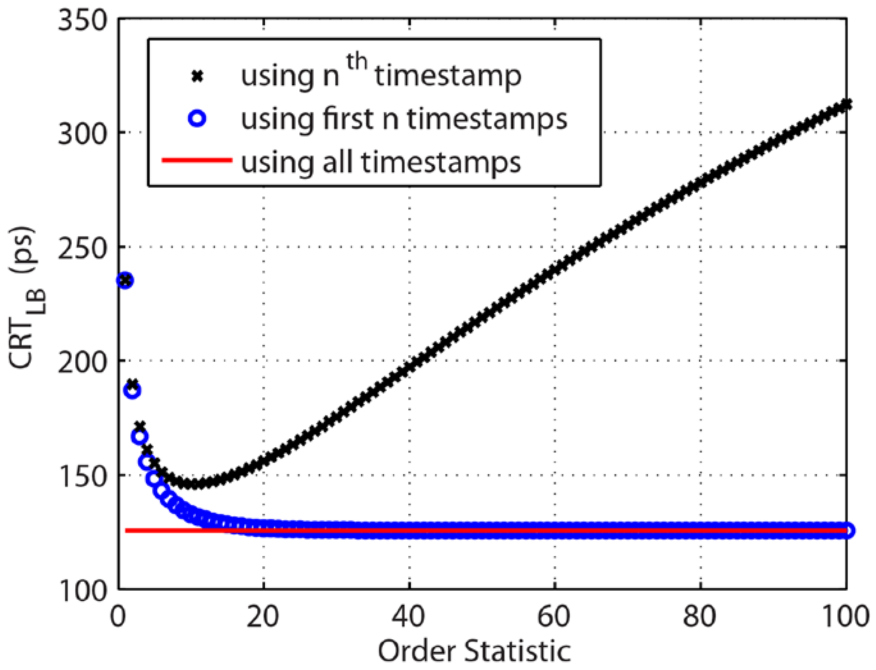

Measured CRT

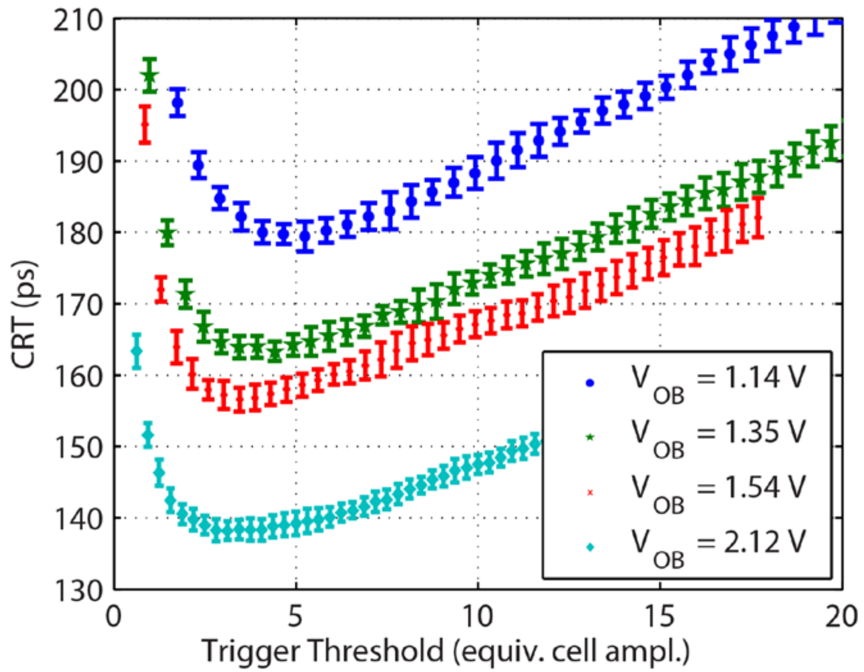

S. Seifert et al, IEEE Transactions on Nuclear Science 59, 190-204, 2012

Comparison to measured values

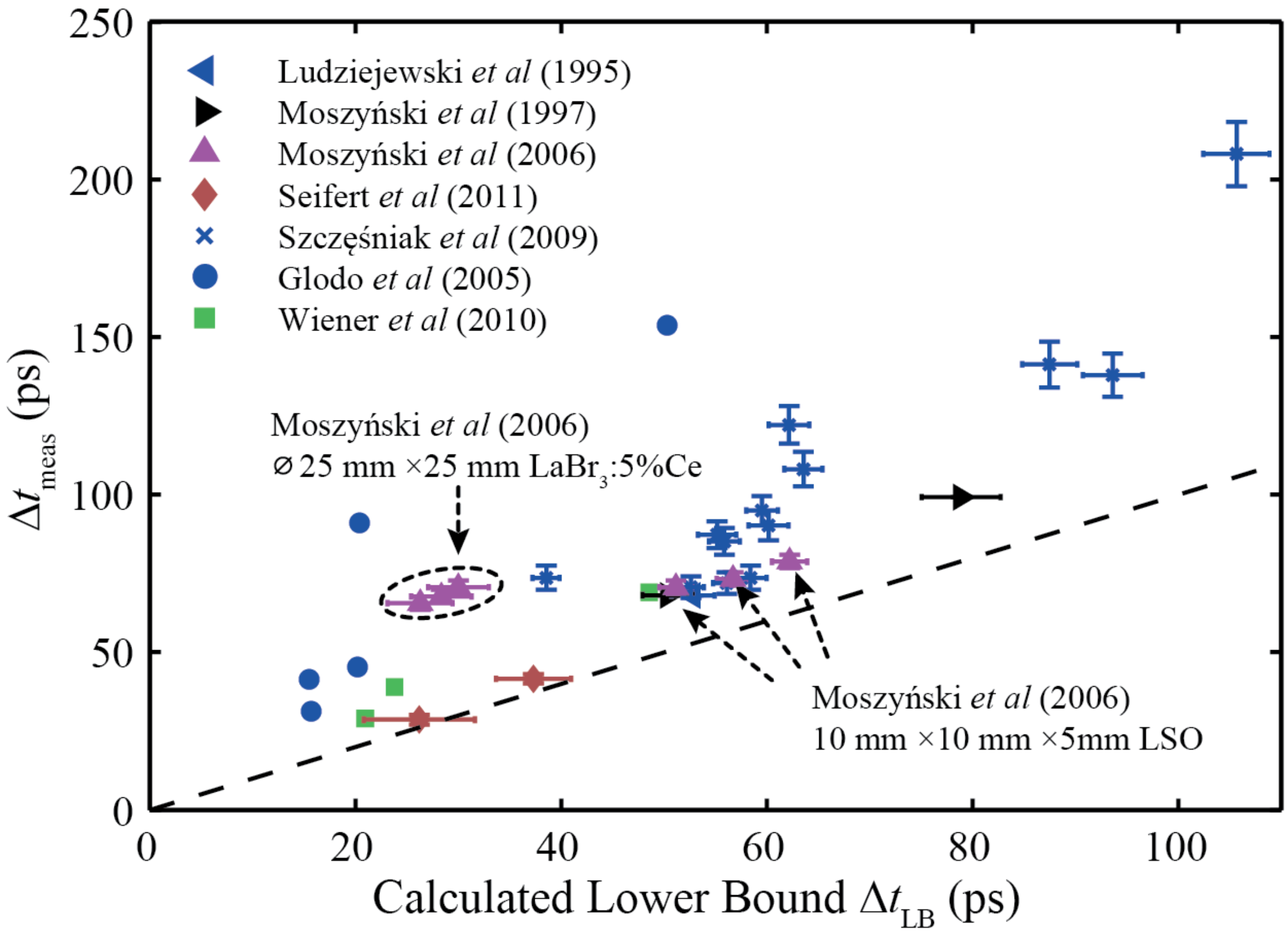

S. Seifert et al, "The lower bound on the timing resolution of scintillation detectors," accepted, Phys Med Biol 2012